UNIVERSITY
OF WARSAW

Doctoral dissertation

$O(N)$ Models and Their Anisotropic Extensions

Andrzej Chlebicki

The thesis written under the supervision of
dr hab. Paweł Jakubczyk
Chair of Condensed Matter Physics,
Institute of Theoretical Physics,
Faculty of Physics, University of Warsaw

Warsaw, November 2023

Contents

Abstract

All in all, it's just another brick in the wall

Pink Floyd, *Another Brick in the Wall, Pt. 2*

In modern physics, there are few field theories more versatile and ubiquitous than the $O(N)$ models. For several decades they have proven invaluable in describing a myriad of physical phenomena. Despite being conceived many years ago, the $O(N)$ models are still subjects of significant developments. This thesis describes a few of the most recent discoveries regarding the classical, bulk phase transitions of the $O(N)$ models and their anisotropic extensions.

The topics discussed in this thesis can be broadly classified as relating to the pure $O(N)$ models or their anisotropic extensions. Regarding the pure $O(N)$ models, we reexamine an old perturbative analysis by Cardy and Hamber [1] predicting a fixed-point collision scenario leading to exotic consequences. Above two dimensions, the collision is expected to induce nonanalytic behavior of critical exponents, while below two dimensions it constitutes a mechanism for the disappearance of the phase transition at the lower critical dimension. We revisit their perturbative analysis and showcase some of its poorly appreciated consequences. We confront these predictions with the results of our nonperturbative renormalization group calculations at the $O(\partial^2)$ order of the derivative expansion. Our calculations confirm the presence of the fixed-point collision below two dimensions and offer robust arguments against the collision scenario above two dimensions. The discussion of this subject, presented in Chapter 3, is based on two articles: *Analyticity of critical exponents of the O(N) models from nonperturbative renormalization* [2] and *Low-temperature behavior of the O(N) models below two dimensions* [3].

The other area explored in this thesis concerns the effects of weak cubic perturbations in the $O(2)$ model. We investigate how the leading scaling exponent of the anisotropic field y_4 varies with the dimension. We offer an accurate determination of y_4 in three dimensions and, subsequently, observe the evolution of y_4 while reducing the dimension towards two. In the vicinity of two dimensions, we observe y_4 approaching zero marking the onset of the nonuniversal behavior related to the Kosterlitz-Thouless physics. We also discuss how the comparative performance

of two alternative approaches to the derivative expansion varies with the dimension. These topics are explored in Chapter 4 based on the article $\mathbb{Z}_4$-*symmetric perturbations to the XY model from functional renormalization* [4]. This article is a product of a collaboration with Carlos A. Sánchez-Villalobos, Paweł Jakubczyk, and Nicolás Wschebor; in the conclusion of the chapter, we disclose the authors' contributions.

Streszczenie

We współczesnej fizyce istnieje niewiele teorii pola bardziej uniwersalnych i wszechobecnych niż modele $O(N)$. Od kilkudziesięciu lat stanowią one nieocenione narzędzie wykorzystywane do opisu niezliczonych zjawisk fizycznych. Pomimo wielu lat, które upłynęły od ich utworzenia, modele $O(N)$ pozostają przedmiotem badań. Niniejsza rozprawa opisuje kilka najnowszych odkryć dotyczących klasycznych przejść fazowych w modelach $O(N)$ i ich anizotropowych rozszerzeniach.

Tematy rozważane w tej rozprawie podzielone są na dwie kategorie: czystych modeli $O(N)$ oraz ich anizotropowych rozszerzeń. W obszarze czystych modeli $O(N)$ weryfikujemy starą analizę perturbacyjną Cardy'ego i Hambera [1] przewidująca zderzenie punktów stałych grupy renormalizacji. Cardy i Hamber twierdzą, że powyżej dwóch wymiarów to zderzenie wywołuje nieanalityczne zachowanie wykładników krytycznych, natomiast poniżej dwóch wymiarów stanowi ono mechanizm zaniku przejścia fazowego w dolnym wymiarze krytycznym. W pierwszej kolejności odtwarzamy ich rozumowanie perturbacyjne, podkreślając jego mało znane konsekwencje. Następnie konfrontujemy ich przewidywania z wynikami naszych obliczeń opartych o nieperturbacyjną grupę renormalizacji w rozwinięciu w pochodnych do rzędu $O(\partial^2)$. Nasze obliczenia potwierdzają obecność zderzenia punktów stałych w wymiarach poniżej dwóch i dostarczają silnych argumentów przeciwko scenariuszowi zderzenia w wymiarach powyżej dwóch. Nasza analiza scenariusza Cardy'ego i Hambera, przedstawiona w Rozdziale 3, oparta jest o dwa artykuły: *Analyticity of critical exponents of the O(N) models from nonperturbative renormalization* [2] oraz *Low-temperature behavior of the O(N) models below two dimensions* [3].

Drugi obszar poruszany w tej rozprawie dotyczy efektów słabych perturbacji kubicznych w modelu $O(2)$. Badamy, w jaki sposób wiodący wykładnik skalowania pola anizotropowego y_4 zmienia się wraz z wymiarem. Precyzyjnie wyznaczamy wartość y_4 w trzech wymiarach, a następnie obserwujemy jego ciągłą ewolucję pomiędzy trzema i dwoma wymiarami. W pobliżu dwóch wymiarów obserwujemy, że y_4 zbliża się do zera, prowadząc do nieuniwersalnych zjawisk związanych z fizyką Kosterlitza-Thoulessa. Badamy również jak precyzja dwóch alternatywnych implementacji rozwinięcia w pochodnych zmienia się wraz z wymiarem. Powyższe

zagadnienia omówione są w Rozdziale 4; przedstawione w nim wyniki pochodzą z artykułu $\mathbb{Z}_4$-*symmetric perturbations to the XY model from functional renormalization* [4]. Ten artykuł powstał we współpracy z Carlosem A. Sánchez-Villalobos, Pawłem Jakubczykiem i Nicolásem Wschebor; w podsumowaniu rozdziału prezentujemy wkład autorów artykułu.

Acknowledgements

> It's awfully considerate of you to think of me here
> And I'm most obliged to you for making it clear
> That I'm not here
>
> Pink Floyd, *Jugband Blues*

I am deeply grateful to my advisor, Paweł Jakubczyk, whose unwavering support has been invaluable throughout this journey. For the past six years, he has been an amazing teacher and an encouraging mentor. His guidance has been essential in shaping the trajectory of my research.

I extend my sincere appreciation to the scientists of Instituto de Física at Universidad de la República in Montevideo for their hospitality during my academic exchange. In particular, I would like to express my gratitude to Nicolás, Carlos, Marcela, and Gonzalo for their generosity, and the welcoming environment they provided. This academic exchange was a transformative experience, exposing me to new perspectives, methodologies, and collaborative opportunities for which I am especially grateful.

A special note of gratitude goes out to my fellow PhD students, in particular, Maciek, Maciej, and Kacper for our countless coffee breaks filled with lively discussions. These breaks were not just refueling moments for caffeine but also essential pauses that fostered a sense of community and collaboration.

I would like to express my heartfelt gratitude to my family and friends whose encouragement has been instrumental throughout this challenging yet rewarding journey. Special thanks are extended to my brother, Zbyszek, for sharing his expertise in programming which significantly enriched my skillset and contributed to the success of my research. I am thankful to Iwona and Błażej for their invaluable assistance in reviewing my grant application and their encouragement in my academic pursuits.

To my wife, Kasia, your love, and patience have been my anchor. Your understanding of the demands of academic life and your encouragement have been indispensable in navigating the challenges of this PhD journey.

Finally, financial support from the Polish National Science Center, the Polish National Agency for Academic Exchange, and the University of Warsaw is gratefully acknowledged. Their support made it possible for me to engage in this enriching academic journey.

Notation and conventions

All models discussed in this thesis are formulated in a d-dimensional Euclidean space. Number N always refers to the number of components of the scalar order parameter.

Position and momentum spaces Letters $\boldsymbol{p}$, $\boldsymbol{q}$, $\boldsymbol{r}$ are reserved to denote vectors in momentum space; letters $\boldsymbol{x}$, $\boldsymbol{y}$, $\boldsymbol{z}$ correspond to the position-space parameters. We introduce the shorthand notation for integrals in position and momentum spaces respectively:

$$\int_{\boldsymbol{x}} := \int d^d\boldsymbol{x}, \quad \int_{\boldsymbol{q}} := \int \frac{d^d\boldsymbol{q}}{(2\pi)^d}. \tag{1}$$

Fourier transform We adopt the following convention for the Fourier transform:

$$f(\boldsymbol{x}) = \int_{\boldsymbol{q}} f_{\boldsymbol{q}} e^{i\boldsymbol{q}\cdot\boldsymbol{x}}, \quad f_{\boldsymbol{q}} = \int_{\boldsymbol{x}} f(\boldsymbol{x}) e^{-i\boldsymbol{q}\cdot\boldsymbol{x}}. \tag{2}$$

The real- and Fourier-space components of the same field share the same symbol. They are distinguished by either the position variable in the bracket, e.g. $\phi(\boldsymbol{x})$, or the momentum in the subscript for the Fourier-space components, e.g. $\phi_{\boldsymbol{q}}$.

Functional derivatives The momentum space functional derivative is defined through a chain rule via the position space functional derivative:

$$\frac{\delta}{\delta\phi_{\boldsymbol{q}}} := \int_{\boldsymbol{x}} \frac{\delta\phi(\boldsymbol{x})}{\delta\phi_{\boldsymbol{q}}} \frac{\delta}{\delta\phi(\boldsymbol{x})} = \int_{\boldsymbol{x}} \frac{e^{i\boldsymbol{q}\cdot\boldsymbol{x}}}{(2\pi)^d} \frac{\delta}{\delta\phi(\boldsymbol{x})}. \tag{3}$$

List of Abbreviations

BZJ	Brézin and Zinn-Justin
CH	Cardy and Hamber
DE	derivative expansion
FP	fixed point
IR	infrared
KT	Kosterlitz-Thouless
LCE	large charge expansion
LPA	local potential approximation
LRO	long-range ordered
MC	Monte Carlo
MW	Morris-Wetterich
NF	Nelson and Fisher
NPRG	nonperturbative renormalization group
NR	Newton-Raphson
PMC	principle of maximal conformity
PMS	principle of minimal sensitivity
PT	perturbation theory
QFP	quasi-fixed point
QLRO	quasi-long-range ordered
RG	renormalization group
RK	Runge-Kutta
UC	universality class
UV	ultraviolet
WP	Wilson-Polchinski

Chapter 1

Introduction

Far, far, far away, way
People heard him say, say
I will find a way, way
There will come a day, day
Something will be done

Pink Floyd, *Let There Be More Light*

1.1 The $O(N)$ models

Symmetries count among the most fundamental concepts in modern physics. They are employed to impose strict constraints on the dynamics and statistics of models, which makes them absolutely indispensable tools in almost every branch of physics. In statistical physics, symmetry is one of the key factors defining the nature of phase transitions allowed to occur in a given model. For this reason, the universality classes (UCs) are typically categorized by symmetry groups, along with spatial dimension and the range of interactions.

A class of symmetry groups that remains ubiquitous in both statistical physics and high-energy physics is the family of N-dimensional orthogonal groups. Models characterized by these symmetries often called the $O(N)$ models, were originally designed to describe phase transitions occurring in ferromagnetic crystals. These early formulations include the Ising model belonging to the $O(1)$ UC, the XY model of the $O(2)$ UC, and the Heisenberg model of the $O(3)$ UC. Nowadays, thanks to the principles of universality, we know that the $O(N)$ UCs describe many more phenomena, inter alia the polymer problem for $N = 0$, the liquid-vapor phase transition for $N = 1$, the helium superfluid transition for $N = 2$ and the chiral phase transition in quantum chromodynamics in the limit of two quark flavors

for $N = 4$ [5–7]. In addition to their wide physical relevance, the $O(N)$ models feature a remarkably simple formulation which has provided a fertile ground for the development of many renormalization group (RG) and conformal field theory techniques [8–10].

Although widely studied for many years, the $O(N)$ models remain subjects of interesting developments. In recent years, an old topic of boundary universality of the three-dimensional $O(N)$ models has received renewed attention due to a discovery of a new boundary UC called "extraordinary-log". This new UC is believed to persist for $2 \leq N < N_c$ with $N_c \approx 5$, though the precise value of N_c remains unsettled [11–14]. Another important discovery concerns a class of previously unknown multicritical fixed points (FPs) of the $O(N)$ models. These FPs share an unusual characteristic - they develop nonanaliticities [cusps] in the $N \to \infty$ limit, thus not lending themselves to the perturbative large-N description. This discovery showcases the limitations of a powerful method which is the large-N expansion [15, 16]. It is also important to mention the advancements in the precision of the determination of universal quantities, such as the critical exponents and the universal amplitude ratios. The recent years saw development of various methods such as conformal bootstrap, Monte Carlo (MC) and functional renormalization group to produce the most precise values [17–27].

As confidence intervals for the values of the critical exponents shrink, sometimes estimates from different methods become incompatible with each other. A prime example of this was the so-called "$O(2)$ controversy". The three-dimensional $O(2)$ UC was studied with many methods including a superfluid ^{4}He space-shuttle experiment [28], MC simulations [29], and perturbative RG methods [30]. While the RG results remained compatible with the rest, the results from the two former methods were in a staggering $\sim 8\sigma$ tension with each other. Conformal bootstrap is a novel tool that offers resolution for such incompatibilities. Unlike the other methods, conformal bootstrap provides strict bounds within which the critical exponents have to be confined. As for the $O(2)$ controversy, a recent conformal bootstrap study has been able to reject the experimental estimate in support of the MC results [31].

1.1.1 Perturbative methods

It is commonly agreed that the UCs of the basic bulk critical transitions in the $O(N)$ models with sufficiently short-range interactions can be parametrized with just two variables: the spatial dimension d and the number of order-parameter components N. The physical realizations of these UCs typically only occur for integer pairs (d, N). However, it has proven useful and convenient in the studies of critical phenomena to treat d and N formally as continuous parameters. The exact meaning of models with noninteger values d or N is a somewhat involved

topic often brushed aside without a detailed explanation. Thanks to path-integral formalism and dimensional regularization, the formulation of field theories in a generic dimension is now well-established and widely employed [10]. In contrast, the rigorous mathematical formulation for models with generic N has been presented only very recently via the language of Deligne categories [32].

Even with the rigorous formulation, it is still difficult to simulate models with generic d and N, e.g. on a lattice. There has been, however, some effort in engineering systems with noninteger values of effective dimension. This includes attempts to simulate systems of nontrivial topology [33, 34] and systems on fractal lattices [35, 36]. The latter, somewhat worryingly, suggests that the critical properties depend on more geometric details than just the Hausdorff dimension of a fractal. The generic values of N have been investigated in a Monte Carlo study of the $O(N)$ loop model [37], and noninteger values of d and N have been recently explored in conformal bootstrap studies [38, 39]. However, the most notable examples of treating d and N as continuous variables include the perturbative RG methods: the $4-\tilde{\epsilon}$ expansion, the $2+\epsilon$ expansion, and the large-N expansion. These perturbative approaches have long been employed to predict the values of the critical exponents and played an invaluable role in the development of the general theory of RG [8, 10, 40].

The three aforementioned perturbative techniques all seek to capture the critical behavior of nontrivial theories by expanding them around the strictly soluble theory with respect to a formally continuous small parameter. The $4-\tilde{\epsilon}$ expansion describes the ϕ^4 model close to its upper critical dimension. The $O(N)$-symmetric ϕ^4 model is a field-theory of an unconstrained N-component scalar field $\boldsymbol{\phi}(\boldsymbol{x})$ governed by the action:

$$\mathcal{S}_{\phi^4} = \int d^d x \left\{ \frac{r}{2}\boldsymbol{\phi}^2(\boldsymbol{x}) + \frac{u}{4!}\left[\boldsymbol{\phi}^2(\boldsymbol{x})\right]^2 + \frac{1}{2}\left[\partial_\mu \boldsymbol{\phi}(\boldsymbol{x})\right]^2 \right\}. \tag{1.1}$$

In the limit $d \to 4^-$, the quartic coupling of the critical FP vanishes and the critical FP collides with the Gaussian fixed point. This allows for the RG β functions to be calculated in a simultaneous expansion in the coupling u and $\tilde{\epsilon} = 4 - d$ in terms of Gaussian expectation values. We note that the $4-\tilde{\epsilon}$ expansion can be applied not only to the models characterized by the $O(N)$ symmetry but also to the models with discrete symmetry groups, e.g. exhibiting cubic anisotropy. We elaborate on this point in the Sec. 1.2.

The $2+\epsilon$ expansion, first proposed by Polyakov [41] and Brézin and Zinn-Justin [42], is a variant of a low-temperature expansion for the nonlinear-σ model near two dimensions. It describes how interactions between the Goldstone modes lead to the decay of the long-range order. In the $O(N)$-symmetric nonlinear-σ model, unlike in the ϕ^4 model, the N-component order parameter is constrained to a unit

length $\boldsymbol{\phi}^2(\boldsymbol{x}) = 1$. The action of the nonlinear-σ model reads simply:

$$\mathcal{S}_{\mathrm{NLS}} = \int d^d x \frac{1}{2g} \left[\partial_\mu \boldsymbol{\phi}(\boldsymbol{x})\right]^2 , \tag{1.2}$$

where g is the spin-wave coupling. Typically, the order parameter is decomposed as $\boldsymbol{\phi}(\boldsymbol{x}) = (\sigma(\boldsymbol{x}), \boldsymbol{\pi}(\boldsymbol{x}))$ into the longitudinal σ field and $N-1$ transversal π fields. Using the constraint $\boldsymbol{\phi}(\boldsymbol{x})^2 = 1$ the action is expressed in terms of the π fields only:

$$\mathcal{S}_{\mathrm{NLS}} = \int d^d x \frac{1}{2g} \left\{ \left[\partial_\mu \boldsymbol{\pi}(\boldsymbol{x})\right]^2 + \frac{\left[\boldsymbol{\pi}(\boldsymbol{x}) \cdot \partial_\mu \boldsymbol{\pi}(\boldsymbol{x})\right]^2}{1 - \boldsymbol{\pi}^2(\boldsymbol{x})} \right\} . \tag{1.3}$$

This form of the action shows explicitly, how nontrivial interactions between the transversal π fields are generated by the constraint imposed on the order parameter.

For weak coupling g [at low temperatures], the dominant contributions to the partition function come from the field configurations satisfying $|\boldsymbol{\pi}(x)| = O(\sqrt{g})$ and $|\partial_\mu \boldsymbol{\pi}(x)| = O(\sqrt{g})$. This means that the interaction term in Eq. (1.3) becomes of higher order in g than the gradient term. One then formulates a diagrammatic expansion around the Gaussian theory [$g = 0$]. A generic β_g^{NLS} function of the $2 + \epsilon$ expansion takes the form:

$$\beta_g^{\mathrm{NLS}} = -\epsilon g + (N-2) f(g, N), \tag{1.4}$$

where $\epsilon = d - 2$ and the function $f(g, N) = \frac{g^2}{2\pi} + O(g^3)$ is deduced perturbatively.

Finally, the large-N expansion is an expansion around the limit $N \to \infty$. In this limit, the $O(N)$ universality class contains the analytically soluble Berlin-Kac [spherical] model [43, 44]. Around the exact solution, the partition function and the correlation functions can be evaluated through the steepest-descent method. This yields the quantities of interest, such as the critical exponents, expressed as a power series in the parameter $\frac{1}{N}$. Importantly, the large-N expansion can be formulated for either the $O(N)$-symmetric ϕ^4 model and the nonlinear-σ model. Moreover, it predicts the same universal properties for both models to any order in $\frac{1}{N}$ [40]. This fact, along with a shared symmetry of the interactions, leads to a widespread belief that these models belong to the same universality class. Most certainly, if the two differ in some way, the nature of that difference would have to be nonperturbative in the large-N limit.

Although the historical significance of these perturbative approaches is difficult to overstate, they are not without their pitfalls. Firstly, the formally small and continuous expansion parameter is typically not small and only formally continuous. Most often, these expansions are employed to access the critical properties of three-dimensional models where $\epsilon = \tilde{\epsilon} = 1$. The expansion series are often asymptotic or even divergent and one has to resort to resummation techniques. Secondly,

by definition, the perturbative approaches cannot describe the nonperturbative effects. These include the role of the vortices in the Kosterlitz-Thouless transition or the multicritical FPs becoming nonanalytical in the $N \to \infty$ limit. Problems with perturbative expansions call for the development of nonperturbative techniques.

Nonperturbative renormalization group (NPRG) methodology based on the Kadanoff-Wilson coarse-graining is not a new idea. The first implementations of NPRG go back as far as the 1970s [45]. The late 1980s and early 1990s saw a revival of the ideas of NPRG with the so-called "effective average action approach" at the forefront. This technique is based on the exact RG-flow equation called the Morris-Wetterich equation [46, 47].

Like the earlier formulations of NPRG, the Morris-Wetterich equation typically cannot be solved exactly and requires some approximate treatment. One particularly successful and widely adopted approximation scheme is the derivative expansion (DE). Although quite accurate even at low expansion orders, for a long time the DE has lacked a method for estimating error bars and its convergence has been questioned. This has changed only very recently with strong arguments being presented for a very rapid convergence of the DE [23, 48] along with techniques for error estimation [21]. A detailed discussion of the effective average action approach and the derivative expansion is relegated to Chapter 2.

1.1.2 Phases and phase transitions

In general, the $O(N)$ models can support three distinct types of phases: disordered, long-range ordered (LRO), and quasi-long-range ordered (QLRO). A disordered phase features a vanishing order parameter and an exponential decay of the correlation function

$$G(r) \propto \exp(-r/\xi), \tag{1.5}$$

where ξ denotes the correlation length. This phase occurs at any dimensions and for any N at sufficiently high temperatures.

A LRO phase is characterized by a nonvanishing order-parameter expectation value. In accord with the Mermin-Wagner theorem [49], in models with continuous symmetry group [$N > 1$], long-range order at nonzero temperatures can exist only above two dimensions. For $N \leq 1$, finite-temperature LRO persists down to the lower critical dimension $d_c(N)$, which for $N = 1$ takes the value $d_c(1) = 1$. In the $O(N)$ models, the second-order ordered-disordered phase transition is always governed by an isolated critical RG FP and therefore it is always characterized by universal, (d, N)-dependent critical exponents.

A QLRO phase, alike a disordered phase, features a vanishing order parameter, but the corresponding correlation function decays as a power-law of the distance

$$G(r) \propto r^{2-d-\eta}, \tag{1.6}$$

where η is the anomalous dimension. This correlation structure is related to a divergent correlation length and arises when the RG flow converges towards a finite-temperature FP in the infrared limit. In the $O(N)$ models, this phase can be found only in a region of the (d, N) plane delimited by $1 < N \leq 2$ and $d_c(N) \leq d \leq 2$, where $d_c(N)$ is the lower critical dimension. Notably, a QLRO phase can only occur for values of (d, N) for which the finite-temperature LRO is prohibited. The lower critical dimension as a function of N varies smoothly from $d_c(2) = 2$ to $d_c(1) = 1$ and is discussed in detail in Chapter 3.

With the exception of the Kosterlitz-Thouless (KT) transition, the phase transition between QLRO and disordered phases is a continuous phase transition controlled by an isolated critical FP. This again means that the critical exponents are universal. A QLRO phase, except for the KT low-temperature phase, is controlled by an isolated stable RG FP giving rise to the universal anomalous dimension η [and the associated correlation function exponent $d-2+\eta$] of the low-temperature phase which is typically different from the critical anomalous dimension.

1.1.3 Kosterlitz-Thouless transition and topological excitations

One of the most famous universality classes admitting the quasi-long-range order is the Kosterlitz-Thouless UC. In the $O(N)$ models with short-range interactions, it is realized only in a single point $(d, N) = (2, 2)$. This exotic UC is widely recognized for the role of topological excitations in the phase transition and its experimental relevance in the context of the helium superfluid transition, superconductivity, liquid crystals, and melting of two-dimensional solids [6].

For the two-dimensional $O(2)$ model, the β_g^{NLS} of the $2+\epsilon$ expansion vanishes for any value of the coupling g. This means that for every value of g, we find a stable RG FP and an infinite correlation length. The two-point correlation function, as predicted by the $2 + \epsilon$ expansion, is characterized by a power-law decay

$$G(r) \propto r^{-\frac{g}{2\pi}}, \tag{1.7}$$

with the value $\frac{g}{2\pi}$ in Eq. (1.7) describing the temperature dependent anomalous dimension η. These are the defining features of a QLRO phase.

In the nonlinear-σ model, the QLRO phase persists at all temperatures for $(d, N) = (2, 2)$. This is somewhat surprising since one should expect that at high temperatures the model becomes disordered with exponential decay of correlations. Corresponding lattice models show exactly that behavior. The difference between the two arises from vortices. These topological excitations are present in the lattice models but remain absent in the nonlinear-σ model as a vortex core would carry infinite energy.

Kosterlitz and Thouless proposed a resolution of this problem [50], for which they were awarded the 2016 Nobel Prize. They have shown that the $O(2)$ Hamiltonian can be decomposed into two decoupled parts: one describing spin waves and the other describing vortex interactions, which incidentally are identical to that of the two-dimensional Coulomb gas. Based on that observation, they devised the RG recursion relations in terms of the spin-wave coupling g and the vortex fugacity y:

$$\beta_g^{\mathrm{KT}} = 4\pi^3 y^2 + O(y^4), \tag{1.8a}$$

$$\beta_{y^2}^{\mathrm{KT}} = \left(4 - \frac{2\pi}{g}\right) y^2 + O(y^4). \tag{1.8b}$$

These equations admit a line of FPs stretching for all values of g at $y^2 = 0$. The FPs with $0 \leq g < \frac{\pi}{2}$ are attractive and control the low-temperature QLRO phase, while the FPs with $g > \frac{\pi}{2}$ are repulsive. The point $g = \frac{\pi}{2}$, $y^2 = 0$ marks the marginal KT FP controlling the phase transition.

Fig. 1.1 visualizes the RG flows governed by Eqs. (1.8). The flows originating in the shaded region, below the dashed separatrix, converge to the line of FPs. This leads to a finite renormalized coupling g_R and vanishing renormalized fugacity $y_R^2 = 0$. In this QLRO phase, all the vortices bind to each other and their effects can be fully absorbed into a redefinition of the spin-wave coupling g. Due to the Coulomb gas analogy, this phase is sometimes called the insulating phase since all the charged particles [vortices] are bound into neutral molecules. At large length scales, $y \to 0$ and one can apply the nonlinear-σ model analysis to calculate the anomalous dimension $\eta = \frac{g_R}{2\pi}$ [with the renormalized spin-wave coupling]. Most notably, at the FP controlling the KT phase transition the anomalous dimension takes the universal value $\eta_{KT} = \frac{1}{4}$. On the other hand, in the disordered [metallic] phase, large vortex fugacity allows vortices to proliferate freely which leads to the destruction of the QLRO. A detailed derivation of the KT equations and an extensive discussion of this model can be found in [6].

Topological excitations play an important role in phase transitions in many models of the $O(N)$ family besides the two-dimensional XY model. In the three-dimensional XY model, vortex excitations do exist and play a central role in the phase transition, just like in two dimensions. One significant difference between the three- and two-dimensional models is that the vortex cores take the form of strings or loops rather than points. Some MC simulations indicate that suppressing the vortices, in the three-dimensional XY model, inhibits the transition and the model remains ordered at all temperatures [51]. The same conclusion can be reached via an analysis of the nonlinear-σ model. The KT analysis based on the vortex-spin-wave decoupling was generalized to the three-dimensional model [52]. Somewhat surprisingly, this generalization yields quite accurate predictions for the correlation

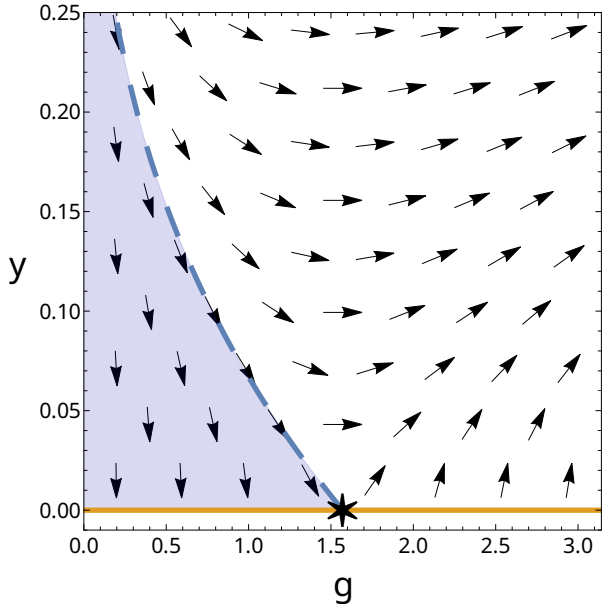

Figure 1.1: RG flows governed by the KT equations 1.8. The orange line marks the line of KT fixed points, the six-pointed star denotes the transition fixed point $g = \frac{\pi}{2}$ and the dashed line denotes a separatrix between the shaded QLRO [insulating] phase and the disordered [metallic] phase.

length exponent ν.

Another interesting example of topological excitations can be found in the three-dimensional Heisenberg model in the form of so-called "hedgehogs". In the Monte Carlo simulations of the Heisenberg model, in which the hedgehog configurations have been artificially suppressed, the phase transition was either completely absent [53] or belonged to a different UC than the three-dimensional $O(3)$ UC [54, 55]. Ref. [55] emphasizes a degree of ambiguity related to how the topological excitations are suppressed, which might explain the differences between various studies. They also claim that the transition in the model with hedgehogs suppressed belongs to the noncompact CP^1 universality class, clearly distinct from the $O(3)$ UC. We are not aware of any further study that supports or disproves this claim.

1.1.4 Cardy-Hamber analysis

In 1977, Nelson and Fisher (NF) extended the Kosterlitz-Thouless equations (1.8) into dimensions $d = 2 + \epsilon$ [56]. It turns out that, for small y^2 and ϵ, it is sufficient to only include the dimension of the coupling g in the function β_g. The modified

equations read:

$$\beta_g^{\mathrm{NF}} = -\epsilon g + 4\pi^3 y^2 + O(y^4), \tag{1.9a}$$

$$\beta_{y^2}^{\mathrm{NF}} = \beta_{y^2}^{\mathrm{KT}} = \left(4 - \frac{2\pi}{g}\right) y^2 + O(y^4). \tag{1.9b}$$

Interestingly, the function β_g^{NF} bears some resemblance to the β_g^{NLS} of the $2+\epsilon$ expansion. Cardy and Hamber (CH) used this observation to construct a unified set of β functions for the $O(N)$ models that captures the second order transitions for $d > 2$ and the KT transition at $(d, N) = (2, 2)$. They proposed:

$$\beta_g^{\mathrm{CH}} = -\epsilon g + (N-2) f(g, N) + 4\pi^3 y^2 + O(y^4), \tag{1.10a}$$

$$\beta_{y^2}^{\mathrm{CH}} = \beta_{y^2}^{\mathrm{KT}} = \left(4 - \frac{2\pi}{g}\right) y^2 + O(y^4). \tag{1.10b}$$

This set of equations reduces to the Nelson-Fisher and Kosterlitz-Thouless equations in the limits $N \to 2$ and $(d, N) \to (2, 2)$ respectively. It also reproduces the β_g^{NLS} function of the $2+\epsilon$ expansion when the vortices are suppressed i.e. when the vortex fugacity vanishes $y^2 \to 0$. It is important to note, that for generic values of (d, N), the Coulomb gas analogy for the vortices breaks down and the physical interpretation of y becomes somewhat ambiguous.

The CH analysis of Eqs. (1.10) is performed in the vicinity of the KT point $(d, N) = (2, 2)$. Therefore $\epsilon = d-2$, $N-2$, and y^2 are all treated as small quantities of the order no higher than $O(\epsilon)$. Importantly, the following reasoning does not require the knowledge of the exact shape of $f(g, N)$, only the assumption that $f(g, 2)/g$ is a monotonic increasing function for small values of g. We introduce a parameter:

$$\Delta = \epsilon \frac{\pi}{2} - (N-2) f\left(\frac{\pi}{2}, N\right) + O(\epsilon^2), \tag{1.11}$$

which determines the existence and stability of the fixed points. In general, equations (1.10) admit two families of nontrivial fixed-point solutions:

$$g_{\mathrm{NF}} = \frac{\pi}{2} + O(\epsilon), \quad y_{\mathrm{NF}}^2 = \frac{\Delta}{4\pi^3}, \tag{1.12}$$

which can be seen as an extension of the FP solution to the Nelson-Fisher Eqs. (1.9) to $N \neq 2$, and

$$\epsilon g_{\mathrm{BZJ}} = (N-2) f(g_{\mathrm{BZJ}}, N) + O(\epsilon^2), \quad y_{\mathrm{BZJ}}^2 = O(\epsilon^2) \tag{1.13}$$

identical to the solution of the $2+\epsilon$ expansion of Brézin and Zinn-Justin (BZJ).

The line $\Delta = 0$, from now on called the CH line, marks the locus of collisions between NF and BZJ fixed-point families. The physics associated with the collision

is quite different depending on whether $d > 2$ or $d < 2$ so the two cases need to be discussed separately. For $d > 2$ and $\Delta > 0$, the NF FP is critical and the BZJ FP is tricritical - it has two unstable perturbations. When Δ crosses zero, the NF FP ceases to be physical as y escapes to the complex domain and the BZJ FP becomes critical. Upon crossing the CH line the critical fixed point changes and the critical exponents are expected to exhibit a nonanalyticity yet remain continuous.

The picture is quite different for $d < 2$. When $\Delta > 0$ the NF FP again serves as a critical fixed point. The BZJ FP, on the other hand, is stable - it has only irrelevant perturbations. This means that the low-temperature behavior is controlled by finite-temperature FP, which leads to quasi-long-range ordering. This important observation has not been made in the original CH paper and mentioned only much later [57] [see also [58]]. For $\Delta < 0$, the NF FP disappears while the BZJ FP becomes arguably nonphysical meaning that no phase transition can occur in this region. This indicates that the lower critical dimension $d_c(N)$ [or conversely $N_c(d)$] can be identified with the CH line below two dimensions. A sketch of the (d, N) plane along with the CH line is presented in Fig. 1.2.

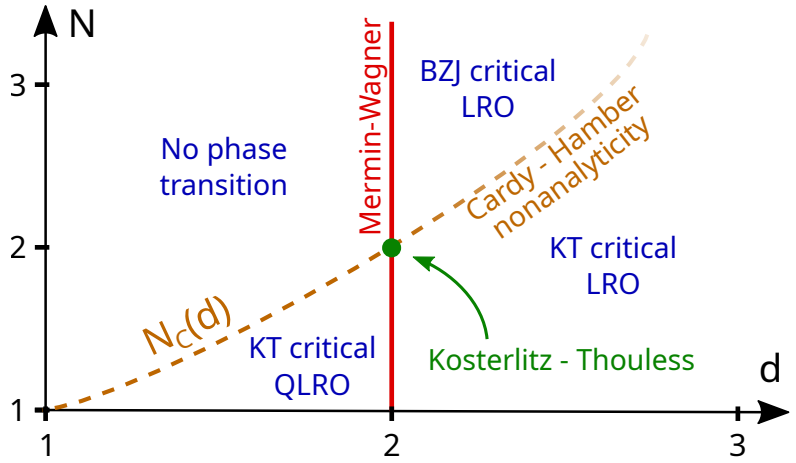

Figure 1.2: Schematic representation of the (d, N) plane in the vicinity of the Kosterlitz-Thouless point $(2, 2)$. The Mermin-Wagner line [$d = 2$, $N > 1$] separates the systems that support the LRO in nonzero temperatures from those that do not. Below two dimensions, for sufficiently small values of N [$N < N_c(d)$] the low-temperature phase is characterized by QLRO, while for $N > N_c(d)$ the system remains disordered for any nonzero temperature. Below two dimensions, the Cardy-Hamber line coincides with $N_c(d)$, while above two dimensions it is a locus of the hypothetical nonanalyticity of the critical exponents predicted within the framework of Ref. [1].

1.1.5 This thesis

In this thesis, we aim to provide a better understanding of the CH scenario for the fixed-point collision. Firstly, we provide a detailed perturbative CH-style analysis and lay out its consequences. In particular, we calculate the critical exponents using the fifth-order β_g^{NLS} function of the $2+\epsilon$ expansion combined with the KT equations in a CH-style reasoning. Subsequently, we compare them with the fixed-point solutions and the associated critical exponents obtained within a nonperturbative framework across the (d, N) plane.

Above two dimensions, we find agreement between the CH-style perturbative predictions and the NPRG results, except for the direct vicinity of the supposed CH line. In this region, we observe no obvious nonanalyticity of the critical exponents. We do observe a pronounced cross-over behavior in the region where the CH line should be located yet only in dimensions not far from two. This indicates some form of smoothed merging of the FP solutions. Moreover, we present arguments to rule out any fixed-point collision within the NPRG approach, except for the dimensions very close to two.

Below two dimensions, our NPRG results align with the CH predictions. We identify both the critical NF FP and the stable BZJ FP and follow them until the lower critical dimension where we observe their collision. Further, we calculate the critical exponents as functions of (d, N) and show a good agreement with the perturbative calculations. We also obtain the correlation function exponent of the QLRO phase - a result never achieved before with any method. Finally, we present the line of lower critical dimensions $d_c(N)$.

1.2 Anisotropic extensions of the $O(N)$ models

In physical systems, the pure $O(N)$ symmetry is oftentimes broken by interactions characterized by a lower-order symmetry. Symmetry-breaking fields or anisotropies can have several effects on the model's behavior ranging from introducing significant corrections to scaling to altering the universal properties or even changing the order of the phase transition. Thus, understanding the response of isotropic fixed points to anisotropic perturbations becomes a very important area of research.

1.2.1 Dangerously irrelevant operators

In the RG theory, the perturbations to a fixed point are classified as either relevant, marginal, or irrelevant. Relevant perturbations increase in magnitude during the RG flow. If the anisotropic perturbation is relevant in the $O(N)$-symmetric FP it implies that either the phase transition becomes first order or there exists an

anisotropic FP that controls the critical phase transition. Marginal perturbations do not change in magnitude upon the RG transformations [up to quadratic terms around the FP] and induce logarithmic corrections to scaling. These are typically associated with a FP collision or the existence of a line of FPs.

The last type of perturbation is called irrelevant. The magnitude of these perturbations decreases with the RG flow. The conventional wisdom dictates that irrelevant operators do not change the universal properties except for inducing additional corrections to scaling and can be neglected sufficiently close to criticality. However, some exceptional couplings break this rule. The irrelevant couplings, which cannot be neglected even very close to criticality are called dangerously irrelevant.

Many prominent examples of dangerously irrelevant couplings can be found in the anisotropic extensions of the $O(N)$ models. Most likely, every irrelevant coupling to the $O(N)$ models characterized by a discrete symmetry group can be classified as dangerously irrelevant for $N \geq 2$ and $2 < d < 4$, as they gap the Goldstone mode. These kinds of models are very much relevant from the experimental point of view, since in real magnetic crystals the spherically symmetric interactions are often supplemented by weak discrete fields reflecting the crystalline symmetry [59].

The effects of the dangerously irrelevant operators due to anisotropies were, to our best knowledge, first addressed by Nelson in Ref. [60]. He argued that the presence of such couplings gives rise to two distinct exponents γ_+ and γ_- controlling divergence of the magnetic susceptibility above and below the critical temperature. Later it was also shown that below T_c such a model exhibits two correlation lengths: ξ - the correlation length of the amplitude mode [similar to that of the pure model] and ξ' connected to the anisotropic field. The latter correlation length ξ' arises due to the instability of the low-temperature Nambu-Goldstone FP with respect to the anisotropic perturbation and indicates the scale at which the order-parameter probability distribution becomes strongly anisotropic.

The correlation length ξ diverges with the exponent ν of the pure model while ξ' diverges with the exponent ν', the value of which depends on the scaling dimension of the anisotropic field y_a. The relation between ν and ν' was addressed in several studies, mostly but not exclusively, based on Monte Carlo methods [61–68]. Recently, there seems to be an agreement on a scaling relation in the form [1]

$$\nu' = \nu \left(1 + \frac{|y_a|}{p}\right), \tag{1.14}$$

with $p = 2$ for classical ferromagnets with irrelevant discrete anisotropies, although it should be noted that Ref. [64] argues for $p = 3$.

[1] Since the considered anisotropic coupling is irrelevant its scaling dimension is negative [$y_a < 0$]. For clarity, y_a is always presented in absolute value $|y_a|$.

In a relatively recent paper, Léonard and Delamotte [65] consider the problem of dangerously irrelevant anisotropies from the perspective of the NPRG. Within that framework, they confirm the scaling relation (1.14) with $p = 2$. Additionally, below the critical temperature, they find two distinct exponents γ_L and γ_T controlling the divergence of longitudinal and transverse susceptibilities respectively. Finally, they derive the scaling relations for the γ exponents:

$$\gamma_+ = \nu(2 - \eta), \tag{1.15a}$$

$$\gamma_T - \gamma_+ = \nu|y_a|, \tag{1.15b}$$

$$\gamma_L - \gamma_+ = \nu|y_a|\frac{4-d}{2}, \tag{1.15c}$$

where Eq. (1.15a) can be recognized as the typical scaling relation derived from the regularity of the correlation function. Although derived specifically for $O(2)$ model with hexagonal anisotropies, Eqs. (1.15) are most likely valid for any irrelevant discrete perturbation to any $O(N)$ model for any $N \geq 2$ in dimensions $2 < d < 4$.

Interestingly, the difference between the high- and the low-temperature exponents becomes more pronounced the more irrelevant the perturbation. This led many MC studies to focus on more irrelevant higher-order anisotropies, e.g. hexagonal rather than cubic, as this makes the separation between length scales ξ and ξ' easier to observe. This might seem counter-intuitive since, typically, the more irrelevant the perturbation the weaker its effects become.

We also note that the relations (1.15) have not been verified with any methods besides the NPRG. It is somewhat surprising that with the exceptions of Refs. [60, 65], to our best knowledge, none of the studies investigating the relation between ν and ν' have addressed the γ exponents of magnetic susceptibility. It would be particularly interesting to see if predictions of Ref. [65] can be confirmed with the MC methodology.

1.2.2 Cubic perturbations in the $O(N)$ models

An anisotropic extension of the $O(N)$ models that received particularly significant attention involves the so-called "cubic interactions". Cubic interactions, as suggested by the name, possess the symmetry of an N-dimensional cube, meaning that they are invariant with respect to the transformations:

$$\phi^i \longleftrightarrow -\phi^i \quad \text{and} \quad \phi^i \longleftrightarrow \phi^j, \tag{1.16}$$

where $i, j \in \{1, 2, \ldots, N\}$ are the order-parameter indices. Like with other discrete anisotropies, it is expected that such interactions might arise in magnetic crystals as a manifestation of the symmetry of either crystalline lattice or cell structure; cubic anisotropies are therefore prevalent in cubic crystals [59].

In three dimensions, the effects of cubic perturbations in the $O(N)$ models, to a large extent, can be understood via the perturbative framework of the $4-\tilde{\epsilon}$ expansion. In this approach, the lowest-order action involving cubic interactions reads:

$$\mathcal{S}_{\phi^4}^{\text{cubic}} = \int d^d x \left\{ \frac{r}{2}\boldsymbol{\phi}^2(\boldsymbol{x}) + \frac{u}{4!}\left[\sum_{i=1}^{N}\phi^i(\boldsymbol{x})^2\right]^2 + \frac{v}{4!}\sum_{i=1}^{N}\phi^i(\boldsymbol{x})^4 + \frac{1}{2}\left[\partial_\mu \boldsymbol{\phi}(\boldsymbol{x})\right]^2 \right\}, \tag{1.17}$$

where u is the isotropic quartic coupling and v describes the strength of the anisotropic interaction. Note that cubic symmetry admits a unique quadratic term $\boldsymbol{\phi}^2$ which is also characterized by the $O(N)$ symmetry. The lowest-order cubic term which is not $O(N)$-symmetric is the quartic $\sum_{i=1}^{N}\phi^i(\boldsymbol{x})^4$ term.

The upper critical dimension of the models characterized by the action (1.17) is equal to four [$d_{\text{uc}} = 4$], similarly to the isotropic variant [$v = 0$]. Close to the upper critical dimension, one can formulate the perturbative expansion around the Gaussian FP [10, 69]. In this case, the perturbative framework involves two β functions expanded simultaneously in 3 variables: $\tilde{\epsilon} = 4 - d$, $u = O(\tilde{\epsilon})$, and $v = O(\tilde{\epsilon})$. To the leading order, the RG equations read:

$$\beta_u^{\phi^4} = -\tilde{\epsilon}u + \frac{1}{8\pi^2}\left(\frac{N+8}{6}u^2 + uv\right), \tag{1.18a}$$

$$\beta_v^{\phi^4} = -\tilde{\epsilon}v + \frac{1}{8\pi^2}\left(2uv + \frac{3}{2}v^2\right). \tag{1.18b}$$

Below four dimensions, these β functions admit four distinct fixed-point solutions:

$$\text{Gaussian FP:} \qquad u_{\text{G}} = 0, \qquad v_{\text{G}} = 0, \tag{1.19a}$$

$$\text{Decoupled Ising FP:} \qquad u_{\text{I}} = 0, \qquad v_{\text{I}} = \frac{16\pi^2\tilde{\epsilon}}{3}, \tag{1.19b}$$

$$O(N)\text{-symmetric FP:} \qquad u_{O(N)} = \frac{48\pi^2\tilde{\epsilon}}{N+8}, \quad v_{O(N)} = 0, \tag{1.19c}$$

$$\text{Cubic FP:} \qquad u_{\text{C}} = \frac{16\pi^2\tilde{\epsilon}}{N}, \qquad v_{\text{C}} = \frac{16\pi^2(N-4)\tilde{\epsilon}}{3N}. \tag{1.19d}$$

The name of the decoupled Ising FP comes from the fact that for $u = 0$, the action (1.17) decouples into N copies of the Ising model. The decoupled Ising FP is tricritical below four dimensions and shares most universal properties of the Ising UC. Interestingly, the decoupled Ising FP, to our best knowledge, has never been identified in lattice models and its domain of attraction outside of the field-theoretic framework remains unclear.

Both the $O(N)$-symmetric and the cubic FPs can be either critical or tricritical depending on d and N. The function $\bar{N}_c(d)$ describes the line in the (d, N) plane where these two FPs collide and swap roles as the operator associated with the cubic symmetry becomes marginal. For $N < \bar{N}_c(d)$ the isotropic FP is critical and the cubic FP tricritical and vice versa for $N > \bar{N}_c(d)$. The schematic RG flows between the four FPs are presented in Fig. 1.3.

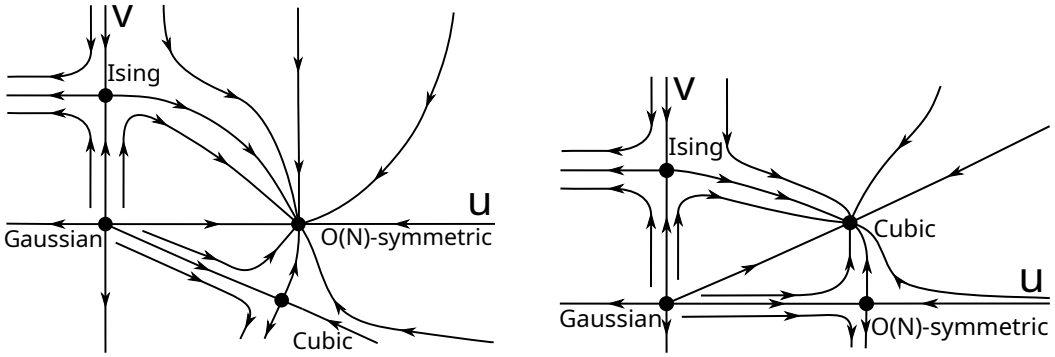

(a) $N < \bar{N}_c(d)$ (b) $N > \bar{N}_c(d)$

Figure 1.3: Schematic representation of the RG flows of the $O(N)$ models with cubic anisotropies in the (u, v) plane in dimensions $2 < d < 4$ [70].

Although the line $\bar{N}_c(d)$ has been a subject of studies for over 40 years, not much is known about its exact shape. Until very recently the value of $\bar{N}_c(3)$ remained elusive, with early estimates ranging between 2.3 and 3.38 [70]. Crucially, there was a disagreement about whether $\bar{N}_c(3)$ is larger or smaller than three. In other words, it was unclear whether the isotropic FP of the three-dimensional Heisenberg model is stable with respect to cubic anisotropy and therefore controls the critical behavior of realistic magnetic crystals with cubic symmetry. This question was apparently resolved by a conformal bootstrap study [71]. It shows that for $N = d = 3$, the cubic anisotropy is relevant at the isotropic FP and consequently $\bar{N}_c(3) < 3$. This agrees with the most recent $4 - \tilde{\epsilon}$ expansion results [70, 72] and was later corroborated by the Monte Carlo calculations [73].

The value of $\bar{N}_c(2)$ remains somewhat unclear. It is sometimes stated that the line $\bar{N}_c(d)$ crosses the point $(d, N) = (2, 2)$ [4, 70, 74]. This statement is based on the fact that the cubic anisotropy is marginal with respect to the FP controlling the Kosterlitz-Thouless transition [75, 76]. There exists, however, quite a simple argument claiming that $\bar{N}_c(d)$ has to be strictly larger than two. To our best knowledge, this reasoning has been first fully articulated in Ref. [71], although parts of it can be found much earlier [see e.g. Ref. [70]].

The case $N = 2$ is quite unique among $O(N)$ models with cubic perturbations, as it possesses a symmetry between the decoupled Ising and the cubic FPs absent

for generic N. For any integer N, the minima of the cubic action (1.17) are 2^N-fold degenerate for $v > 0$ - pointing to the vertices of N-dimensional hypercube, and $2N$-fold degenerate for $v < 0$ - pointing to the faces of the hypercube. For $N = 2$, action minima are 4-fold degenerate both for $v > 0$ and $v < 0$. Under a $\frac{\pi}{4}$ rotation:

$$(\phi_1, \phi_2) \longmapsto \frac{1}{\sqrt{2}} (\phi_1 + \phi_2,\ \phi_1 - \phi_2)\,. \tag{1.20}$$

the minima of the action map onto the maxima and vice versa. Moreover, this transformation preserves the form of the action (1.17) with a redefinition of the quartic couplings:

$$u' = u + \frac{3}{2}v, \quad v' = -v. \tag{1.21}$$

Such mapping can exist only for $N = 2$ due to the same degree of minima degeneracy.

Importantly, the rotation (1.20) interchanges the cubic and the decoupled Ising FPs, which means that the two FPs share all critical exponents. Moreover, the symmetry between the two FPs requires that a collision between the cubic and the $O(N)$-symmetric FPs is also a collision with the Ising FP. Such a collision, however, can occur only at the Gaussian FP where the four FP families (1.19) intersect, which happens only in the upper critical dimension. Moreover, the decoupled Ising FP and the cubic FP were found isolated from the KT line of fixed points in the two-dimensional $O(2)$ model with cubic anisotropies [77]. Therefore, the collision between the cubic and the $O(N)$-symmetric FPs most likely does not take place for $N = 2$ below four dimensions. This implies that $\bar{N}_c(d)$ should be strictly larger than two in any dimension.

1.2.3 Cubic perturbations in the two-dimensional $O(2)$ model

As discussed in Sec. 1.1.3, the long-range order cannot survive in the two-dimensional $O(2)$ model at finite temperatures due to the Mermin-Wagner theorem [49]. Despite that, the model still admits a phase transition - the vortex unbinding KT transition between a disordered phase and a QLRO phase. The situation changes when we consider symmetry-breaking interactions such as cubic anisotropies. The explicit $O(2) \to \mathbb{Z}_4$ symmetry-breaking allows for the formation of the LRO, which leads to a question of the stability of the QLRO in the presence of weak discrete perturbations.

This topic was addressed in the seminal paper by José et al. [75]. Working with the generalized Villain model and employing brilliant duality relations, they devised the RG equations for the $O(2)$ universality class with $\mathbb{Z}_q$-symmetric perturbations for any integer $q > 1$. Here, we will focus only on $q = 4$ describing

the cubic perturbations. The recursion relations derived by José et al. describe RG flow of three couplings: g - the spin-wave coupling, y_0 - related to the vortex fugacity and y_4 - the $\mathbb{Z}_4$-symmetric anisotropic field. The proposed RG equations read:

$$\beta_g = 2\pi^3 y_0^2 \exp\left(-\frac{\pi^2}{g}\right) - 8\pi g^2 y_4^2 \exp\left(-4g\right), \tag{1.22a}$$

$$\beta_{y_0} = \left(\frac{\pi}{2} - g\right)\left(\frac{-2}{g}\right) y_0. \tag{1.22b}$$

$$\beta_{y_4} = \left(\frac{\pi}{2} - g\right)\frac{4}{\pi} y_4. \tag{1.22c}$$

When the anisotropy vanishes [$y_4 = 0$], Eqs. (1.22) reduce to the KT recursion relations (1.8) after the substitution $y^2 = y_0^2 \exp(-\pi^2/g)$. We note that these equations are valid only to the leading order in y_0 and y_4.

Eqs. (1.22) admit two lines of fixed points:

$$\text{Isotropic KT FPs:} \quad g \in [0, +\infty[, \qquad y_0 = y_4 = 0, \tag{1.23a}$$

$$\text{Anisotropic FPs:} \quad g = \frac{\pi}{2} + O(y_4^2, y_0^2), \quad y_4 = \pm y_0, \tag{1.23b}$$

intersecting at the point of the KT transition $g = \frac{\pi}{2}$, $y_0 = y_4 = 0$. The eigenvalue analysis shows, that the cubic perturbation is relevant at the isotropic FPs below the KT transition point [$g < \frac{\pi}{2}$] and irrelevant above [$g > \frac{\pi}{2}$]. This means that the KT QLRO phase is unstable towards arbitrarily weak $\mathbb{Z}_4$-symmetric fields in favor of the LRO. The phase diagram deduced by José et al. is presented in Fig. 1.4.

The existence of the anisotropic line of FPs and the associated nonuniversality of the critical exponents have been confirmed by later studies using either fixed-dimension perturbative expansion [74] or MC methods [78]. However, the MC based Ref. [79] raises some questions about the correspondence between the lattice models used in MC simulations and the generalized Villain model employed by José et al. The authors of Ref. [79] report a "bubble" of the KT QLRO phase present in the phase diagram of the XY model for weak $\mathbb{Z}_4$-symmetric fields. This stands in contrast to the claims of José et al. that the QLRO phase can occur only when the cubic field vanishes [see Fig. 1.4].

This disagreement was apparently resolved in Ref. [77]. They show that for weak anisotropic fields, one observes a cross-over between KT-like and critical behaviors. The length scale associated with this cross-over diverges very quickly with the diminishing strength of the anisotropic field. It is postulated that for weak anisotropic fields, the cross-over scale is already beyond the reach of the MC simulations which might give rise to an apparent presence of the KT QLRO phase.

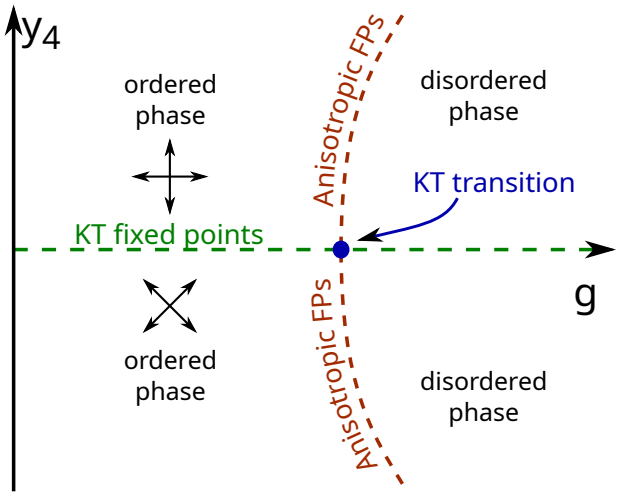

Figure 1.4: Projection of the phase diagram of the two-dimensional $O(2)$ model with cubic perturbations onto the (g, y_4) plane according to Ref. [75]. The second-order order-disorder phase transitions are controlled by the anisotropic FPs. The KT QLRO phase is confined to a line $y_4 = 0$.

There have been many attempts at experimental verification of the picture presented by Ref. [75]. Taroni et al. [80] present an exhaustive overview of experimental studies of phase transitions in two-dimensional materials attributed to a wide variety of universality classes ranging from 3- and 4-states Potts to Ising, XY, and XY with cubic anisotropies (XY+$\mathbb{Z}_4$). They collect and analyze the distribution of the reported values of the β exponent, controlling the behavior of the order parameter near the transition.

Taroni et al. show that the experimental values for the β exponent cover a wide range from roughly 0.1 up to 0.25 which they call a "universal window". The presented distribution of the β exponent is bimodal with strong peaks at $\beta \approx 0.12$ and $\beta \approx 0.23$. The former peak is interpreted as related to the two-dimensional Ising universality class. Importantly, it is argued that materials of the XY+$\mathbb{Z}_4$ UC can display scaling similar to that of the Ising UC for sufficiently strong anisotropies.

The presence of the latter peak is even more interesting. It has been shown that the pure two-dimensional XY model is subject to very strong finite-size effects. In the QLRO phase, the magnetization vanishes as slowly as

$$\langle m \rangle \sim L^{-\frac{1}{8\pi K_R}}, \tag{1.24}$$

where L denotes the linear extent of the system and K_R is the renormalized spin-wave stiffness taking values larger than $K_R \geq \frac{2}{\pi}$ [81, 82]. The small value of the exponent in Eq. (1.24) means that finite-size effects remain very much relevant even

in the macroscopic systems. Interestingly, the magnetization near the transition temperature in finite systems [to some extent] seems to follow a power-law with an effective exponent $\beta_{\text{eff}} \approx 0.23$ [82–84]. Even more surprising is the fact that this effective exponent seems to take a universal value. Taroni et al. interpret the second peak of the β exponent distribution as a manifestation of that finite-size effect.

One more important point raised in Ref. [80] is that the theory of José et al. predicts that the β exponent should diverge as $\beta \sim y_4^{-1}$ and therefore its distribution is presumably unbounded. The experimental data, however, remains strangely confined to the small universal window. Taroni et al. argue that the apparent contradiction might arise due to the presence of strong finite-size effects. As the true exponent β describing the magnetization in the thermodynamic limit increases, the importance of the finite-size corrections magnifies rapidly. It is thus conceivable, that in the experiments the finite-size effects overshadow the true β exponent of the XY+$\mathbb{Z}_4$ UC and that the observed scaling is related to the effective finite-size exponent.

1.2.4 This thesis

In this thesis, we employ the nonperturbative renormalization to offer a new perspective on the $O(2)$ model with cubic anisotropies. We begin by addressing the three-dimensional model for which, so far, the NPRG estimates for the scaling dimensions were quite far off compared to the values obtained by most other methods. We identify the problem lying in the previous approaches and offer an estimate standing in agreement with most estimates given in the literature.

Subsequently, we continuously lower the dimension and observe how the scaling dimensions of several dominant operators evolve between three and two dimensions. In this manner, we observe that the dominant cubic perturbation changes its character from irrelevant to marginal as the dimension approaches two.

Chapter 2

Nonperturbative Renormalization Group

So, so you think you can tell
Heaven from hell?
Blue skies from pain?
Can you tell a green field
From a cold steel rail?

Pink Floyd, *Wish you were here*

In the introduction, we outlined the major perturbative renormalization group (RG) schemes and emphasized their undeniable impact on the fields of statistical and high-energy physics. These methods, however, are not without their pitfalls, calling for the development of an alternative approach. The idea of formulating a renormalization group approach not relying on any sort of perturbative expansion is not a new one. In fact, it can be traced as far back as the 1970s to the exact RG scheme proposed by Wilson and Kogut [85]. They derived an exact RG equation governing the flow of interactions based on the idea of gradually integrating out the degrees of freedom in the momentum space. In the following years, several alternative exact approaches have been formulated, including the Wegner-Houghton differential generator [86] and the Wilson-Polchinski (WP) approach [87].

However, for around 20 years the nonperturbative renormalization group (NPRG) methods have seen limited use. Some approximate schemes have been developed to provide descriptions of wetting [88, 89] and unbinding transitions [90]. However, for bulk critical phenomena those early approaches were quite inaccurate when compared to popular methods such as perturbative RG and Monte Carlo [91–94], except for the exact results obtained mostly in the perturbative regimes [45, 85, 86, 95]. The main problem of the early NPRG methods was that the exact

equations were almost always insoluble, while the approximation schemes were not well-supported and were often seen as uncontrolled. Moreover, the perturbative RG methods were tremendously successful at the time and the NPRG techniques often seemed unnecessary.

A sort of revival of Wilson's idea came about in the 1990s in the form of the so-called effective average action approach, also known as the Morris-Wetterich (MW) approach. This method, put forward independently by Wetterich [46], Morris [47], and Bonini et al. [96], describes the flow of the effective average action Γ_k [the generator of the infrared (IR) cutoff vertex functions]. This stands in contrast with the WP approach, which describes the flow of the generator of the IR-cutoff connected correlation functions W_k. A priori, it is not obvious why this change should make a difference. After all, both the MW equation and the WP equation are exact, they describe the same underlying physics, and both are analytically insoluble. However, judging by the significant attention the MW equation has recently attracted, it seems to be a significantly more practical method than the WP approach. Over the last 30 years, the NPRG methods have been developing rapidly and have been employed in many fields of modern physics ranging from statistical mechanics and quantum many-body physics to gravity and high-energy physics [7, 97–99].

Throughout this chapter, we explain the methodology of the effective average action approach to the NPRG employed in this thesis. In Sec. 2.1 we define the effective average action and derive the Morris-Wetterich equation governing its RG flow. Sec. 2.2 introduces the approximation scheme of the derivative expansion and explains how the RG-flow equations are derived. In Sec. 2.3, we discuss the role of the infrared regulator. We introduce the most common choices for this function, and how to reduce the dependence of the estimates of the physical quantities on the spurious parameters introduced by the regulator choice. Further, we discuss the topics of convergence of the derivative expansions and the techniques for error bar estimation. Finally, in Sec. 2.4, we discuss specific applications of the derivative expansion and the challenges involved therein. We show, how the derivative expansion can be used to capture the Kosterlitz-Thouless (KT) transition, the difficulties appearing in the studies of the low-temperature phase, and the methodological modifications required in the studies of the anisotropic models.

2.1 Effective Average Action

The effective average action approach follows Wilson's idea of gradually integrating out the degrees of freedom. For a given momentum scale k, the order-parameter degrees of freedom are divided into the rapid, "active" modes [with momentum $|\boldsymbol{q}| \gg k$] and the slow, "frozen" modes [with momentum $|\boldsymbol{q}| \ll k$]. The thermal

fluctuations of the frozen modes are suppressed, while the fluctuations of the active modes are taken into account. In this picture, the RG flow takes the form of "gradually activating" the modes within a shell $k \approx |\boldsymbol{q}|$. This is implemented by introducing a family of functionals $\Gamma_k[\phi]$ called the effective average action. At the ultraviolet (UV) scale $k = \Lambda$, the effective action takes the form of the microscopic action. As the scale shifts down towards IR limit $k \to 0$, progressively all fluctuations become accounted for and the effective action approaches the Gibbs free energy.

To define Γ_k, we first introduce the scale-dependent IR-cutoff partition function:

$$\mathcal{Z}_k[h] = \int \mathcal{D}\varphi \exp\left\{-\mathcal{S}[\varphi] - \mathcal{R}_k[\varphi] + \int_{\boldsymbol{q}} \varphi_{\boldsymbol{q}} h_{-\boldsymbol{q}}\right\}, \tag{2.1}$$

where $\mathcal{S}[\varphi]$ is the microscopic action of the scalar order parameter φ and $\mathcal{R}_k[\varphi]$ is the IR regulating term responsible for damping the fluctuations of the frozen modes. The proper choice of $\mathcal{R}_k$ is central to this scheme. We want the IR-regulating term to be a quadratic functional of the field that provides a large [or infinite] mass to the slow modes, leaving the rapid modes essentially unchanged. For an arbitrary field φ, we define:

$$\mathcal{R}_k[\varphi] := \frac{1}{2}\int_{\boldsymbol{q}} R_k(\boldsymbol{q}^2)\varphi_{\boldsymbol{q}}\varphi_{-\boldsymbol{q}}, \tag{2.2}$$

where R is the IR regulator function, on which we impose two essential requirements: $R_k(\boldsymbol{q}^2 \ll k^2) \gg \boldsymbol{q}^2$ and $R_k(\boldsymbol{q}^2 \gg k^2) \ll \boldsymbol{q}^2$. In practice, it is often convenient to choose a large, but finite mass $R_k(\boldsymbol{q}^2 \ll k^2) \propto Z_k k^2$ with Z_k denoting the order-parameter renormalization factor which we shall define later. Such a choice secures two important limits:

- In the UV limit, $R_\Lambda(\boldsymbol{q}^2) \gg \boldsymbol{q}^2$ for any $\boldsymbol{q}$; the regulator provides large mass to all the modes and effectively freezes all order-parameter fluctuations and the scale-dependent effective function takes the bare value [up to an additive factor].

- In the IR limit, $\lim_{k\to 0} R_k(\boldsymbol{q}^2) \to 0$ for any $\boldsymbol{q}$; all fluctuations are restored and the scale-dependent partition function reaches the exact value.

In the exact treatment, the universal quantities should not depend on the choice of the regulator function. This, however, is no longer true when approximations are performed. We relegate the discussion of the regulator dependence and the typical choices of regulators to Sec. 2.2, where we discuss our approximation scheme.

We now define the IR-cutoff Helmholtz free energy $W_k[h] = \log(\mathcal{Z}_k[h])$[1]. The effective average action is its Legendre transform with a subtracted regulator term:

$$\Gamma_k[\phi] + W_k[h] = \int_{\boldsymbol{q}} \phi_{\boldsymbol{q}} h_{-\boldsymbol{q}} - \mathcal{R}_k[\phi], \tag{2.3}$$

with

$$\phi_{\boldsymbol{q}} = \frac{\delta W_k[h]}{\delta h_{-\boldsymbol{q}}} \quad \text{and} \quad h_{\boldsymbol{q}} = \frac{\delta \Gamma_k[\phi]}{\delta \phi_{-\boldsymbol{q}}} + R_k(\boldsymbol{q}^2)\phi_{\boldsymbol{q}}. \tag{2.4}$$

We emphasize a distinction between the fields φ and ϕ. The former is the fluctuating order parameter and the functional integration variable in Eq. (2.1). The latter, on the other hand, is the IR-cutoff thermal average of the order parameter and an argument of Γ_k.

Having defined Γ_k we again inspect the IR and UV limits. Recovering the IR limit is straightforward since all the regulator terms vanish identically. $W_0[h]$ is by definition the Helmholtz free energy, and $\Gamma_0[\phi]$ its Legendre transform - the Gibbs free energy. Calculating the UV limit, however, is somewhat more involved. Let us take the definition of $h_{\boldsymbol{q}}$ from Eq. (2.4) and insert it into Eq. (2.3). We find:

$$-\Gamma_k[\phi] = W_k[h(\phi)] - \mathcal{R}_k[\phi] - \int_{\boldsymbol{q}} \frac{\delta \Gamma_k[\phi]}{\delta \phi_{\boldsymbol{q}}} \phi_{\boldsymbol{q}}. \tag{2.5}$$

We subsequently exponentiate both sides and substitute $\exp(W_k[h]) = \mathcal{Z}_k[h]$ from Eq. (2.1) to obtain:

$$\begin{aligned} \exp(-\Gamma_k[\phi]) = &\exp\left\{-\mathcal{R}_k[\phi] - \int_{\boldsymbol{q}} \frac{\delta \Gamma_k[\phi]}{\delta \phi_{\boldsymbol{q}}} \phi_{\boldsymbol{q}}\right\} \times \\ &\int \mathcal{D}\varphi \exp\left\{-\mathcal{S}[\varphi] - \mathcal{R}_k[\varphi] + \int_{\boldsymbol{q}} \left[\frac{\delta \Gamma_k[\phi]}{\delta \phi_{\boldsymbol{q}}} \varphi_{\boldsymbol{q}} + R_k(\boldsymbol{q}^2)\varphi_{\boldsymbol{q}}\phi_{-\boldsymbol{q}}\right]\right\}. \end{aligned} \tag{2.6}$$

With a shift of the integration variable $\Delta = \varphi - \phi$, Eq. (2.6) can be further reorganized into:

$$\exp(-\Gamma_k[\phi]) = \int \mathcal{D}\Delta \exp\left\{-\mathcal{S}[\phi + \Delta] - \mathcal{R}_k[\Delta] + \int_{\boldsymbol{q}} \frac{\delta \Gamma_k[\phi]}{\delta \phi_{\boldsymbol{q}}} \Delta_{\boldsymbol{q}}\right\}. \tag{2.7}$$

In the UV limit, the regulator function diverges [or almost diverges] for any $\boldsymbol{q}$ sharpening the regulator term $\mathcal{R}_k[\Delta]$ to [almost] a functional Dirac delta function $\delta[\Delta]$. This means that, in the UV limit, the effective action is [almost] equal to the microscopic action up to an additive constant $\Gamma_\Lambda[\phi] \simeq \mathcal{S}[\phi] + C$. The equality becomes exact if the regulator truly diverges $R_\Lambda(\boldsymbol{q}^2) = \infty$.

[1] Up to a $-k_B T$ factor which plays no role in what follows.

At this point, it becomes obvious why the regulator term $\mathcal{R}_k[\phi]$ had to be subtracted in the definition of Γ_k [see Eq. (2.3)]. In the UV limit, $\mathcal{R}_k[\phi]$ does not vanish; on the contrary - it becomes very large. Had it not been subtracted we would not have recovered the [approximate] equality $\Gamma_\Lambda[\phi] \simeq \mathcal{S}[\phi] + C$ in the UV limit.

2.1.1 Morris-Wetterich Equation

The essential role in any RG scheme is played by the flow equations or the so-called β functions. The flow equation for the effective average action Γ_k can be quite straightforwardly derived following the steps presented e.g. in Ref. [100]. We first act with the derivative with respect to scale $(k\partial_k|_h)$ on the IR-cutoff Helmholtz free energy to find:

$$\begin{aligned} k\partial_k|_h W_k[h] &= \frac{-1}{2\mathcal{Z}_k[h]} \int \mathcal{D}\varphi \left(\int_{\boldsymbol{q}} k\partial_k R_k(\boldsymbol{q}^2)\varphi_{\boldsymbol{q}}\varphi_{-\boldsymbol{q}} \right) \times \\ &\qquad \exp\left\{ -\mathcal{S}[\varphi] - \mathcal{R}_k[\varphi] + \int_{\boldsymbol{q}} \varphi_{\boldsymbol{q}} h_{-\boldsymbol{q}} \right\} \\ &= \frac{-1}{2\mathcal{Z}_k[h]} \left(\int_{\boldsymbol{q},\boldsymbol{p}} k\partial_k R_k(\boldsymbol{q}^2) \frac{\delta^2}{\delta h_{\boldsymbol{p}} \delta h_{\boldsymbol{q}}} \right) \mathcal{Z}_k[h] \\ &= \frac{-1}{2} \int_{\boldsymbol{q},\boldsymbol{p}} \dot{R}_k(\boldsymbol{q}^2) \delta\left(\boldsymbol{p}+\boldsymbol{q}\right) \left(\frac{\delta^2 W_k[h]}{\delta h_{\boldsymbol{p}} \delta h_{\boldsymbol{q}}} - \frac{\delta W_k[h]}{\delta h_{\boldsymbol{p}}} \frac{\delta W_k[h]}{\delta h_{\boldsymbol{q}}} \right), \end{aligned} \tag{2.8}$$

where we introduced $\dot{R}_k(\boldsymbol{q}^2) := k\partial_k R_k(\boldsymbol{q}^2)$. Since $W_k[h]$ is the Legendre transform of $\Gamma_k[\phi] + \mathcal{R}_k[\phi]$ we have:

$$\frac{\delta W_k[h]}{\delta h_{\boldsymbol{q}}} = \phi_{-\boldsymbol{q}} \quad \text{and} \quad \int_{\boldsymbol{r}} \left[\frac{\delta^2 W_k[h]}{\delta h_{\boldsymbol{p}} \delta h_{\boldsymbol{r}}} \right] \left[\frac{\delta^2 \Gamma_k[\phi]}{\delta \phi_{\boldsymbol{r}} \delta \phi_{\boldsymbol{q}}} + \delta(\boldsymbol{r}+\boldsymbol{q}) R_k(\boldsymbol{q}^2) \right] = \delta(\boldsymbol{p}+\boldsymbol{q}). \tag{2.9}$$

With these observations, we can rewrite the flow equation for W_k as:

$$k\partial_k|_h W_k[h] = -\frac{1}{2} \int_{\boldsymbol{q}} \dot{R}_k(\boldsymbol{q}^2) \left[\left(\Gamma_k^{(2)} + R_k \right)^{-1}_{\boldsymbol{q},-\boldsymbol{q}} - \phi_{\boldsymbol{q}} \phi_{-\boldsymbol{q}} \right], \tag{2.10}$$

where $\Gamma_k^{(2)}$ is the second functional derivative of Γ_k and the inverse is understood in the operator sense.

To obtain the flow equation for the effective average action we act with the $(k\partial_k|_h)$ operator on the Legendre transform equation (2.3). We find:

$$k\partial_k|_h \left(\Gamma_k[\phi] + W_k[h] \right) = \int_{\boldsymbol{q}} \left[\left(h_{\boldsymbol{q}} - R_k(\boldsymbol{q}^2)\phi_{\boldsymbol{q}} \right) \left(k\partial_k|_h \phi_{-\boldsymbol{q}} \right) - \frac{1}{2} \dot{R}_k(\boldsymbol{q}^2) \phi_{\boldsymbol{q}} \phi_{-\boldsymbol{q}} \right]. \tag{2.11}$$

After substitution of the flow of $W_k[h]$ from Eq. (2.10), Eq. (2.11) becomes:

$$k\partial_k|_h\,\Gamma_k[\phi] = \frac{1}{2}\int_{\boldsymbol{q}} \dot{R}_k(\boldsymbol{q}^2)\left(\Gamma_k^{(2)} + R_k\right)^{-1}_{\boldsymbol{q},-\boldsymbol{q}} + \int_{\boldsymbol{q}} \left(h_{\boldsymbol{q}} - R_k(\boldsymbol{q}^2)\phi_{\boldsymbol{q}}\right)\left(k\partial_k|_h\,\phi_{-\boldsymbol{q}}\right). \tag{2.12}$$

The differentiation with respect to scale in Eq. (2.12) is taken keeping the source h fixed. We need to change the variables so that the derivative is taken keeping the order parameter ϕ fixed. On the left-hand side of Eq. (2.12), we perform the replacement:

$$k\partial_k|_h\,\Gamma_k[\phi] = k\partial_k|_m\,\Gamma_k[\phi] + \int_{\boldsymbol{q}} \left(k\partial_k|_h\,\phi_{-\boldsymbol{q}}\right)\frac{\delta\Gamma_k[\phi]}{\delta\phi_{-\boldsymbol{q}}}. \tag{2.13}$$

Recalling the value of $\frac{\delta\Gamma_k[\phi]}{\delta\phi_{-\boldsymbol{q}}}$ from Eq. (2.4) we get a cancellation that simplifies Eq. (2.12) to:

$$k\partial_k\Gamma_k[\phi] = \frac{1}{2}\int_{\boldsymbol{q}} \dot{R}_k(\boldsymbol{q}^2)\left(\Gamma_k^{(2)} + R_k\right)^{-1}_{\boldsymbol{q},-\boldsymbol{q}}. \tag{2.14}$$

Equation (2.14) known as the MW equation was independently derived in Refs. [46, 96, 101].

The derivation presented above was specific to a single-component scalar field theory. It can, however, be easily generalized. The main modifications lies in the way the regulator term $\mathcal{R}_k$ is constructed [see Eq. (2.2)] and how it relates to the derivatives with respect to sources [see Eq. (2.8)]. For example, in theories of N-component real scalar fields, with which we work in this thesis, the proper regulator term takes the form:

$$\mathcal{R}_k[\boldsymbol{\phi}] := \frac{1}{2}\int_{\boldsymbol{q}} R_k(\boldsymbol{q}^2)\sum_{i=1}^{N}\phi^i_{\boldsymbol{q}}\phi^i_{-\boldsymbol{q}}. \tag{2.15}$$

This requires that in Eq. (2.8) [and all subsequent steps] the indices of the field are traced over. The more general form of the Morris-Wetterich equation reads:

$$k\partial_k\Gamma_k = \frac{1}{2}\mathrm{Tr}\left\{\dot{R}_k\left(\Gamma_k^{(2)} + R_k\right)^{-1}\right\}, \tag{2.16}$$

with the trace operator involving integration over internal momenta and summation over internal indices.

Among other NPRG schemes, the MW equation is distinguished by several properties that make it a convenient basis for approximations not relying on perturbation theory. These include:

- **One-loop structure** - the trace in the MW equation always involves only a single momentum integral. Moreover, one can often take advantage of the rotational invariance to reduce this single integral to a one-dimensional integral, which greatly simplifies the calculation complexity. A diagrammatic representation of Eq. (2.16) is shown in Fig. 2.1.

- **One-Particle Irreducible (1PI) structure** - only the 1PI diagrams contribute to the flow equations for the effective action as well as for all the vertex functions.

- **Decoupling of short- and long-range physics** - thanks to the regulator term $\dot{R}_k$ in the MW equation only momenta $q \lesssim k$ contribute to the flow at any scale k. This ensures that the RG flow is regular and does not suffer from UV divergences.

- **Infrared regularity** - at any finite scale k the infrared regulator R_k provides the order parameter with a finite mass. In this way, the theory is safe from IR divergences. At the same time, the singularities of Γ_k, expected when studying phase transitions, appear only in the limit $k \to 0$. At finite scales, however, Γ_k remains regular which allows for the development of approximation schemes based on the series expansion of the effective action.

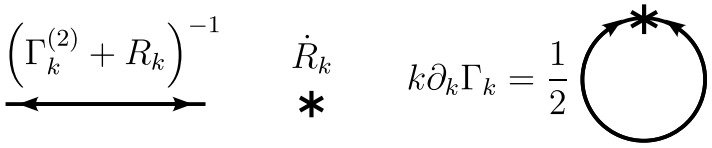

Figure 2.1: Diagrammatic representation of the Morris-Wetterich equation (2.16). The continuous lines with arrows denote the "dressed propagator" $\left(\Gamma_k^{(2)} + R_k\right)^{-1}$ and the asterisks denote the scale derivative of the regulator $\dot{R}_k$.

The Morris-Wetterich equation has provided a fertile ground for research in statistical physics and far beyond. It has been used in quantum theories involving both bosons and fermions, as well as gauge theories and even gravity. A wide range of applications of the MW equation based NPRG is thoroughly discussed in Ref. [99].

2.2 Derivative Expansion

The MW equation is exact but seldom can it be solved analytically. Thus, it requires an approximation scheme. The common approximations for the NPRG

rely on imposing some parametrization on the effective action Γ_k and solving the MW equation in the restricted functional space. One such approach called the derivative expansion (DE), relies on the observations of the previous section.

Let us recall that the structure of the MW equation ensures that at any given scale only the slow modes [$q \lesssim k$] contribute to the flow. Thus, when developing an approximation scheme, we mostly focus on the low-momentum structure of the vertex functions. This is the essential idea behind the derivative expansion; it is an expansion of the effective action [and consequently the vertex functions] in the momentum of the order-parameter modes. One expects such an expansion to be well-behaved as long as Γ_k is regular. Conveniently, thanks to the presence of the IR regulator, regularity of Γ_k is secured at any finite scale k.

In practice, the DE is performed by imposing a specific ansatz on Γ_k including terms with no more than a specified number of differential operators $\partial_\mu = \frac{\partial}{\partial x^\mu}$ acting on the order parameter. The form of the ansatz differs between models since at any given order one should include all the symmetry-allowed terms. As an example, we present the most general ansätze for the three leading orders of the DE for the $O(N)$ models with generic N:

$$\Gamma_k^{\mathrm{LPA}} = \int_{\boldsymbol{x}} \left\{ U(\rho) + \frac{1}{2} \left(\partial_\mu \phi^i\right)^2 \right\}, \tag{2.17a}$$

$$\Gamma_k^{\partial^2} = \int_{\boldsymbol{x}} \left\{ U(\rho) + \frac{Z_\pi(\rho)}{2} \left(\partial_\mu \phi^i\right)^2 + \frac{Z_\sigma(\rho) - Z_\pi(\rho)}{4\rho} \left(\partial_\mu \rho\right)^2 \right\}, \tag{2.17b}$$

$$\begin{aligned} \Gamma_k^{\partial^4} = \Gamma_k^{\partial^2} + \int_{\boldsymbol{x}} \Bigg\{ & \frac{W_1(\rho)}{2} \left(\partial_\mu \partial_\nu \phi^i\right)^2 + \frac{W_2(\rho)}{2} \left(\partial_\mu \partial_\nu \rho\right)^2 \\ & + W_3(\rho) \partial_\mu \rho \partial_\nu \phi^i \partial_\mu \partial_\nu \phi^i + \frac{W_4(\rho)}{2} \phi^i \partial_\mu \phi^j \partial_\nu \phi^j \partial_\mu \partial_\nu \phi^i \\ & + \frac{W_5(\rho)}{2} \phi^i \partial_\mu \rho \partial_\nu \rho \partial_\mu \partial_\nu \phi^i + \frac{W_6(\rho)}{4} \left[\left(\partial_\mu \phi^i\right)^2 \right]^2 + \frac{W_7(\rho)}{4} \left(\partial_\mu \phi^i \partial_\nu \phi^i\right)^2 \\ & + \frac{W_8(\rho)}{2} \partial_\mu \phi^i \partial_\nu \phi^i \partial_\mu \rho \partial_\nu \rho + \frac{W_9(\rho)}{2} \left(\partial_\mu \phi^i\right)^2 \left(\partial_\nu \rho\right)^2 + \frac{W_{10}(\rho)}{4} \left[\left(\partial_\mu \rho\right)^2 \right]^2 \Bigg\}. \end{aligned} \tag{2.17c}$$

In Eqs. (2.17), we used ρ to denote the $O(N)$ invariant $\phi^i \phi^i / 2$ and, to simplify the notation, we suppressed the scale dependence of the parametrizing functions U, Z_σ, Z_π, and W_i as well as the position dependence of the fields ϕ and ρ.

The derivative expansion reduces the incredible complexity of a general functional Γ_k and recasts it into just a couple of single-parameter functions. However, the simplicity of the ansätze (2.17) can be almost deceptive. While at the leading and next-to-leading orders the flow equations, which shall be discussed shortly, are manageable, their complexity grows extremely rapidly with each subsequent order. The leading order - the local potential approximation (LPA) involves just

one function - the local potential, while the flow equation fits in a single line. At the order $O(\partial^2)$, we are dealing with three functions, and the flow equations fit on a single page. At order $O(\partial^4)$, the flow equations for the thirteen parametrizing functions can only be derived on a computer and become too long for a human to read. The order $O(\partial^6)$ has never been implemented except for $N = 1$ [21, 23].

In some particular cases, the effective action ansatz as well as the flow equations can be greatly simplified. For example, when studying the Ising universality class (UC) [$N = 1$], $(\partial_\mu \phi^i)^2$ and $(\partial_\mu \rho)^2$ terms in Γ_k become proportional and the function $Z_\pi(\rho)$ decouples from physics and can be removed from the parametrization. For $N = 1$ at the order $O(\partial^4)$, there are only three independent four-derivative terms instead of ten present for generic N. Thanks to the reduction of the Γ_k ansatz, the DE up to the order $O(\partial^6)$ has been employed to study the Ising UC in three dimensions [21]. Similar reduction, although not as spectacular, can be achieved for higher integer values of N, e.g. for $N = 2$ at the order $O(\partial^4)$, just one function can be removed from the ansatz without loss of generality.

The difficulties related to the rapidly increasing complexity of the flow equations are counteracted by the fact that the DE converges quite rapidly and is surprisingly accurate even at low orders of the expansion. Already at the next-to-leading order, the DE becomes one-loop exact in three distinct perturbative regimes: $2 + \epsilon$ [for $N > 2$], $4 - \tilde{\epsilon}$, and $N \to \infty$ [102, 103]. This suggests that the DE offers a reasonable interpolation between the perturbative regimes. Moreover, thanks to their one-loop 1PI structure, the flow equations can be very efficiently implemented numerically. Even the highly complex flow equations of the $O(\partial^4)$ level can be integrated with a fairly limited numerical effort when compared with other methods such as conformal bootstrap or Monte Carlo, leading to results of comparable accuracy. We shall expound on the subject of convergence and accuracy of the DE in Sec. 2.3.

2.2.1 Flow equations

Once the effective action ansatz has been adopted, the flow equations are readily derived by calculating the flow of the vertex functions and expanding them in momenta. This is done by acting on the MW equation with the functional derivatives:

$$k\partial_k \Gamma^{(n)}_{k;i_1\boldsymbol{p}_1,\ldots,i_n\boldsymbol{p}_n} = \frac{1}{2}\mathrm{Tr}\left\{ \dot{R}_k \frac{\delta^n \left(\Gamma^{(2)} + R_k\right)^{-1}}{\delta\phi^{i_1}_{\boldsymbol{p}_1} \ldots \delta\phi^{i_n}_{\boldsymbol{p}_n}} \right\}. \tag{2.18}$$

Each functional derivative either acts on a "dressed propagator" generating a new $\Gamma^{(3)}$ vertex or on an existing vertex raising its order. Thus, the flow equations for the $\Gamma^{(n)}$ functions can be elegantly represented by one-loop 1PI diagrams. For example, the flow equation for $\Gamma^{(2)}_{k;i\boldsymbol{p},j-\boldsymbol{p}}$ function can be found by evaluating two

diagrams presented in Fig. 2.2.

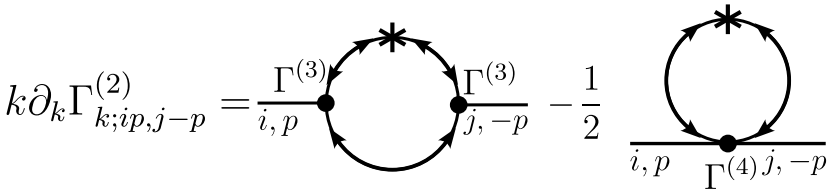

Figure 2.2: Diagrammatic representation of the flow equation for the $\Gamma^{(2)}_{k;i\boldsymbol{p},j-\boldsymbol{p}}$ function. The continuous lines with arrows denote the "dressed propagator" $\left(\Gamma^{(2)}_k + R_k\right)^{-1}$, the asterisks denote the scale derivative of the regulator $\dot{R}_k$ and the dots with n lines denote the n-point vertex functions. The external legs of the diagram are labeled with corresponding field indices and momenta.

At this point, it becomes important to discuss two alternative approaches to deriving the flow equations in the DE. The first is realized by directly following the steps outlined above. It is sometimes called the "ansatz" approach because it relies on extracting the equations directly from the effective action ansatz. The second approach is based on an interpretation of the DE as an expansion of the vertex functions in the external momenta. The prescription of this scheme is to calculate all necessary vertex functions keeping track of the neglected corrections. When we plug the vertex functions into the flow equations, we find that some terms coming from products of vertices are of the same order in momenta as the corrections neglected by the imposition of the effective action ansatz. We therefore should neglect these higher-order terms to keep the momentum expansion consistent. This approach is sometimes called "strict" because it strictly controls the momentum expansion.

It might be argued, however, that the name "strict" is a misnomer and may lead to confusion as it suggests some form of exactness. On the contrary, the whole idea of this approach is to truncate the terms that would appear if we adopted the equations coming from the ansatz at face value. To avoid confusion we will adopt the more neutral names: "ansatz" and "truncated", when referring to the respective schemes.

The advantage of the truncated approach lies in the reduction of the flow equations. At the order $O(\partial^2)$, the difference between the two schemes is minor, but at the order $O(\partial^4)$ the truncated scheme equations become many times shorter than the ansatz scheme equations. The price to pay for the reduction lies in the accuracy of the calculations, but its severity varies with the dimension. In three dimensions, the difference between the predictions of the two variants of the DE is negligible both at the $O(\partial^4)$ and $O(\partial^2)$ orders. We note that the DE calculations at the order $O(\partial^4)$ [$O(\partial^6)$ for $N = 1$ of Refs. [20, 21, 23] were performed only in

the truncated variant. As will be discussed in detail in Sec. 4.3, the truncated approach performs significantly worse than the ansatz approach when the dimension approaches two. In particular, the truncated scheme does not recover the onset of the KT physics as accurately as the ansatz scheme.

After calculating the flow of the vertex functions we evaluate them in a uniform field configuration $[\boldsymbol{\phi}_{\boldsymbol{q}} = \boldsymbol{\phi}\delta_{\boldsymbol{q},0}]$ and expand it in powers of the external momenta to obtain the flow of the parametrizing functions. At this point, it becomes convenient to specify the basis in the order-parameter space. In the $O(N)$-symmetric theory, without loss of generality, we can select

$$\phi^1(\boldsymbol{x})^2 = 2\rho(\boldsymbol{x}) \quad \text{and} \quad \phi^i(\boldsymbol{x}) = 0 \text{ for } 1 < i \leq N. \tag{2.19}$$

In this basis, one identifies the β functions:

$$\beta_U^k(\rho) = k\partial_k U_k(\rho) = k\partial_k \Gamma[\boldsymbol{\phi}]|_{\text{Uniform}}\,, \tag{2.20a}$$

$$\beta_{Z_\sigma}^k(\rho) = k\partial_k Z_\sigma(\rho) = \frac{1}{2d}\,\Delta_{\boldsymbol{p}}|_{\boldsymbol{p}=0}\left(k\partial_k \Gamma^{(2)}_{k;1\boldsymbol{p},1-\boldsymbol{p}}\right)\Big|_{\text{Uniform}}\,, \tag{2.20b}$$

$$\beta_{Z_\pi}^k(\rho) = k\partial_k Z_\pi(\rho) = \frac{1}{2d}\,\Delta_{\boldsymbol{p}}|_{\boldsymbol{p}=0}\left(k\partial_k \Gamma^{(2)}_{k;2\boldsymbol{p},2-\boldsymbol{p}}\right)\Big|_{\text{Uniform}}\,, \tag{2.20c}$$

with $\Delta_{\boldsymbol{p}} = \sum_{i=1}^d \partial_{p_i}^2$ denoting the Laplacian operator in the momentum space. A similar, though much more involved procedure holds for the terms of higher order in the DE [21].

The β functions of Eq. (2.20) contain the most important physical information and could be used to obtain the renormalized quantities but are not yet suitable for the analysis of RG fixed points. For this purpose, we need to transform them into a dimensionless form. This is achieved by multiplying each quantity X by the scale raised to the power of its canonical dimension $\tilde{X} = Xk^{d_X}$. At the $O(\partial^2)$ order of the DE, the rescaling takes the form:

$$\tilde{\rho} = \rho k^{2-d-\eta_k},\ \tilde{U}_t(\tilde{\rho}) = U_k(\rho)k^{-d},\ \tilde{Z}_{\sigma,t}(\tilde{\rho}) = Z_{\sigma,k}(\rho)k^{\eta_k},\ \tilde{Z}_{\pi,t}(\tilde{\rho}) = Z_{\pi,k}(\rho)k^{\eta_k}. \tag{2.21}$$

In Eq. (2.21), we introduced two new quantities: the "running anomalous dimension" η_k and the "renormalization time" $t = -\log(k/\Lambda)$. The former is the logarithmic derivative of the order-parameter renormalization $\eta_k = -k\partial_k \log(Z_k)$ and serves as a precursor for the fixed-point anomalous dimension. To close the set of equations, we choose an arbitrary constant $\tilde{\rho}_\eta$ and impose

$$\tilde{Z}_{\pi,t}(\tilde{\rho}_\eta) = Z_{\pi,k}(\rho_\eta)/Z_k \equiv 1 \tag{2.22}$$

defining Z_k[2]. The renormalization time is introduced to transform the flow equations into a stationary form. After the rescaling the equation for any parametrizing

[2]When studying the critical fixed points, either of the functions Z_π and Z_σ can be used in

function $\tilde{F}_t(\tilde{\rho})$ takes the form:

$$\partial_t \tilde{F}_t(\tilde{\rho}) = d_F \tilde{F}_t(\tilde{\rho}) - (d - 2 + \eta_k)\tilde{\rho}\tilde{F}'_t(\tilde{\rho}) - \tilde{\beta}_F(\tilde{\rho}) \tag{2.23}$$

with $\tilde{\beta}_F(\tilde{\rho}) = k^{-d_F}\beta_F^k(\rho)$ denoting the dimensionless loop contribution to the flow. The superscript denoting the scale-dependence in $\tilde{\beta}$ has been dropped since the dimensionless $\tilde{\beta}$ functions are only implicitly RG-time dependent.

2.2.2 Fixed points and critical exponents

Some universal quantities such as critical exponents can be extracted from the fixed point solutions to the RG-flow equations or their direct vicinity. It is thus beneficial to develop methods for finding the fixed-point solutions. In the DE, it is tremendously difficult to obtain analytical fixed point (FP) solutions without additional approximations and outside of the perturbative regime; we are unaware of any such achievements. The typical choice is to resort to numerical analysis.

In the so-called "functional approach" to the DE, we attempt to solve the discretized form of the set of flow equations of the form (2.23). This is achieved by representing the functions on a finite grid spanned on the interval $[0, \tilde{\rho}_{\mathrm{Max}}]$ and approximating the $\tilde{\rho}$ derivatives of parametrizing functions by finite differences. We thus transform a small set of nonlinear partial differential equations into a large set of ordinary differential equations suitable for numerical treatment. The details of the numerical methods employed in this thesis are discussed in Appendix B. Typically, the loop integrals cannot be performed analytically and are approximated with finite sums. The Gauss-Legendre quadrature rules used to perform the momentum integrals in the calculations of the present thesis are discussed in Ref. [104].

From this point, one can follow one of two routes: integrate the flow equations or search for the FP solutions. To integrate the flow equations one first needs to specify the initial condition for the effective action. When studying only the universal properties of the critical transitions, it is typical to select a microscopic action with a "Mexican-hat" potential[3]:

$$\Gamma_\Lambda[\boldsymbol{\phi}] = \mathcal{S}[\boldsymbol{\phi}] = \int_{\boldsymbol{x}} \left[\frac{u_0}{8} \left(\boldsymbol{\phi}^2 - \phi_0^2 \right)^2 + \frac{1}{2} \left(\partial_\mu \boldsymbol{\phi} \right)^2 \right]. \tag{2.24}$$

Eq. (2.22) to define the order-parameter renormalization. This is no longer true when investigating the low-temperature behavior. In this case, models with $N > 1$ require the renormalization factor to be defined via Z_π, while for $N = 1$ one has to use Z_σ since it is the only of the two functions retaining the physical significance.

[3]We note that for our purpose the specific form of the microscopic action has no impact on the results.

Subsequently, one needs to numerically integrate this initial value problem from the microscopic scale $k = \Lambda$ $[t = 0]$ until all the couplings become renormalized. In this thesis, we employ the adaptive step Runge-Kutta-Fehlberg method described in Appendix B.4.

One could ask why not integrate the equations down to the limit $k \to 0$. This, however, turns out to be numerically infeasible and, luckily, unnecessary. The flow equations are easiest to implement numerically in terms of the dimensionless quantities. In these terms, the limit $k \to 0$ corresponds to infinite renormalization time $t \to \infty$ and the limit itself is often singular. In practice, it is sufficient to integrate the flows to the scale at which all the *dimensionful* quantities become renormalized and their flow is negligible. This corresponds to integrating the flow down to some finite scale k_{Min} significantly lower than the inverse correlation length $k_{\mathrm{Min}} \ll \xi^{-1}$.

Once the integration method is implemented, the ϕ_0 parameter of the initial condition (2.24) can be tuned over consecutive flow simulations to approach the critical manifold. From the flows passing sufficiently close to the FP, one can directly extract the information about the anomalous dimension η, the correlation length exponent ν and leading corrections to scaling exponents [if the employed method offers a sufficient precision]. The flow integration method also presents access to nonuniversal information; it can be used inter alia to draw the phase diagram, calculate the renormalized quantities, and observe the cross-over behaviors. In the studies of multicritical points [FPs with two or more relevant directions], flow integration can become burdensome as it requires fine-tuning of several parameters.

The approach alternative to the flow integration is the fixed point search. It relies on directly solving the fixed point equation

$$\partial_t \Gamma^*[\boldsymbol{\phi}] = 0. \tag{2.25}$$

At this point, it becomes convenient to introduce a symbol $\mathcal{F}_t(\tilde{\rho})$ denoting a dimensionless vector of all parametrizing functions, e.g. at the order $O(\partial^2)$ we have

$$\mathcal{F}_t^{\partial^2}(\tilde{\rho}) = \left\{ \tilde{U}(\tilde{\rho}), \tilde{Z}_\sigma(\tilde{\rho}), \tilde{Z}_\pi(\tilde{\rho}) \right\}. \tag{2.26}$$

In terms of $\mathcal{F}$, the FP equation (2.25) takes just as simple form

$$\partial_t \mathcal{F}^*(\tilde{\rho}) = 0. \tag{2.27}$$

In the functional form, Eq. (2.27) describes a set of nonlinear ordinary differential equations. After the discretization outlined above, they reduce to a very large set of algebraic equations. These equations can be quite easily solved by several

methods. In this thesis, we employ the Newton-Raphson method explained in Appendix B.3.

The FP search method is a very efficient way to obtain values of the critical exponents. The anomalous dimension η is itself encoded in the FP solution while the other critical exponents are extracted from the linearization of the RG flow around the FP. We write:

$$\partial_t \mathcal{F} = \underbrace{\partial_t \mathcal{F}^*}_{0} + M(\mathcal{F}^*)\,(\mathcal{F} - \mathcal{F}^*) + O\left((\mathcal{F} - \mathcal{F}^*)^2\right), \tag{2.28}$$

where M is the matrix of first derivatives of the flow equations:

$$M(\mathcal{F})_{a\tilde{\rho}_i, b\tilde{\rho}_j} := \frac{\partial\left(\partial_t \mathcal{F}_{a\tilde{\rho}_i}\right)}{\partial \mathcal{F}_{b\tilde{\rho}_j}} \tag{2.29}$$

also known as the Jacobian. When evaluated at a fixed point, the matrix M is often called the stability matrix. In the definition (2.29), indices a, b enumerate the functions in $\mathcal{F}$ while the indices $\tilde{\rho}_i$, $\tilde{\rho}_j$ refer to the points on the discrete $\tilde{\rho}$ grid. The matrix (2.29) does not contain the rows and columns corresponding to values fixed by external constraints, e.g. the row and the column corresponding to $\tilde{Z}_\pi(\tilde{\rho}_\eta)$ are absent because the value $\tilde{Z}_\pi(\tilde{\rho}_\eta) = 1$ is fixed in the rescaling procedure to define the anomalous dimension. Similarly, the regularity of the effective action requires that the functions $\tilde{Z}_\sigma(\rho)$ and $\tilde{Z}_\pi(\rho)$ take the same value in the limit $\tilde{\rho} \to 0$, and thus the values $\tilde{Z}_\sigma(0)$ and $\tilde{Z}_\pi(0)$ should be treated as a single parameter when calculating the stability matrix.

The eigenvalues e_l of the stability matrix describe the scaling dimensions of the eigenoperators of the RG transformation. In our sign convention, the positive eigenvalues correspond to the relevant operators, and the negative to the irrelevant. For the critical FP, enumerating the eigenvalues in the descending order we identify the correlation length exponent $\nu = 1/e_1$ related to the dominant eigenvalue, and the correction to scaling exponents $\omega_i = |e_{i+1}|$ [105]. The stability matrix is not symmetric and therefore some of its eigenvalues may take complex values. The complex eigenvalues always appear as conjugate pairs: e and $\bar{e}$.

The fixed point search approach is a very efficient and precise method to identify the critical exponents. It requires substantially less computational effort than the flow integration and has the capacity for the calculation of an arbitrary number of the RG eigenvalues without worrying about the nonlinear corrections that could spoil the estimation of the critical exponents from the flow. The disadvantage of this method lies in the limited number of quantities that it allows to calculate, which are essentially restricted to the critical exponents. Even some universal quantities such as the universal amplitude ratios cannot be extracted from the fixed point alone.

We emphasize that the stability matrix (2.29) is defined after the discretization. However, the stability matrix $M(\mathcal{F}^*)$ has a functional counterpart stability operator $\mathcal{M}(\mathcal{F}^*)$, which describes the true linearization of the RG equation around the functional solution to the FP equation. Its kernel is defined as:

$$\mathcal{M}(\mathcal{F})_{a\tilde{\rho},b\tilde{\rho}'} := \frac{\delta\left(\partial_t \mathcal{F}_a(\tilde{\rho})\right)}{\delta \mathcal{F}_b(\tilde{\rho}')}. \tag{2.30}$$

We are unaware of any studies investigating the stability operator $\mathcal{M}(\mathcal{F}^*)$ or its spectrum, though there is no lack of pressing questions. Physical arguments tell us that the spectrum of $\mathcal{M}(\mathcal{F}^*)$ should be bounded from above and, at least partially, discrete. Yet it remains unclear, why this should be the case from the mathematical point of view.

More importantly, however, the notion of convergence of the stability matrices to the stability operator upon tightening and expanding the grid has not been well defined and certainly not fully understood. Many modern DE studies rely on the assumption that the several lowest eigenvalues [in absolute value] of the stability matrix converge to the several lowest eigenvalues of the stability operator when the grid spacing goes to 0 and the grid size $\tilde{\rho}_{\mathrm{Max}}$ goes to infinity. This belief is founded on strong, yet only phenomenological arguments and crucially lacks a proof based on mathematical principles.

2.2.3 Further approximations

The DE can be very efficiently implemented numerically, but it is still quite demanding, especially at higher orders or when applied to models with symmetries more complex than $O(N)$. This can be circumvented by performing additional approximations on top of the DE.

One such approximation is the so-called LPA' scheme. It is essentially an intermediate step between the LPA and $O(\partial^2)$ orders of the DE. In this approach, the function $Z_{\pi,k}(\rho)$ is reduced to a flowing constant, and $Z_{\sigma,k}(\rho)$ is either reduced to a flowing constant or assumed equal $Z_{\pi,k}(\rho)$ depending on the implementation. Typically, at the LPA' level, the normalization point $\tilde{\rho}_\eta$, used in the normalization condition $\tilde{Z}(\tilde{\rho}_\eta) = 1$, is set equal to the minimum of the dimensionless local potential.

The advantage of the LPA' approach lies in a spectacular reduction of the numerical complexity. Not only does it remove the effort required to calculate the β functions for Z_σ and Z_π at each point of the grid, but also allows the momentum integrals to be calculated analytically when a particularly convenient IR regulator is employed. Despite its simple formulation, LPA' properly captures many aspects of long-distance physics on the qualitative level [99], including even some signatures

of the KT transition [106]. We also note, that the LPA' is sufficient to reproduce exactly the one-loop predictions from $2+\epsilon$, $4-\tilde{\epsilon}$ and large-N expansions.

Another route for simplifying the flow equations relies on truncating the parametrizing functions in powers of the order parameter. This allows us to reduce a complex functional structure of the parametrizing functions to a small set of parameters. The expansion is typically performed around $\rho = 0$ or around the minimum of the local potential ρ_0, with the latter showing better performance in three dimensions [107]. Convergence of the field truncation was also analyzed in Refs. [108, 109]. Already 20 years ago, this method was used to obtain the critical exponents of the three-dimensional $O(N)$ models at the order $O(\partial^2)$ [110] and of the three-dimensional Ising UC [$N = 1$] at the order $O(\partial^4)$ [111]. Only very recently have the field truncated calculations been extended to the $O(\partial^4)$ order for $N \neq 1$ [112] [also in three dimensions].

The field truncated approach is not new and its fairly rapid convergence in three dimensions and above is well-documented. It turns out, however, that in the case of the $O(N)$ models below dimension $d \lesssim 2.5$, this type of expansion does not reproduce the expected critical behavior when carried out beyond the lowest sensible order:

$$U(\rho) = \frac{u_2}{2} \left(\rho - \rho_0\right)^2 . \tag{2.31}$$

Worryingly, the range of dimensions where this problem occurs seems to grow with the employed order of the field truncation. An interesting exception lies in the perturbative regime $d - 2 \ll 1$, $N > 2$ where the field truncation seems to converge properly. The reasons for the inadequacy of the high-order field expansion in low dimensions remain unclear to us and require future clarifying studies.

2.3 Infrared Regulator

So far, we have barely discussed the IR regulator function R_k and the regulator dependence of the results. In the exact treatment, our results should not depend on the choice of the regulator but this property becomes spoiled by approximations such as the DE. It is therefore necessary to develop a consistent method for minimizing the dependence on the nonphysical parameters.

Introducing the effective average action approach we have required that the regulator function has to take large values for low momenta [$R_k(\boldsymbol{q}^2 \ll k^2) \gg \boldsymbol{q}^2$] and vanish rapidly at large momenta [$R_k(\boldsymbol{q}^2 \gg k^2) \approx 0$]. We also suggested that it might be convenient to separate the dimensionful and the dimensionless parts of the regulator; we write

$$R_k(\boldsymbol{q}^2) = Z_k k^2 r\left(\boldsymbol{q}^2/k^2\right), \tag{2.32}$$

where r is a dimensionless function of a single dimensionless parameter $\boldsymbol{q}^2/k^2$. The regulator r should take a finite value at $\boldsymbol{q}^2/k^2 = 0$ and vanish quickly for $\boldsymbol{q}^2/k^2 \gg 1$.

The constraints imposed on the regulator are not very restrictive and there are many candidates for that role. Through the years, several different candidate functions were tried and tested. Nowadays, the most commonly used regulators include:

$$r_{\text{Wetterich}}(y) = \alpha \frac{y}{e^y - 1}, \tag{2.33a}$$

$$r_{\text{Exponential}}(y) = \alpha \exp(-y), \tag{2.33b}$$

$$r_{\text{Litim}-n}(y) = \alpha \, (1-y)^n \, \Theta(1-y). \tag{2.33c}$$

2.3.1 Principle of Minimal Sensitivity

The true physical result should not depend on the scheme through which it has been calculated; in particular, it should be independent of the employed regulator function. However, the approximate results, e.g. coming from the derivative expansion, typically show some level of regulator dependence which has to be investigated and understood to offer an accurate estimate of the physical quantity in question. This problem can be, to some extent, ameliorated by employing the principle of minimal sensitivity (PMS).

The PMS is a method designed to optimize the estimate of a physical quantity within a single regulator family. Each regulator function presented in Eq. (2.33) carries a free parameter α that has to be fixed. To determine an optimized estimate of the quantity Q we first calculate the functional profile $Q(\alpha)$. Subsequently, we select the value $Q(\alpha_{\text{PMS}})$ corresponding to the stationary point:

$$\left.\frac{\partial Q(\alpha)}{\partial \alpha}\right|_{\alpha_{\text{PMS}}} = 0. \tag{2.34}$$

The PMS has proven very useful, often significantly improving the estimates of the DE calculations [21, 23, 110, 111]. Interestingly, the PMS-optimized quantities not only lie closer to the physical values of said quantities but also show a smaller spread across the regulator families - strongly reducing the regulator dependence of the results [21, 23]. It has to be noted, however, that in some rare cases, the function $Q(\alpha)$ features none or more than one stationary point, and the PMS becomes insufficient as a regulator-fixing tool.

Early on, the PMS was also criticized as an ad hoc solution without a physical foundation. This changed recently after the PMS was linked to the minimal breaking of the conformal symmetry. In the exact theory, the fixed point solutions should fulfill the conformal Ward identity. When approximations are employed,

however, this identity becomes broken. In a recent study [48], Balog et al. formulated the principle of maximal conformity (PMC), stating that the regulator should be selected in such a way that the breaking of the conformal Ward identity is minimal. They also showed that for the three-dimensional $O(1)$ UC the PMC and the PMS yield almost the same optimized regulator suggesting that the PMS can be treated as an effective substitute for the PMC [PMS being significantly easier to implement in practice than PMC]. This is particularly important for the cases in which the PMC cannot be implemented, e.g. at the LPA and $O(\partial^2)$ orders of the DE. Moreover, the PMC could be used to optimize regulators when the PMS fails, e.g. when the quantity of interest has more than one stationary point. Discussion of the rationale for the PMS and fixing regulator dependence has been continued in Ref. [113].

The results presented in this thesis, unless explicitly stated otherwise, were obtained with the Wetterich regulator (2.33a).

2.3.2 Convergence of Derivative Expansion and Error Bars

Since its inception, the DE has faced criticism based on the fact that it does not have a manifest small parameter controlling the series expansion. It was noted, that the DE accuracy seems to be better when the anomalous dimension η becomes small. This led to a phenomenological postulate that the small parameter of the DE should be connected to η [100]. This postulate, however, was not supported by any fundamental arguments.

Similarly to the physical rationale for the PMS, this question has been resolved in a recent push for a more foundational understanding of the DE [23]. Balog et al. showed that the small parameter of the derivative expansion can be identified by investigating the universal structure of the two-point function $\Gamma^{(2)}$. Furthermore, they argued that the dispersion of the PMS-optimized results should decrease by a factor of between 4 and 9 with each subsequent order of the derivative expansion.

Based on those findings, De Polsi et al. formulated a technique for estimating error bars in the DE [21]. This technique relies on a comparison between consecutive orders of the DE. Let us consider a physical quantity Q. The dispersion $\Delta Q^{(s)}$ at the order $O(\partial^s)$ is calculated via a simple procedure:

- We find the PMS values at the order of our calculation $Q^{(s)}_{\mathrm{PMS}}$ and the preceding order $Q^{(s-2)}_{\mathrm{PMS}}$. The necessity for comparison with the lower order means that the error bars cannot be estimated at the LPA order with this method.

- If we employ different families of regulators, we can improve the estimates at each order by adopting $\bar{Q}^{(s)}_{\mathrm{PMS}}$ corresponding to the central value across

families of regulators. The value $\bar{Q}^{(s)}_{\mathrm{PMS}}$ is the basic estimate for Q at order $O(\partial^s)$.

- The error bars are calculated from the fact that the distance between the DE estimate $\bar{Q}^{(s)}_{\mathrm{PMS}}$ and the true value should reduce by a factor of between 4 and 9 with each subsequent order. Assuming the pessimistic case we write

$$\Delta Q^{(s)} = \frac{\left|\bar{Q}^{(s)}_{\mathrm{PMS}} - \bar{Q}^{(s-2)}_{\mathrm{PMS}}\right|}{4}. \tag{2.35}$$

The steps outlined above lead to very conservative estimates for the error bars that can often be improved upon. Typically, the consecutive orders of the DE yield alternating results. By alternating we mean that at the order $O(\partial^{s-2})$ the PMS value corresponds to a minimum [maximum], while at the order $O(\partial^s)$ the PMS value corresponds to a maximum [minimum] lying below [above] the results of the previous order. In such cases, these PMS values can be thought of as the upper and the lower bounds for the quantity of interest respectively. This means that half of the range of the error bars $\bar{Q}^{(s)}_{\mathrm{PMS}} \pm \Delta Q^{(s)}$ lies outside of our bounds. Thus, it makes sense to shift the central estimate by half of $\Delta Q^{(s)}$ and divide the dispersion by half. This yields an improved estimate:

$$\bar{Q}^{(s)}_{\mathrm{Improved}} = \frac{7\bar{Q}^{(s)}_{\mathrm{PMS}} + \bar{Q}^{(s-2)}_{\mathrm{PMS}}}{8}, \tag{2.36a}$$

$$\Delta Q^{(s)}_{\mathrm{Improved}} = \frac{\left|\bar{Q}^{(s)}_{\mathrm{PMS}} - \bar{Q}^{(s-2)}_{\mathrm{PMS}}\right|}{8}. \tag{2.36b}$$

The procedure for determination of the error bars is visualized in Fig. 2.3.

Most often, this procedure leads to proper estimation of the error bars. Sometimes, however, the two consecutive orders of the DE coincidentally yield very similar results and the error bars become artificially reduced. In such a case, some ad hoc method has to be developed to restore the estimated dispersion to a reasonable range. In Ref. [21] this kind of "crossing" of the critical exponents was showcased for ω in three dimensions around $N = 4$. Based on the fact that the DE is exact in the large-N limit, De Polsi et al. postulated that the dispersion should be monotonously falling with N. This allowed them to interpolate the error bars to the cases where the raw estimates were too narrow.

Another drawback of this method becomes apparent when different regulator families yield significantly different results [which sometimes happens at higher orders of the DE]. In those cases, one has to factor in the error coming from the choice of the regulator function $\Delta_{\mathrm{reg}}Q$. For more details on the error bar estimation, we refer to Ref. [21].

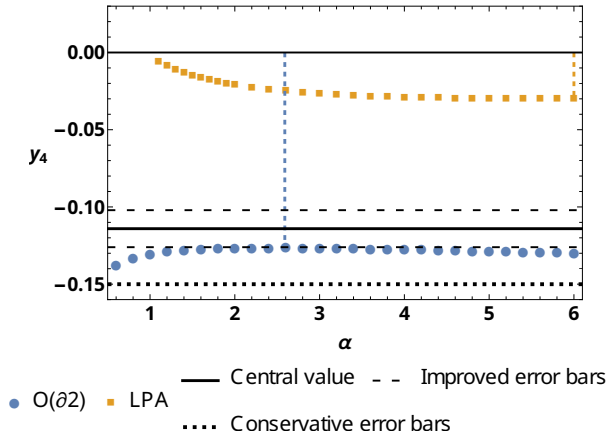

Figure 2.3: Visualization of the error bar estimation procedure for the critical exponent y_4 [the definition and discussion of this exponent are relegated to Chapter 4]. Circles and squares denote the results of two consecutive orders of the DE - $O(\partial^2)$ and LPA respectively with vertical lines indicating the PMS values. The dotted line denotes the lower bound of the conservative error bars. The results from consecutive orders are alternating so the improved estimates are employed [see Eq. (2.36)]; the dashed lines denote the improved error bars and the solid line denotes the improved central value. The lower improved bound passes through the PMS value of the $O(\partial^2)$ level and the upper improved bound coincides with the conservative upper bound.

2.3.3 Near-Optimal Regulator

In recent studies, the significance of the PMS in the precise evaluation of critical indices has been emphasized, particularly upon increasing the truncation order [21, 48]. However, the benefits of employing PMS remain somewhat limited at the $O(\partial^2)$ order of the DE, with notable improvements primarily observed in the immediate vicinity of two dimensions. Additionally, it is important to note that employing the PMS significantly inflates the required computational resources. As a result, researchers focused on qualitative analysis, rather than striving for high-precision estimates, may find it advantageous to opt for a fixed, near-optimal regulator and forego further fine-tuning.

Within this section, we choose the $O(2)$ model as a reference point to determine a near-optimal value for α for the Wetterich regulator [see Eq. (2.33a)] for the $O(N)$ models in dimensions between two and three. Our analysis is illustrated in Fig. 2.4, which showcases the variation of the PMS value of α as determined for either the correlation length exponent ν or the anomalous dimension η as the dimension changes. A substantial increase in the variability of α_{PMS} in lower dimensions is

evident, with no PMS value found in the immediate vicinity of two dimensions. More importantly, the chart indicates that $\alpha = 2$ approximates the "average" value of $\alpha_{\rm PMS}$ for this model in this range of dimensions.

To gain further insights, we explore the disparity between the PMS-optimized critical exponents and the near-optimal exponents calculated using $\alpha = 2$. Fig. 2.5 provides a side-by-side comparison of the values of anomalous dimensions as computed with the optimal and near-optimal regulators. Except for dimensions very close to two, the differences between the two scenarios are negligible. This discrepancy is further highlighted in the subsequent illustration in Fig. 2.6, which portrays the relation between η and α for a series of dimensions in proximity to two. It becomes apparent why the PMS value of α cannot be determined in dimensions very close to two, specifically for $d \lesssim 2.01$.

An alternate approach for optimizing the regulator, designed specifically for the KT transition, was introduced in Ref. [114]. Details of this procedure will be discussed in Sec. 2.4.1. For now, it is worth noting that Ref. [114] identified an "optimal" value of $\alpha_{\rm opt} \approx 2.0$. Importantly, this "optimal" value, similar to $\alpha_{\rm PMS}$, exhibits weak dependence on the renormalization point $\tilde{\rho}_\eta$. This provides further support for the proposition that critical exponents' near-optimal values can be derived from calculations using the Wetterich regulator with $\alpha = 2$.

In certain sections of this thesis, we obtain results by keeping the regulator fixed at $\alpha = 2.0$ rather than employing the PMS procedure. We deem it essential to emphasize that the differences between the PMS values of critical exponents [when $\alpha_{\rm PMS}$ can be determined] and the values obtained at $\alpha = 2$ are relatively minor. Moreover, our validation confirms that the key findings obtained with the near-optimal regulator remain unchanged even when PMS regulators are used [where applicable, specifically in dimensions significantly separated from two].

2.4 Applications of the Derivative Expansion

2.4.1 Kosterlitz-Thouless Transition

The Kosterlitz-Thouless transition is a famously unusual and elusive phase transition. The presence of topological excitations and the essential singularity of the correlation length make it notoriously difficult to capture. Despite these difficulties, many important characteristics of the KT transition have been properly described within the DE framework. However, there also remain significant challenges, inter alia the failure of the PMS to determine the critical exponents such as the anomalous dimension. Since the KT transition plays a central role in this thesis it is important to discuss in detail the performance of the DE concerning that transition.

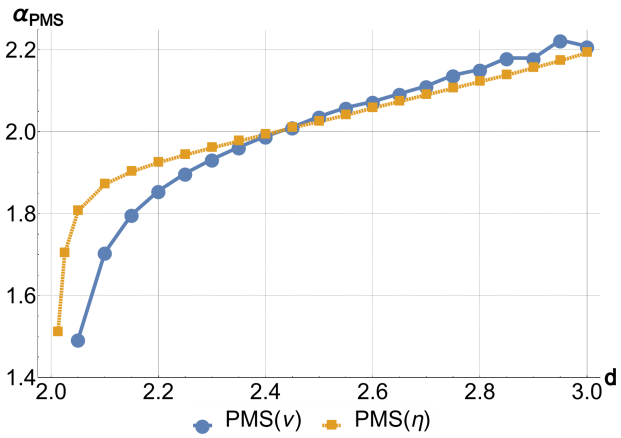

Figure 2.4: Evolution of the PMS values of the regulator parameter α depending on dimension d for $N = 2$. A substantial increase in its variation occurs when the dimension approaches two. No PMS value is found in the immediate vicinity of two dimensions. Figure from Ref. [2].

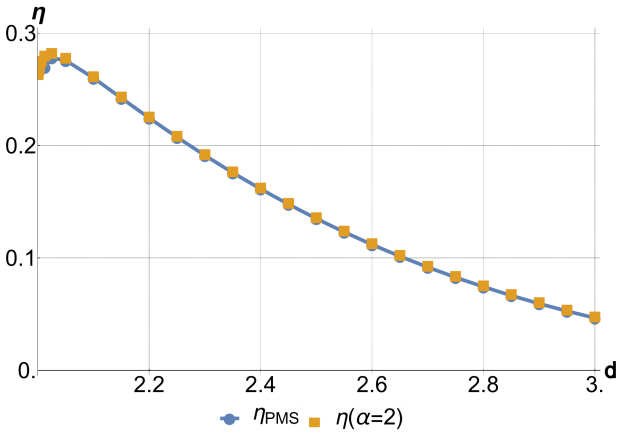

Figure 2.5: Comparison of the anomalous dimension η of the $O(2)$ model as function of dimension calculated for $\alpha = 2$ and α_{PMS}. Figure from Ref. [2].

At the LPA order, we find no transition at all for $(d, N) = (2, 2)$.

Improving the truncation to the LPA' level, we find a significant change. Strictly speaking, no phase transition occurs for $(d, N) = (2, 2)$, but some signatures of the KT transition can be identified. As we mentioned before, the DE at the LPA' order recovers exactly the one-loop results of the $2 + \epsilon$ expansion. This can be easily seen in the field truncated approach. One finds that the $\tilde{\beta}_{\tilde{\rho}_0}$ function

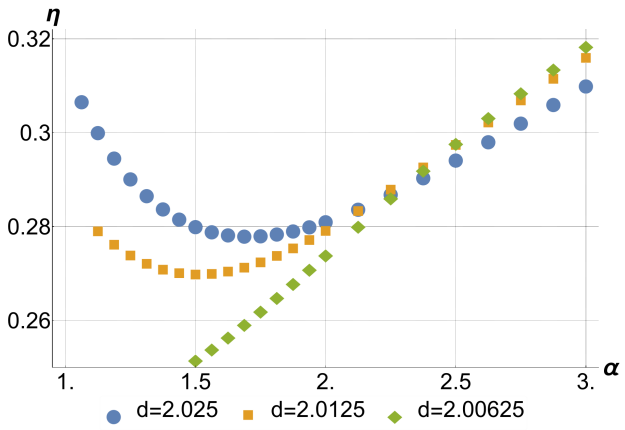

Figure 2.6: Variation of the anomalous dimension η of the $O(2)$ model depending on α for a sequence of dimensions in the close vicinity of two. No PMS value is found in sufficiently low dimensions. Figure from Ref. [2].

for the flow of the dimensionless minimum of the potential $\tilde{\rho}_0$ reads

$$\tilde{\beta}_{\tilde{\rho}_0} = \epsilon\tilde{\rho}_0 + C(N-2) + O(\tilde{\rho}_0^{-1}, \epsilon) \tag{2.37}$$

in a double expansion around large $\tilde{\rho}_0$ and small ϵ [106]. In Eq. (2.37), C denotes a constant that can take any positive value under a proper rescaling. One easily verifies that the $\tilde{\beta}_{\tilde{\rho}_0}$ function is equivalent to the leading order β_g function of the $2+\epsilon$ expansion (1.4) with the potential minimum proportional to the inverse temperature $\tilde{\rho}_0^{-1} \propto g$.

At the KT point $(d, N) = (2, 2)$, the $\tilde{\beta}_{\tilde{\rho}_0}$ function vanishes up to terms of order $O(\tilde{\rho}^{-2})$ [115]. At low temperatures, the RG flows [regardless of the initial condition] converge to a line characterized by a very slow RG flow. Since the flows are slow, yet not exactly static, this line is often called a line of quasi-fixed points (QFPs). During the drift along the line of QFPs, the temperature $\tilde{\rho}_0^{-1}$ and the anomalous dimension η slowly increase up to a point of an abrupt cross-over. After the cross-over, the flow becomes very rapid and quickly ends up in a disordered phase. The cross-over point has been identified with an anomalous dimension $\eta \simeq 0.24$ very close to that of the KT transition $\eta_{\mathrm{KT}} = 1/4$ [106]. This result, however, has to be treated with caution since no analysis of regulator dependence was performed in that study.

Another important finding concerns the role of the longitudinal fluctuations in the KT transition. To understand it, Jakubczyk and Metzner [116] employed the DE at the LPA' with the minimal field truncation [see Eq. (2.31)]. They found that by discarding the longitudinal fluctuations one may recover many properties

of the KT low-temperature phase including a finite spin-wave stiffness, a vanishing order parameter, and an algebraic decay of the order parameter with the exponent η proportional to the temperature at low temperatures.

More quantitative agreement between the NPRG and the KT theory can be found when the $O(\partial^2)$ order of the DE is employed. This scheme was used to recover the line of QFPs with an even slower drift along the line [114, 115]. Importantly, Ref. [114] identifies a true FP at the endpoint of the line of QFPs with $\eta \simeq 0.24$ and the universal jump of spin-wave stiffness $\Delta K_R \simeq 0.64$. These results stand in very good agreement with the results of the KT theory with $\eta_{\mathrm{KT}} = 1/4$ and $\Delta K_{\mathrm{KT}} = 2/\pi \approx 0.637$.

One of the obstacles in capturing the KT transition at the order $O(\partial^2)$ arose from the failure of the PMS. Thus, an alternative method for fixing the regulator dependence had to be proposed. At the order $O(\partial^2)$, the drift along the line of QFPs is so slow that its direction could be reversed just by tuning the free parameter α of the regulator function. For low temperatures T, the optimal value $\alpha_{\mathrm{opt}}(T)$ is therefore selected such that the drift stops and the flow reaches a true fixed point [114]. The transition temperature T_{KT} is then determined as the highest temperature for which the regulator can be optimized in this way. The endpoint of the line of QFPs can be then extracted from the flow at the transition temperature T_{KT} with the optimized regulator. Importantly, if the regulator tuning is abandoned, the transition takes the form of an extremely sharp cross-over into a phase characterized by an enormously large (but finite) correlation length which would be practically indistinguishable from infinite in an experiment or simulation [114, 115]. Further studies also showed that the DE at the order $O(\partial^2)$ can be used to accurately recover nonuniversal properties of the KT transition such as entropy and specific heat [117].

For further reading on the KT transition studied with various truncations of the functional RG, we refer to Refs. [118–123].

2.4.2 Low-temperature behavior

The critical state is far from being the only area of interest in equilibrium statistical physics. Another important area of study concerns the low-temperature properties such as the equations of state. Finding these, often nonuniversal, quantities is necessary to gain a full understanding of a given model. However, low-temperature behavior is notoriously difficult to capture with both perturbative and nonperturbative methods.

The DE-based NPRG is no different in this regard. The problem of describing low-temperature behavior with the functional approach lies in the structure of the flow equations. Let us recall that the equations take the form of one-loop 1PI diagrams with lines representing "dressed propagators", which at the $O(\partial^2)$ level

of the DE take the form:

$$G_\sigma^{-1}(\rho, q) = U'(\rho) + 2\rho U''(\rho) + q^2 Z_\sigma(\rho) + R(q^2), \qquad (2.38)$$
$$G_\pi^{-1}(\rho, q) = U'(\rho) + q^2 Z_\pi(\rho) + R(q^2).$$

Both propagators and consequently all terms in the β functions, suffer from poles in momentum q. At finite scales, these poles remain on the imaginary axis, however as we approach the infrared limit in the low-temperature phase, $U'(0)+R(0) \to 0^+$ taking the poles closer to the real axis. Ref. [124] delves deep into the subject of the ordered phase singularities and finds the analytical solutions close to the singularities at the LPA level. So far, at the $O(\partial^2)$ level of the DE, no analytical solution has been proposed and one has to employ numerical methods. However, the computational cost of achieving any given precision diverges as the pole of the propagator approaches the real axis.

One possible cure for the low-temperature divergences was employed in Ref. [125] [see also [126]]. In the long-length-scale part of the flow, the $\tilde{\rho}$ grid was no longer considered on the interval $[0, \tilde{\rho}_{\mathrm{Max}}]$, focusing instead on a close vicinity of the minimum of the local potential $[\tilde{\rho}_0 - \delta\tilde{\rho}_{\mathrm{min}}, \rho_0 + \delta\tilde{\rho}_{\mathrm{max}}]$. This approach is similar to the field expansion described in Sec. 2.2.3, since it focuses only on a direct vicinity of the minimum of the local potential, but retains more information and seems to be better-controlled. Despite discarding some physical information, this approach seems stable and reliable, and it can be used to capture renormalized quantities in the ordered phase.

In this thesis, besides the critical state, we are investigating the quasi-long-range order. Such phases are controlled by regular, stable RG fixed points. Therefore, we are not dealing with true nonanalyticities that might arise in the long-range ordered phase and do not need to resort to schemes such as those proposed in Refs. [124–126]. For most of our purposes, it turns out sufficient to adopt extremely precise numerical algorithms.

An alternative route for avoiding the singularities of the β functions relies on the expansion of the parametrizing functions into the Taylor series around the minimum of the local potential described in Sec. 2.2.3. In Sec. 3.4, we employ the power-series expansion as a supplementary tool to outline the expected results and to describe the parts of the (d, N) plane that we were not able to access within the functional scheme. To avoid the instabilities in low dimensions, we refrain from employing high orders of the expansion settling for the minimal truncation with $Z_\sigma(\rho)$ and $Z_\pi(\rho)$ reduced to flowing constants and the local potential parametrized as:

$$U(\rho) \approx \frac{u_2}{2} (\rho - \rho_0)^2 . \qquad (2.39)$$

Henceforth, we shall refer to the scheme relying on the field expansion as the "minimal truncation" [in contrast to the functional scheme described earlier].

2.4.3 Anisotropic Models

The discussion of the DE was so far mostly restricted to models with the $O(N)$ symmetry. To describe the models with anisotropic interactions we need to introduce some generalizations. The following reasoning will be specifically devoted to models characterized by a two-component scalar order parameter and cubic anisotropies but we will also mention possible generalizations to higher-order anisotropies and larger values of N.

We first need to promote the $O(N)$-symmetric ansätze (2.17) to the most general form invariant upon the cubic symmetry transformations:

$$\phi^1 \longleftrightarrow -\phi^1 \quad \text{and} \quad \phi^1 \longleftrightarrow \phi^2. \tag{2.40}$$

The only difference between the ansätze at the LPA level takes the form of promoting the local potential to the $\mathbb{Z}_4$-symmetric function of $\boldsymbol{\phi}$. At the $O(\partial^2)$ level, however, a new term appears; the $O(2)$-symmetric term $(\partial_\mu\rho)^2$ is split into two independent $\mathbb{Z}_4$-symmetric terms:

$$\phi^1\phi^2\partial_\mu\phi^1\partial_\mu\phi^2 \quad \text{and} \quad \left[\left(\phi^1\right)^2 - \left(\phi^2\right)^2\right]\left[\left(\partial_\mu\phi^1\right)^2 - \left(\partial_\mu\phi^2\right)^2\right]. \tag{2.41}$$

The full $\mathbb{Z}_4$-symmetric LPA and $O(\partial^2)$ level ansätze take the form:

$$\Gamma^{\text{LPA}}_{\mathbb{Z}_4} = \int_{\boldsymbol{x}} \Big\{ U(\phi^1,\phi^2) + \frac{1}{2}\left(\partial_\mu\phi^i\right)^2 \Big\}, \tag{2.42a}$$

$$\begin{aligned}\Gamma^{\partial^2}_{\mathbb{Z}_4} &= \int_{\boldsymbol{x}} \Big\{ U(\phi^1,\phi^2) + \frac{Z(\phi^1,\phi^2)}{2}\left(\partial_\mu\phi^i\right)^2 + T(\phi^1,\phi^2)\phi_1\phi_2\partial_\mu\phi_1\partial_\mu\phi_2 \\ &\qquad + \frac{W(\phi^1,\phi^2)}{4}\left[\left(\phi^1\right)^2 - \left(\phi^2\right)^2\right]\left[\left(\partial_\mu\phi^1\right)^2 - \left(\partial_\mu\phi^2\right)^2\right] \Big\},\end{aligned} \tag{2.42b}$$

where U, Z, T, and W are functions invariant with respect to transformations (2.40). The $O(2)$ symmetry of the action (2.42) is restored when all the parametrizing functions become rotationally invariant and, at the $O(\partial^2)$ level, when $T(\phi^1,\phi^2) \equiv W(\phi^1,\phi^2)$.

The cubic symmetry constraints on the vector of parametrizing functions $\mathcal{F}$ can be imposed in many ways. The direct parametrization via the field $\boldsymbol{\phi} = (\phi^1,\phi^2)$ is one of the less efficient ones. We shall introduce two more convenient parametrizations involving either the polar decomposition or representation via invariants.

The polar decomposition relies on introducing two fields: ρ and θ via the conditions

$$\phi^1(\boldsymbol{x}) = \sqrt{2\rho(\boldsymbol{x})}\cos(\theta(\boldsymbol{x})), \quad \phi^2(\boldsymbol{x}) = \sqrt{2\rho(\boldsymbol{x})}\sin(\theta(\boldsymbol{x})). \tag{2.43}$$

The field ρ is defined identically to that of the $O(2)$-symmetric case. As we shall see, this parametrization makes the symmetry constraints quite simple, although it also requires careful treatment. When the order parameter $\boldsymbol{\phi}$ vanishes, polar coordinates become degenerate. In the isotropic models, this is not a problem since by definition the effective action has no polar dependence. With the anisotropies present, we have to keep in mind the fact that when the order parameter vanishes, the anisotropic interactions vanish as well. More specifically, the lowest order cubic term reads

$$\tau = \frac{\left(\phi^1\phi^2\right)^2}{2} = \frac{\rho^2 \sin^2(2\theta)}{2}. \tag{2.44}$$

Therefore to preserve the regularity of $\mathcal{F}(\phi^1, \phi^2)$, we need to impose that at small ρ the vector of parametrizing functions $\mathcal{F}$ behaves as:

$$\partial_\theta \mathcal{F}(\rho, \theta) = \mathcal{F}^2 \sin(4\theta)\rho^2 + \mathcal{F}^3 \sin(4\theta)\rho^3 + O(\rho^4), \tag{2.45}$$

where $\mathcal{F}^2$ and $\mathcal{F}^3$ are vectors of constants. Although Eq. (2.45) looks straightforward, its numerical implementation might present a challenge and has to be meticulously performed.

In the (ρ, θ) parametrization, any $\mathbb{Z}_p$ symmetry [for integer p] is imposed by requiring that for any ρ the parametrizing functions fulfill:

$$\mathcal{F}(\rho, \theta) = \mathcal{F}(\rho, 2\pi/p + \theta) \quad \text{and} \quad \mathcal{F}(\rho, \theta) = \mathcal{F}(\rho, 2\pi/p - \theta). \tag{2.46}$$

An efficient way to implement these constraints is to represent $\mathcal{F}$ on a strip $\rho \in [0, +\infty[$, $\theta \in [0, \pi/p]$ with the boundary conditions

$$\partial_\theta \mathcal{F}(\rho, \theta)|_{\theta=0} = \partial_\theta \mathcal{F}(\rho, \theta)|_{\theta=\pi/p} = 0. \tag{2.47}$$

The polar representation is a convenient choice for functional treatment. The domain of the parametrizing functions has a rectangular shape, which can be straightforwardly implemented. The numerical calculations, however, have to be performed on a two-dimensional field grid, which greatly increases the computational effort. As a consequence, there have been only a few successful attempts at implementing the NPRG retaining the full functional dependence with respect to two invariants [127, 128], with the full $O(\partial^2)$ order DE calculation performed only very recently [4].

A major drawback of the polar representation relates to the care required for the treatment of the boundaries. Typically, the general expressions for the flow equations cannot be numerically evaluated at the boundaries due to spurious non-analyticities. To avoid these problems, one needs to find the boundary expressions analytically which requires significant effort. These issues might be, to some extent, ameliorated by replacing the polar angle θ with the variable $\xi = \cos(p\theta) \in [-1, 1]$.

In this alternative parametrization, both the symmetry constraints (2.46) and the boundary conditions (2.47) become naturally fulfilled.

An approach alternative to the polar decomposition relies on parametrizing $\mathcal{F}$ in terms of the invariants of the symmetry transformations. For any even anisotropy $\mathbb{Z}_p$ in the $O(2)$ model, there are just two algebraically independent invariants. It is common to select: $\rho = \phi^i\phi^i/2$ - the $O(N)$ invariant and τ_p - the p^{th} order $\mathbb{Z}_p$-symmetric polynomial of the order parameter. For the cubic symmetry, we shall use

$$\tau = \frac{\left(\phi^1\phi^2\right)^2}{2}, \tag{2.48}$$

where subscript 4 was dropped for brevity. We note that in the $O(N)$ models with cubic perturbations, there are N independent cubic invariants, of which τ, after promotion to $\tau' = \sum_{i\neq j}\left(\phi^i\phi^j\right)^2/2$, represents the one of the lowest order.

In the (ρ, τ) parametrization, the boundary problems arising in the polar parametrization are mostly absent. The flow equations are manifestly regular, except for the limit $\rho \to 0$ which is not particularly difficult to resolve. This parametrization is therefore particularly useful for the field-truncated approach. The functional approach, on the other hand, does present a serious technical challenge in this parametrization. The domain of the parametrizing functions takes the form of a wedge $\rho \in [0, +\infty[$, $\tau \in [0, \rho^2/2]$, which is nontrivial from the numerical perspective.

Most NPRG studies of discrete anisotropies so far relied on the expansion in both ρ and τ invariants [65, 77, 129, 130]. While this approach seems to be well-suited for the three-dimensional models, close to two dimensions the field expansion seems not to converge properly even in the isotropic models. Additionally, it seems that to properly recover the KT transition, present in two dimensions when anisotropies vanish, one needs to retain the functional dependence with respect to the $O(2)$ invariant ρ [106, 114–117, 121, 122]. We therefore introduce an intermediate scheme, in which we truncate $\mathcal{F}$ in powers of τ and treat ρ on the functional level.

The truncation in τ reduces the dimension of the domain of $\mathcal{F}$ for a price of increasing the number of the parametrizing functions. The LPA and $O(\partial^2)$ DE

ansätze for the τ-expanded approach at the $O(\tau)$ order read:

$$\Gamma_{\mathrm{E}}^{\mathrm{LPA}} = \int_{\boldsymbol{x}} \Big\{ U(\rho) + \tau U^1(\rho) + \frac{1}{2} \left(\partial_\mu \phi^i\right)^2 \Big\}, \tag{2.49a}$$

$$\begin{aligned} \Gamma_{\mathrm{E}}^{\partial^2} = \int_{\boldsymbol{x}} \Bigg\{ & U(\rho) + \tau U^1(\rho) + \frac{Z_\sigma(\rho) + \tau Z_\sigma^1(\rho)}{2} \left(\partial_\mu \phi^i\right)^2 \\ & - \frac{Z_\sigma(\rho) - Z_\pi(\rho) + \tau \left[Z_\sigma^1(\rho) - Z_\pi^1(\rho)\right]}{4\rho} \left[\left(\phi^1 \partial_\mu \phi^2\right)^2 + \left(\phi^2 \partial_\mu \phi^1\right)^2 \right] \\ & + T(\rho) \phi^1 \phi^2 \partial_\mu \phi^1 \partial_\mu \phi^2 \Bigg\}. \end{aligned} \tag{2.49b}$$

The subscript E of the effective action Γ_{E} stands for "expanded". The $O(2)$ symmetry is restored to the ansätze when the functions U^1, Z_σ^1, Z_π^1 vanish identically and $T = \frac{Z_\sigma - Z_\pi}{2\rho}$.

A further improvement of the numerical efficiency might be achieved by a replacement $T \to T' + \frac{Z_\sigma - Z_\pi}{2\rho}$ in the ansatz (2.49b). In this way, we separate the isotropic and anisotropic contributions to the flow of the effective action. The β_T function contains both isotropic and anisotropic contributions, while $\beta_{T'}$ - vanishes in the isotropic models. Thus, β_T contains the redundant information already carried in the β_{Z_σ} and β_{Z_π}; removing that redundancy should lead to some reductions in the flow equations. Moreover, having a purely anisotropic $\beta_{T'}$ safeguards against the anisotropies being accidentally generated by numerical errors in the integration of the RG flow.

In Chapter 4, we investigate the character of the cubic perturbations to the $O(2)$-symmetric model in varying dimensions. Apart from the physical questions, a significant part of the discussion therein will be devoted to a comparison of the efficacy of the fully functional approach in the polar decomposition (ρ, θ) representation and the τ-expanded approach.

Chapter 3

Cardy-Hamber scenario revisited

> Thunder in the other course of heaven
> Things cannot be destroyed once and for all
>
> Pink Floyd, *Chapter 24*

In this chapter, we discuss our contributions to reassess and verify the scenario put forward by Cardy and Hamber (CH). In Sec. 3.1, we offer a detailed reexamination of the perturbative CH-style analysis. We attempt to offer a better intuition about the fixed-point collision by charting the trajectories followed by the fixed points upon shifting dimension. We highlight the fact, that the CH scenario implies the existence of a quasi-long-range ordered (QLRO) low-temperature phase below two dimensions for $N_c(d) < N < 2$ and show that the universal anomalous dimension η of the low-temperature phase can be calculated perturbatively. This section constitutes a, hopefully, more pedagogical, restatement of the original CH analysis [1] with an emphasis placed on insights drawn from later contributions [3, 57, 58].

In Sec. 3.2 we address some possible concerns about the suitability of our methodology for investigating the CH scenario. First, we gauge the capacity of the derivative expansion (DE) to detect nonanalyticities. To that end, we compare the results of our calculations with the exact expressions for the critical exponents featuring nonanalyticities, but in a context distinct from the CH scenario. Subsequently, we discuss the role of topological excitations in the CH scenario and whether they can be captured within the framework of the DE. The results of this section were originally presented in Ref. [2].

Sec. 3.3 addresses the CH claims in the top-right quadrant of the (d, N) plane $[d > 2,\ N > 2]$. Contrary to the perturbative analysis, the nonperturbative calculations show no apparent nonanalyticity of several critical exponents. We do, however, note a cross-over in the behavior of the critical exponents occurring

close to the presumed position of the supposed line of nonanalyticities. These cross-overs are also associated with the rapid departure of the nonperturbative renormalization group (NPRG) results from the predictions of the $2+\epsilon$ expansion. Finally, our analysis of the subdominant renormalization group (RG) eigenvalue excludes the possibility of the fixed point (FP) collision occurring in the manner outlined by Cardy and Hamber, except perhaps for dimensions very close to two. The results and conclusions presented in this section come from Ref. [2].

Sec. 3.4 is devoted to the consequences of the CH scenario in the bottom-left quadrant of the (d, N) plane [$d < 2,\ N < 2$]. In this region, our results align with the CH scenario. We identify the two FP solutions and track their critical exponents across the quadrant. As expected, close to two dimensions, the critical exponents stand in good agreement with the prediction of the $2 + \epsilon$ expansion. Finally, we chart the line $N_c(d)$ and show how it compares to the predictions of CH and of Ref. [58]. This section discusses the results originally published in Ref. [3].

In Sec. 3.5, we conclude this chapter with a summary of our findings and a brief discussion.

We emphasize that this chapter is not concerned with obtaining the most accurate estimates of the critical exponents across the (d, N) plane. Our goal is to understand the general trends in the behavior of the critical exponents, verify the predictions of the CH scenario, and estimate the shape of the CH line. For this reason, throughout the present chapter, we do not employ the methodology for estimating the error bars and often refrain from optimizing our estimates via the principle of minimal sensitivity (PMS).

The NPRG flow equations used in the calculations described in this chapter are presented in Appendix A.

3.1 Perturbative analysis

The CH reasoning is based on the assumption that the RG equations of the $O(N)$ models should be analytical in the (d, N) plane. If that is true, then we should be able to derive a unified set of RG equations valid in the entire plane. Of course, we should not hope to recreate the exact RG functions for the entire plane, but we could combine the perturbative β functions to widen their range of applicability.

The idea of combining insights from different perturbative schemes has been applied in several different contexts. Ref. [131] uses the fact, that the $2+\epsilon$ and the large-N expansions overlap to any order in a double expansion to obtain the $O(\epsilon^4)$ coefficients of the critical exponents. Ref. [132], on the other hand, combines the $2 + \epsilon$ and the $4 - \tilde{\epsilon}$ expansions to perform a variational resummation aiming to extract the critical exponents in three dimensions.

A similar, and notably earlier, approach to combining the perturbative β functions came from Cardy and Hamber [1]. They proposed to combine the RG equations of the $2+\epsilon$ expansion [see Eq. (1.4)] with the Kosterlitz-Thouless (KT) recursion relations [1] [see Eq. (1.8)]. The universal behavior described by such a system of equations should, in principle, be physical in the vicinity of the KT point $(d, N) = (2, 2)$ in the (d, N) plane. This is a substantial improvement compared to the KT theory restricted to the KT point and the $2+\epsilon$ expansion valid only for $\frac{d-2}{N-2} \ll 1$.

The equations proposed by CH read:

$$\beta_g^{\mathrm{CH}} = -\epsilon g + (N-2) f(g, N) + 4\pi^3 y^2 + O(y^4), \tag{3.1a}$$

$$\beta_{y^2}^{\mathrm{CH}} = \left(4 - \frac{2\pi}{g}\right) y^2 + O(y^4). \tag{3.1b}$$

Importantly, the function $f(g, N)$ in Eq. (3.1a) so far has only been studied perturbatively in powers of g. We emphasize that the following reasoning is fairly general and does not require the knowledge of the exact shape of $f(g, N)$, only the assumption that $f(g, 2)/g$ is a monotonic increasing function for small values of g. However, later on, we are going to exploit the expansion of f to the highest known order [131]:

$$\begin{aligned} f(g, N) = {} & \frac{g^2}{2\pi} + \frac{g^3}{4\pi^2} + \frac{g^4(N+2)}{32\pi^3} \\ & - \frac{g^5\left(N^2 - 18N\zeta(3) - 22N + 54\zeta(3) + 34\right)}{192\pi^4} + O(g^6). \end{aligned} \tag{3.2}$$

We also note, that while the spin-wave coupling g retains a clear physical interpretation in the entire (d, N) plane, this is not true for y^2. At the KT point $[(d, N) = (2, 2)]$, y^2 describes the vortex fugacity, but its physical interpretation becomes somewhat ambiguous for other values of d and N. In specific contexts, parameters analogous to y^2 may retain their physical meaning in different dimensions [52, 133, 134].

Due to their perturbative nature, Eqs. (3.1) have to be analyzed in the direct vicinity of the KT point. In the following reasoning, $N-2$ and y^2 will be treated as small quantities of order not larger than $O(\epsilon)$. With that assumptions, Eqs. (3.1) admit two families of nontrivial fixed-point solutions. One of the families is identical to that of the $2+\epsilon$ expansion of Brézin and Zinn-Justin (BZJ) [41, 42],

$$\epsilon g_{\mathrm{BZJ}} = (N-2) f(g_{\mathrm{BZJ}}, N) + O(\epsilon^2), \quad y^2_{\mathrm{BZJ}} = O(\epsilon^2). \tag{3.3}$$

[1] The KT recursion relations are derived perturbatively to the leading order in the vortex fugacity y^2.

It exists whenever $\hat{\epsilon} = \epsilon/(N-2)$ is positive and not too large. Assuming the form (3.2) of the function f, the condition (3.3) can be satisfied by several nontrivial solutions, of which all but one can be discarded as nonphysical artifacts of the g expansion. From now on, we shall use the term BZJ FP to describe the solution to (3.3) with the lowest positive value of g_{BZJ}, which is the only physical. When the BZJ FP exists, the spin-wave coupling is found perturbatively in terms of $\hat{\epsilon}$:

$$g_{\mathrm{BZJ}} = 2\pi\hat{\epsilon} + O(\hat{\epsilon}^2). \tag{3.4}$$

The second fixed-point family reads

$$g_{\mathrm{NF}} = \frac{\pi}{2} + O(\epsilon), \quad y^2_{\mathrm{NF}} = \frac{\Delta}{4\pi^3} \tag{3.5}$$

where

$$\Delta = \epsilon\frac{\pi}{2} - (N-2)f\left(\frac{\pi}{2}, N\right) + O(\epsilon^2). \tag{3.6}$$

The CH Eqs. (3.1) in a form restricted to $N = 2$ were first derived by Nelson and Fisher (NF) in Ref. [56] [see Eq. (1.9)]. The solution (3.5) is essentially an extension of the solution to the NF equations to $N \neq 2$, hence we call this family the NF FPs. The NF FP does exist only in the subset of the (d, N) plane where Δ is positive.

The parameter Δ plays an essential role in the following analysis, as its sign determines the existence and stability of the fixed-point solutions to Eqs. (3.1). Moreover, the condition $\Delta = 0$ defines the Cardy-Hamber line at which the two families of FPs collide. A sketch of the (d, N) plane including the CH line is presented in Fig. 3.1.

The CH analysis predicts a widely different physical behavior for N above and below two. For $N > 2$, the FP collision should lead to a nonanalyticity of the critical exponents across the CH line, while for $N < 2$ the FP collision marks the lower critical dimension $d_c(N)$ [or conversely $N_c(d)$]. These two cases are discussed separately in the following sections.

3.1.1 N larger than two

We first analyze the top halfplane [$N > 2$] of the (d, N) plane [see Fig. 3.1]. In this setting, below two dimensions there are no nontrivial FP solutions and the zero-temperature FP [$g^* = 0$] is unstable; there is no phase transition. We therefore focus only on the top-right quadrant [$d > 2$, $N > 2$].

Fig. 3.2 shows how the FP solutions to the CH Eqs. (3.1) for $N = 2$ and $N = 2.5$ evolve with the shifting dimension. When $N = 2$, the picture is fairly simple. In two dimensions, we find the KT line of FPs with the relevancy of the vortex fugacity y^2 changing at the point $g^* = \pi/2$, while in higher dimensions

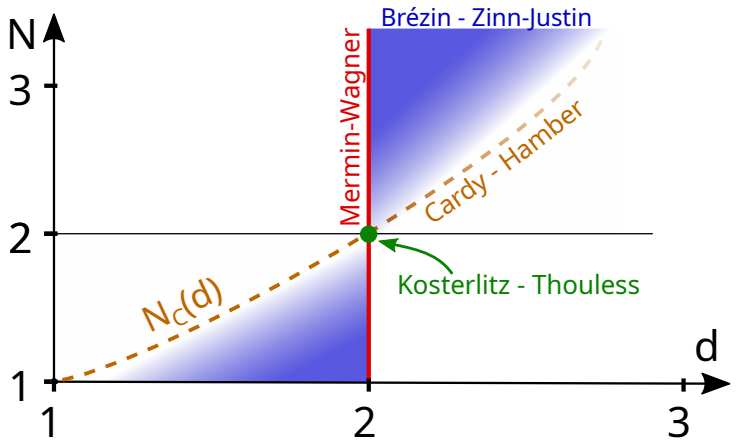

Figure 3.1: Schematic representation of the (d, N) plane in the vicinity of the Kosterlitz-Thouless point $(2, 2)$. The Mermin-Wagner line [$d = 2$, $N > 1$] separates the systems that support the long-range order at nonzero temperatures from those that do not. Blue shading denotes the region of the (d, N) plane where the parameter $\hat{\epsilon} = \frac{d-2}{N-2}$ is small and positive. The brown dashed line marks the Cardy-Hamber line $\Delta = 0$. For $d < 2$, the CH line coincides with $N_c(d)$, while for $d > 2$ it is a locus of the hypothetical nonanalyticity of the critical exponents. Figure from Ref. [3].

there is just one critical FP that springs from the point at which the vortices are marginal.

When N is larger than two, there are no lines of FPs. In low dimensions, Δ is negative [see Eq. (3.6)] which leads to an imaginary value of y_{NF} and a nonphysical character of the NF FP. We, therefore, only find the critical BZJ FP. With the growing dimension Δ increases until it reaches zero and the NF FP springs from the BZJ FP. Then the NF FP takes the role of the critical FP, as the BZJ FP develops a second unstable direction and becomes tricritical.

To develop a better intuition about the collision, it is useful to look at the evolution of the RG eigenvalues upon shifting the dimension. The two dominant eigenvalues of the BZJ and the NF FPs as functions of dimension are presented in Fig. 3.3. This chart also visualizes two important implications of the CH scenario: nonanalyticity of the critical exponents, and vanishing of the subdominant eigenvalue at the CH line. In the perturbative picture, the nonanalyticity takes the form of discontinuity of the first derivative of the eigenvalues. We note that in the exact picture, the nonanalyticity could take the form of discontinuity of any higher derivative. Possibly, it could even be avoided altogether if the collision is smooth enough. On the other hand, the vanishing of the subdominant eigenvalue is a necessary condition for the fixed-point collision to occur.

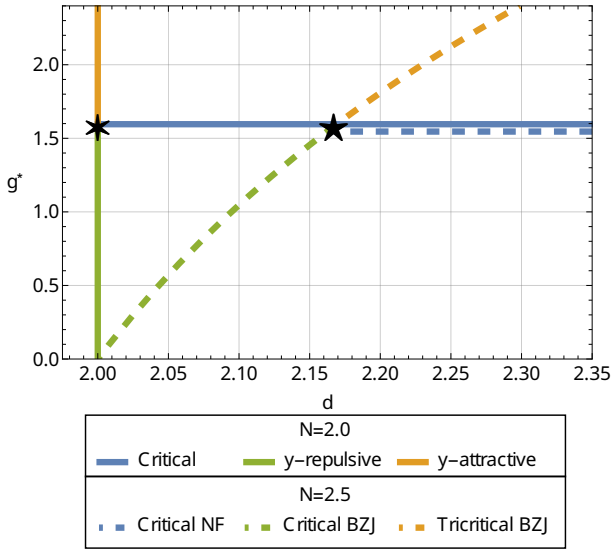

Figure 3.2: Fixed-point spin-wave coupling g^* solutions to Eq. (3.1) as functions of dimension. The $N = 2$ solutions [solid lines] are divided into three families: the critical FPs [blue], y-attractive FPs of the KT line of FPs [green], and y-repulsive FPs of the KT line of FPs [orange]. The $N = 2.5$ solutions [dashed lines] are similarly divided into three families: the critical NF FPs [blue], the critical BZJ FPs [green], and the tricritical BZJ FPs [orange]. Stars denote the points of collision between the NF and BZJ FP families. Both the blue horizontal lines correspond to $g^* = \pi/2$ and were separated slightly for clarity.

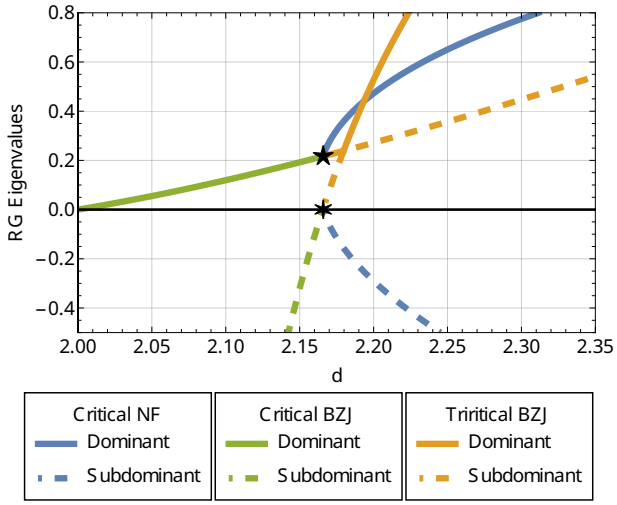

Figure 3.3: RG eigenvalues of the FP solutions to Eq. (3.1) as functions of dimension for $N = 2.5$. The dominant eigenvalues of each FP are marked by solid lines, and the subdominant eigenvalues by the dashed lines. Graph presents the eigenvalues of three families of FP solutions distinguished by colors: the critical NF FPs - blue, critical BZJ FPs - green, and the tricritical BZJ FPs - orange. Stars denote the values of the eigenvalues upon the FP collision.

3.1.2 N smaller than two

A different picture presents itself in the bottom-left quadrant of the (d, N) plane [see Fig. 3.1]. The CH paper notes that the NF FP is critical and controls the phase transition when $\Delta > 0$ and that there is no phase transition for $\Delta < 0$. However, Cardy and Hamber also state that only the NF FP is real for $N < 2$. It is nonetheless rather evident from Eq. (3.1a), that the BZJ FP also exists in this quadrant, and, as we argue below, controls the low-temperature phase present in the $\Delta > 0$ part of the (d, N) plane below two dimensions. This fact was first explicitly stated in Ref. [57] and alluded to earlier in Ref. [58].

For negative values of ϵ, the zero-temperature trivial fixed point $[g^* = 0]$ is unstable, which prevents the formation of the long-range order at any finite temperatures, in accord with the Mermin-Wagner theorem. However, at the same time, a new infrared stable FP appears. Specifically, for $\epsilon < 0$ and $\Delta > 0$, the BZJ FP is a stable finite-temperature FP which emerges from the zero-temperature FP as ϵ crosses zero. In this region, the NF FP controls the transition between the disordered and the QLRO phases.

Let us note, that at the BZJ FP the vortex fugacity vanishes. This means, that at this FP the condensation energy of a vortex diverges and the model can be described solely by spin waves. As a consequence, many properties of this FP,

including the leading RG eigenvalue $e_1 = \nu^{-1}$ and the anomalous dimension η, are identical to those predicted by the nonlinear-σ model, which opens a way to calculate the structure of correlations in the QLRO phase via the perturbative means of the $2 + \epsilon$ expansion. This remark was first presented in Ref. [3].

Above the CH line [see Fig. 3.1], when Δ becomes negative, the NF FP ceases to exist. At the same time, the BZJ FP attains a single relevant direction while its attraction domain shrinks to a subset of the $y^2 = 0$ line. This fixed point does not control any phase transition. This is because, as we deduce from Eq. (3.1), the RG flows cannot cross between the regions $y^2 = 0$ and $y^2 > 0$. The difference between these two regions concerns the presence of vortex-like excitations, which can appear when $y^2 > 0$, but cannot appear when $y^2 = 0$. For this reason, the models corresponding to those two regions are subject to very distinct physics. This thesis primarily focuses on the models with $y^2 > 0$. From this perspective BZJ FP acts simply as a repulsive FP for $\Delta < 0$. We, therefore, expect that no phase transition takes place for $\Delta < 0$ and consequently that the condition $\Delta = 0$ defines the line of lower critical dimensions [in the bottom-left quadrant of the (d, N) plane]. The CH scenario for the fixed-point collision for $N < 2$ is illustrated in Fig. 3.4.

To complete the picture we also present the RG eigenvalues of different FP solutions. The two dominant eigenvalues of the BZJ and the NF FPs as functions of dimension are presented in Fig. 3.5. The chart shows that, for $N < 2$, it is the dominant eigenvalue that vanishes upon the FP collision. Since the collision marks the lower critical dimension, there is no nonanalyticity of the critical exponents associated with the collision.

We emphasize the contrast between the physical implications of the CH scenario above and below $N = 2$. For $N > 2$, the collision takes place between the critical and the tricritical FPs. The second-order phase transition takes place between the disordered and the long-range ordered phases, and the critical exponents exhibit [within this approach] nonanalyticities at the line of the collisions [$\Delta = 0$]. For $N < 2$, on the other hand, the critical FP collides with the FP controlling the low-temperature behavior. The phase transitions take place between the disordered and the QLRO phases, and the line of the collisions marks the lower critical dimensions $d_c(N)$ [or conversely $N_c(d)$].

3.2 Suitability of the NPRG

Let us briefly depart from the discussion of the CH scenario. Since the derivative expansion is an approximation, there might be some objections regarding its suitability to analyze the exotic physics of the CH scenario. It is important to note, that the DE yields quite accurate values of the critical exponents for the $O(N)$

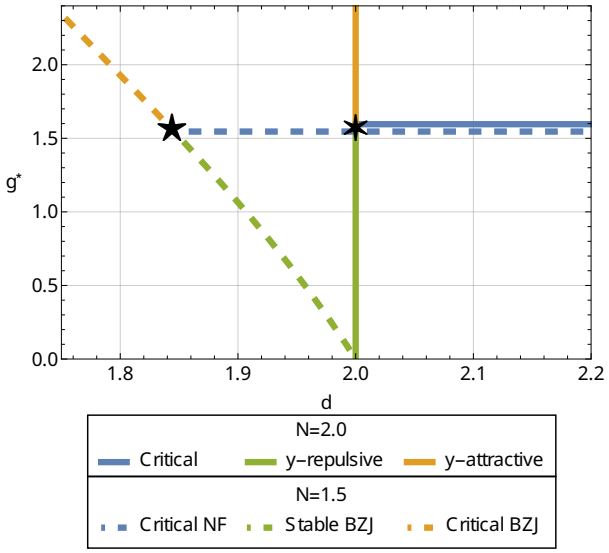

Figure 3.4: Fixed point spin-wave coupling g^* solutions to Eq. (3.1) as functions of dimension. The $N = 2$ solutions [solid lines] are divided into three families: the critical FPs [blue], y-attractive FPs of the KT line of FPs [green], and y-repulsive FPs of the KT line of FPs [orange]. The $N = 1.5$ solutions [dashed lines] are similarly divided into three families: the critical NF FPs [blue], the infrared stable BZJ FPs [green], and the critical [nonphysical] BZJ FPs [orange]. Stars denote the points of collision between the NF and BZJ FP families. Both the blue horizontal lines correspond to $g^* = \pi/2$ and were separated slightly for clarity.

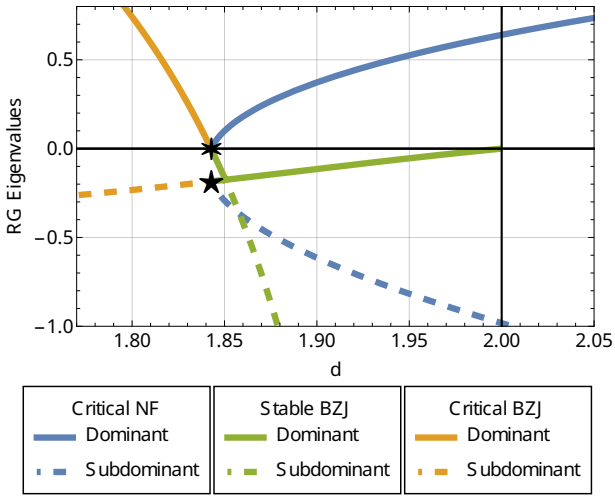

Figure 3.5: RG eigenvalues of the FP solutions to Eq. (3.1) as functions of dimension for $N = 1.5$. The dominant eigenvalues of each FP are marked by solid lines, and the subdominant eigenvalues by the dashed lines. Graph presents the eigenvalues of three families of FP solutions distinguished by colors: the critical NF FPs - blue, stable BZJ FPs - green, and the critical [nonphysical] BZJ FPs - orange. Stars denote the values of the eigenvalues upon the FP collision.

models with integer value (d, N) even at low orders of the expansion. Nevertheless, it remains unclear whether some important aspects of the $O(N)$ models' physics are not suppressed in this approach. In the present section, we address two significant concerns regarding its capacity for detecting nonanalyticities and capturing the effects of vortices.

3.2.1 Detecting nonanalyticities

The derivative expansion of NPRG is an approximate scheme based on numerical calculations. It is not immediately obvious that such a methodology is suitable to detect a nonanalytic behavior of the critical exponents, such as that predicted by the CH analysis. For this reason, we find it instructive to benchmark our method against an exact result predicting nonanalyticities. Such an exact reference point is provided by Ref. [135] presenting the exact values of the critical exponents in the two-dimensional models with $-2 \leq N \leq 2$. Crucially, in the limit $N \to 2$, both the inverse correlation length exponent ν^{-1} and the anomalous dimension η feature square-root-like nonanalyticities. In this section, we calculate these two critical exponents at the $O(\partial^2)$ order of the DE and compare our results with the exact ones to gauge the capacity of our methodology to detect nonanalyticities.

In two dimensional $O(N)$ models, the exact critical exponents are as follows

[135]:

$$\nu^{-1} = 4 - 2t \,, \qquad \eta = 2 - t/2 - 3/(2t) \,, \tag{3.7}$$

with t defined through $N = -2\cos(2\pi/t)$ on a branch $t \in [1, 2]$. For N close to two, the exponents are readily expanded in terms of $\delta = 2 - N$ as follows:

$$\nu^{-1} = \frac{4}{\pi}\sqrt{\delta} + O(\delta) \,, \qquad \eta = \frac{1}{4} + \frac{1}{4\pi}\sqrt{\delta} + O(\delta) \,. \tag{3.8}$$

These expressions reveal a manifest divergence of the first derivatives of the critical exponents in the limit $N \to 2^-$ providing a benchmark for our results.

The exponents ν^{-1} and η as obtained in our DE calculations are compared to their exact values in Fig. 3.6. Our results for ν^{-1} oscillate around the exact values, being underestimated close to $N = 2$ and overestimated for lower values of N. Our results for the anomalous dimension η as a function of N take shape very similar to the exact behavior with two exceptions. Our results are systematically overestimated by around 0.04 for most of the inspected values of N and feature a drop around $N = 2$ much more substantial than that observed in the exact behavior. Despite the differences, our results exhibit a manifest singularity of the first derivatives of the critical exponents in the limit $N \to 2^-$ in the form closely resembling the exact behavior.

To inspect this point further we performed a power-law fit for both critical exponents around $N = 2$. For ν^{-1} the fit yields an exponent of 0.45 fairly close to the exact value of 1/2. For the anomalous dimension, our results feature a drop significantly more rapid than the exact expression leading to a significantly overestimated exponent of around 0.77.

A mixed performance of the $O(\partial^2)$-order DE in this case calls for a comment. We believe, that the inaccuracies of our calculations stem mostly from two factors. Firstly, the presented results are not PMS-optimized; they were obtained with the near-optimal regulator [see Sec. 2.3.3]. Employing the PMS could offer particular improvement to our estimation of η, as in the $O(N)$ models at the $O(\partial^2)$ order the PMS value of η typically corresponds to the minimum as a function of α [see Fig. 2.6 and Ref. [21]], and therefore our results can be expected to lie above the PMS-optimized value.

The second, and arguably more significant, factor is the relatively low order of the DE employed in our calculations. We emphasize that the DE is known to be the most accurate when the dimension d is high and the anomalous dimension η is low [21, 23, 48, 99]. Thus, the two-dimensional $O(N)$ models [for $N \leq 2$] constitute a particularly unfavorable case for our methodology and a significant overestimation of η is to be expected. Despite the noted inaccuracies, our results unambiguously demonstrate that the $O(\partial^2)$ DE is capable of capturing the nonanalyticities of the critical exponents.

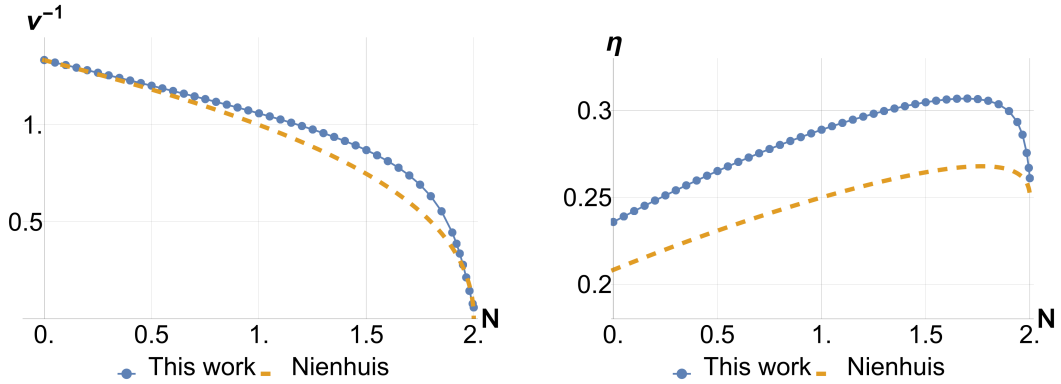

Figure 3.6: The critical exponents ν^{-1} and η as functions of N in two dimensions. The singular first derivatives at $N = 2$ are clearly visible. Figure from Ref. [2].

3.2.2 The role of vortices

The FP collision is not the only phenomenon predicted to occur at the CH line. The CH scenario also indicates that the relevance [in the RG sense] of vortex-like excitations changes upon crossing the CH line. Below the CH line [high dimensions, low N] vortices are supposedly relevant, while above the CH line [low dimension, high N] they become irrelevant.

The central role of the topological excitations raises a question about the capacity of the DE to capture the consequences of the CH scenario. Indeed, vortices [or other topological excitations] do not enter the DE description as separate degrees of freedom and it is not immediately obvious whether their effects are captured by our methodology. To explore this question we recall the discussion of the topological excitations in Sec. 1.1.3. In that section, we introduced several studies showing that in the absence of the topological excitations, some phase transitions would be either absent or belong to a completely different universality class. More precisely, when the topological excitations are suppressed:

- the KT transition of the two-dimensional XY model does not take place and the algebraic phase extends to arbitrarily large temperatures;
- the three-dimensional XY model remains ordered at any finite temperature and the phase transition does not take place [51];
- the phase transition in the three-dimensional Heisenberg model is either absent or belongs to a different universality class characterized by a very large anomalous dimension $\eta \approx 0.6$ [53–55].

As discussed in Sec. 2.4.1, the KT transition is fully captured with the DE only when the fine-tuned IR regulator is employed; when an arbitrary regulator is used,

the transition takes the form of an extremely sharp cross-over. Nevertheless, the picture presented by the $O(\partial^2)$ DE is clearly distinct from that of the spin-wave description expected for the model with suppressed vortices.

The picture presented by the two other examples is even more transparent. The DE calculations for these models show the behavior as expected of the models admitting the topological excitations, very accurately reproducing the expected values of the critical exponents [21]. This indicates that the relevant excitations are indeed captured within our methodology.

3.3 Analyticity of the critical exponents

In this section, we discuss the CH scenario in the top-right quadrant of the (d, N) plane $[d > 2, N > 2]$ within the framework of the NPRG. We search for the CH line addressing three distinct phenomena predicted by the CH scenario: nonanalyticity of the critical exponents $e_1 = \nu^{-1}$ and η, vanishing of the subleading RG eigenvalue e_2 and nonanalyticity of the fixed-point profiles [as functions of (d, N)].

In an attempt to detect the CH line, we identify a [functional] fixed point corresponding to (d, N) located far away from the expected nonanalyticity. This can be done by integrating the flow; tuning the initial condition so that the system flows sufficiently close to a fixed-point solution. We subsequently study the evolution of ν^{-1} and η as either d or N varies towards the region where the CH line should be found. In practice, we either gradually decrease d or increase N. The fixed point at (d, N) serves as the initial condition for the fixed-point equations at $(d - \delta d, N)$ or $(d, N + \delta N)$, which [after discretization] are solved using standard algebraic routines. We were able to scan the (d, N) plane and extract numerically the functions $\eta(d, N)$ and $\nu^{-1}(d, N)$ traversing the region where the CH line is expected.

We note, that the procedure of finding the fixed point becomes progressively harder when the dimension approaches two and the step in the (d, N) plane must then be tiny. This is [at least partially] related to the fact that, at low dimensions, the profile of the fixed-point effective potential acquires increasingly strong variation at large $\tilde{\rho}$. For selected choices of (d, N), we checked the results against those obtained by integration of the flow. We note that for $N > 2$ we were not able to solve the fixed-point equations in dimensions arbitrarily close to two, but anyway significantly lower than the anticipated position of the CH line.

Sections 3.3.1 and 3.3.2 are devoted to the analysis of the inverse correlation length exponent ν^{-1} and the anomalous dimension η along horizontal and vertical trajectories in the (d, N) space respectively. In a region where the CH line is expected, we note a cross-over behavior sharpening as the dimension becomes close to two, yet without direct indications of true nonanalytic behavior. In Sec.

3.3.3, we investigate the subleading RG eigenvalue e_2 along vertical trajectories in the (d, N) plane; e_2 shows no signs of nonanalyticity and stays widely separated from zero. Finally, Sec. 3.3.4 explores the functional profiles of the RG FPs. We again identify a cross-over behavior, sharpening upon approaching two dimensions but without explicitly nonanalytic behavior.

The results presented in this section are obtained with the near-optimal regulator [Wetterich regulator with $\alpha = 2$], rather than optimized via the PMS [see Sec. 2.3.3]. We verified the independence of our conclusions with regard to this choice.

3.3.1 d-dependence

Fig. 3.7 presents the dependence of the inverse correlation length exponent ν^{-1} and the anomalous dimension η for a sequence of values of N. The left panel of the figure, presenting the exponent ν^{-1}, shows a clear distinction between the case of $N = 2$ and the cases of $N > 2$. In high dimensions, all curves [except that for $N = \infty$] follow a similar trajectory. Upon decreasing the dimension, one by one, they rapidly transition from the low-N-like [high-dimension-like] behavior to the large-N-like behavior. This transition occurs for any finite $N > 2$ upon crossing some characteristic dimension $\tilde{d}_c(N)$. The curve corresponding to $N = 2$ does not feature this kind of transition. Instead of vanishing smoothly, it tends to zero nonanalytically in a square-root-like fashion in agreement with the CH-style analysis. The behavior of ν^{-1} is reminiscent of the CH scenario, however, the observed transition between the low-N-like and the large-N-like behaviors takes the form of an apparently smooth cross-over rather than the nonanalytic cusp predicted in the CH scenario [see Fig. 3.3].

A similar picture can be seen in the right panel of Fig. 3.7 presenting the anomalous dimension η as a function of the dimension. In high dimensions, all the curves follow a similar trajectory which might be understood as the low-N-like behavior. Upon crossing some characteristic dimension $\tilde{d}_c(N)$ each of the curves corresponding to $N > 2$ detaches from this trajectory to approach zero in the limit $d \to 2$. In this case, however, the corrections to the $N = \infty$ value are more substantial than for ν^{-1}. We note that in low dimensions, our results for the anomalous dimension align very well with the predictions of the $2 + \epsilon$ expansion $\eta_{2+\epsilon} = \hat{\epsilon} + O(\hat{\epsilon}^2)$ with $\hat{\epsilon} = \frac{d-2}{N-2}$. The only curve not aligned with the predictions of the $2 + \epsilon$ expansion is, as expected, the one corresponding to $N = 2$. In the limit $d \to 2$, the anomalous dimension reaches a nonzero value $\eta(d \to 2, N = 2) \approx 0.27$ in an apparently nonanalytical fashion.

The transition between the low-N-like and the large-N-like behavior presents a picture quite similar to that of the CH scenario and it might be tempting to associate the characteristic dimension $\tilde{d}_c(N)$ with the CH line. It is immediately

obvious that $\tilde{d}_c(N)$ increases with N, and takes the value $\tilde{d}_c(2) = 2$ in agreement with the CH-style analysis. Furthermore, the line $\tilde{d}_c(N)$ seems situated quite closely to the predicted position of the CH line. However, we emphasize that the observed transition is smooth [or at least of the $\mathcal{C}^2$ type] and does not provide any signs of the FP collision. On the contrary, it indicates a smooth transition between the regimes controlled by the $2+\epsilon$ and $4-\tilde{\epsilon}$ expansions.

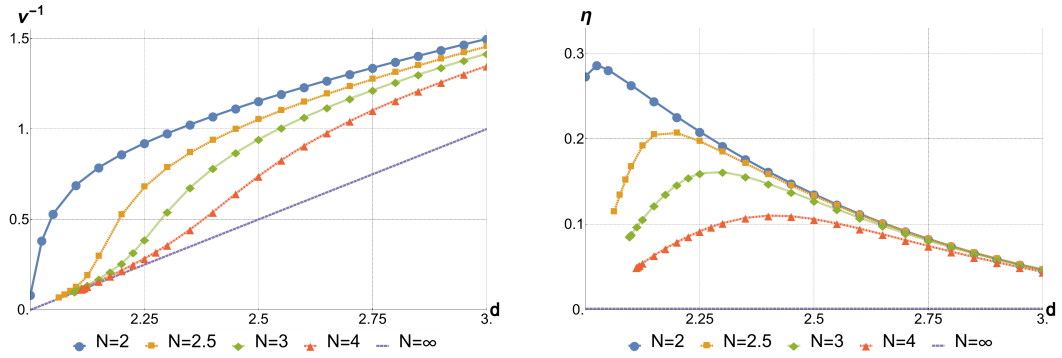

Figure 3.7: The critical exponents ν^{-1} and η as functions of d for a sequence of values of N. The lines corresponding to $N = \infty$ present the exact results of the large-N expansion: $\nu^{-1}(d, N = \infty) = d - 2$, and $\eta(d, N = \infty) = 0$. Figure form Ref. [2].

3.3.2 N-dependence

An analysis similar to that of the previous section can also be performed along vertical lines in the (d, N) plane. The N-dependence of the ν^{-1} and η exponents calculated in a sequence of dimensions is shown in Fig. 3.8. We first note, that the data marked by the blue circles was introduced in Sec. 3.2.1 where we compared the DE results to the exact expressions of Ref. [135]. Let us recall that in two dimensions both exponents feature a square-root-like nonanalyticity in the limit $N \to 2^-$. When the dimension is raised, the square-root-like nonanalyticity is progressively smoothed into a cross-over. At the large-N side of the cross-over, our results precisely match the predictions of the $2+\epsilon$ expansion [131]. Interestingly, the divergence between the $2+\epsilon$ expansion and our results is extremely rapid and occurs very closely to the spot of the cross-over.

At this point, we are ready to offer a phenomenological definition of the position of the cross-over line $\tilde{N}_c(d)$. Let us note that, at the KT point $[(d, N) = (2, 2)]$, $\eta(d = 2, N)$ is discontinuous while $\nu^{-1}(d = 2, N)$ features a discontinuity of the first derivative with respect to N. Although the discontinuity of η becomes smoothed above two dimensions, it leaves a fingerprint in the form of a very large [negative]

value of the first derivative $\partial_N \eta$. On the same note, the discontinuity of $\partial_N \nu^{-1}$, leaves a fingerprint in the form of a large [positive] value of the second derivative $\partial_N^2 \nu^{-1}$. Thus, the extrema of $\partial_N^2 \nu^{-1}$ and $\partial_N \eta$ should indicate the line of the cross-overs $\tilde{N}_c(d)$.

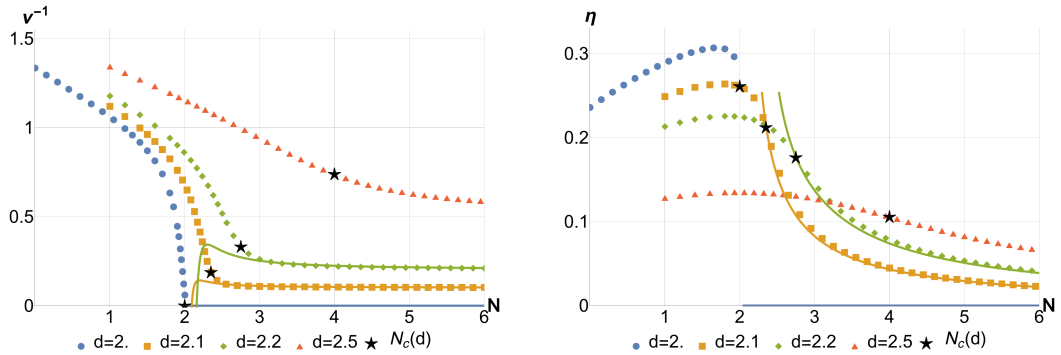

Figure 3.8: The critical exponents ν^{-1} and η as functions of N in a sequence of dimensions. Continuous lines denote the $2+\epsilon$ expansion predictions; the lines corresponding to $d = 2.5$ were removed to avoid obscuring the illustration. The stars indicate our estimate of $\tilde{N}_c(d)$ [see the main text]. Figure from Ref. [2].

These derivatives, along with the associated cross-over points, are plotted as functions of N in Fig. 3.9. The values at the extrema diminish [in absolute value] upon increasing dimension indicating progressive smoothing of the cross-overs between the low-N-like and the large-N-like behaviors. In fact, between dimensions $d = 2.75$ and $d = 3$, the maximum of $\partial_N^2 \nu^{-1}$ disappears altogether. We emphasize that these derivatives seem to diverge only at the KT point and provide no indication of nonanalyticities of any kind except at that point.

In Fig. 3.10, we sketch the line of cross-overs obtained by tracing the extrema of $\partial_N^2 \nu^{-1}$ and $\partial_N \eta$. Our two criteria for $\tilde{N}_c(d)$ precisely align with each other suggesting their common origin and possible physical implications. We also compare the obtained line of cross-overs $\tilde{N}_c(d)$ to the CH line as calculated in Ref. [1]. We find that in the vicinity of the KT point $(d, N) = (2, 2)$, the two curves lie very close to each other, although the inclination of $\tilde{N}_c(d)$ is slightly larger than that of the CH line. We relegate the discussion of this slight discrepancy to Sec. 3.4.3.

3.3.3 Subdominant eigenvalue

The perturbative CH-style analysis, at the highest available order of the perturbative expansion, predicts that the nonanalyticity of the critical exponents takes the form of discontinuity of first derivatives of the RG eigenvalues. In Sec. 3.1.1, however, we emphasized that in the exact picture, this nonanalyticity might be

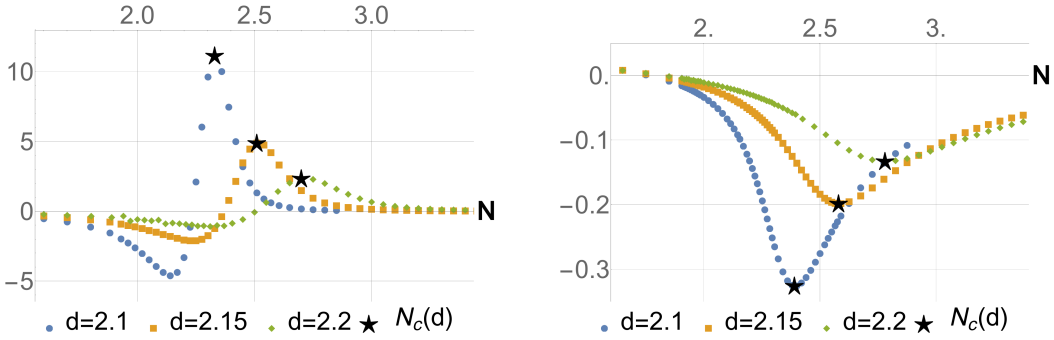

(a) $\partial_N^2 \nu^{-1}$ (b) $\partial_N \eta$

Figure 3.9: The derivatives of the critical exponents as functions of N in a sequence of dimensions. The stars indicate the maxima/minima, which serve as our defining property of the $\tilde{N}_c(d)$ line. Figure from Ref. [2].

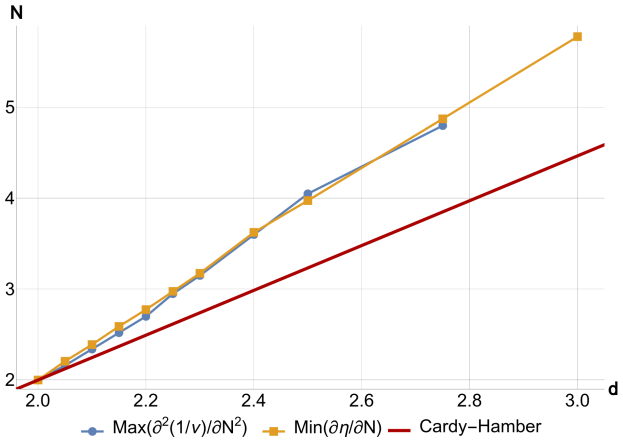

Figure 3.10: Loci of the maxima of $\partial_N^2 \nu^{-1}$ and the minima of $\partial_N \eta$ compared to the CH line [as calculated in Ref. [1]]. Figure from Ref. [2].

smoothed and take a different form or even be avoided altogether. Thus, the fact that our calculations do not reveal any obvious nonanalyticity of the critical exponents is not a sufficient argument to reject the CH scenario in the top-right [$d > 2$, $N > 2$] quadrant of the (d, N) plane.

In this section, we attempt to observe a phenomenon being a necessary consequence of the FP collision as predicted by the CH scenario in this part of the (d, N) plane. A collision of RG FPs is always associated with a vanishing of an RG eigenvalue corresponding to the eigenvector connecting the colliding FPs. In our case, we expect the subdominant RG eigenvalue e_2, connected with the leading correction to scaling exponent ω, to vanish identically on the CH line in dimensions

above two.

The results of our $O(\partial^2)$-order DE calculations for e_2 are presented in Fig. 3.11. The eigenvalue is calculated as a function of N in a sequence of dimensions $d > 2$. The figure shows that e_2 remains substantially separated from zero in the entire investigated region of the (d, N) plane. Furthermore, we can expect that the eigenvalue does not vanish at any larger value of N since our results converge quickly to the predictions of the large-N expansion [40].

There is an important deficiency in our methodology that has to be acknowledged at this point. The $O(\partial^2)$ order of the DE does not properly reproduce the vanishing of the subdominant eigenvalue at the KT transition in the two-dimensional $O(2)$ model. For this reason, we opted to only present the fully reliable data corresponding to dimensions sufficiently distant from two [$d \geq 2.25$], keeping in mind that the accuracy of the DE is expected to increase with increasing dimension and N.

We further note that in three dimensions our results can be treated as fully accurate. As a point of comparison for our results, we have shown the estimates of the $O(\partial^4)$ order DE from Ref. [21]. The results of Ref. [21] are entirely compatible with the best estimates for e_2 from other methods, such as the most recent Monte Carlo (MC) calculations, and were chosen as a reference due to the abundance of data points available for comparison. We emphasize that, in three dimensions, the differences between our results and those of Ref. [21] are almost negligible. Moreover, these more accurate results are even a bit further separated from zero than ours.

Our results indicate that the subdominant eigenvalue e_2 is substantially separated from zero in dimensions $d \gtrsim 2.2$ for any value of N. As a consequence, the FP collision envisaged by Cardy and Hamber can only possibly take place in dimensions close to two, meaning that the CH line would have to either terminate at some point (d_t, N_t) or become vertical reaching the limit $N \to \infty$ in some finite dimension. Neither of these possibilities can be supported by available perturbative arguments or any of our findings. This leads us to believe that the CH prediction for the FP collision is not realized in the top-right [$d > 2$, $N > 2$] quadrant of the (d, N) plane.

Rejecting the CH scenario, however, we are left with an intriguing question regarding the mechanism of the changing relevance of vortices. As argued in Sec. 1.1.3 and reiterated in Sec. 3.2.2, suppression of vortices and hedgehogs in the three-dimensional $O(2)$ and $O(3)$ models changes the universality class (UC) of the transition indicating the RG-sense relevance of these topological excitations. Our results properly capture the vortex-dominated physics of these models and reproduce the predictions of the vortex-suppressing $2 + \epsilon$ expansion below the line of the cross-overs. This suggests that vortices should be relevant above the cross-

over line and irrelevant below. This is further supported by Ref. [136] arguing that the $2+\epsilon$ expansion continued to three dimensions should describe the CP^1 UC [clearly distinct from the Heisenberg UC]. With the CH scenario rejected, the mechanism of the changing relevance remains unknown and calls for future clarification.

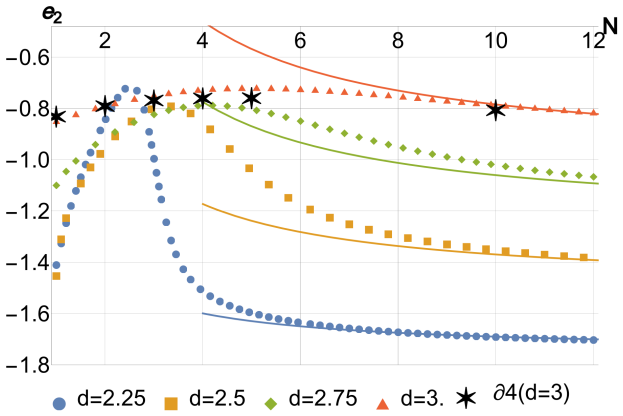

Figure 3.11: The subdominant eigenvalue e_2 as function of N in a sequence of dimensions. The continuous lines denote the predictions of the large-N expansion [40], and the stars denote the results of derivative expansion at order $O(\partial^4)$ for the three-dimensional models from Ref. [21]. Figure from Ref. [2].

3.3.4 Fixed-point profiles

In the CH scenario, we can identify entities suffering from nonanalyticities other than just critical exponents. Recalling Fig. 3.2 we can observe that the spin-wave coupling g^* of the critical FP exhibits a nonanalyticity upon the FP collision. A similar behavior can be expected to occur in different RG schemes describing the same UC. Although the FP structure is not a universal feature, its exploration might offer us a better understanding of the physics underlying the cross-over observed in the behavior of critical exponents.

Fig. 3.12 presents the evolution of the functions parametrizing the FP action upon shifting dimension. In three dimensions, the form of the effective potential $\tilde{U}$ is almost identical to the "mexican-hat" potential[2], while the fluctuation suppressors $\tilde{Z}_\sigma$ and $\tilde{Z}_\pi$ only negligibly differ from unity. In other words, the effective

[2]Observe that the right panel of Fig. 3.12 presents the first derivative of the effective potential $\tilde{U}'(\tilde{\rho})$. The derivative $\tilde{U}'(\tilde{\rho})$ is essentially linear in $\tilde{\rho} = \phi^i\phi^i/2$ meaning that the potential itself is of order 4 in terms of the order parameter $\boldsymbol{\phi}$.

action very much resembles the action of the ϕ^4 model with a weak quartic coupling, highlighting the accessibility of the three-dimensional model to perturbative description via the $4 - \tilde{\epsilon}$ expansion.

Upon lowering the dimension we observe slow evolution - the minimum of the local potential $\tilde{U}^*$ becomes more pronounced, while the value of $\tilde{Z}_\pi$ around the minimum becomes relatively low. $\tilde{Z}_\sigma$ remains relatively static until the CH [cross-over] line is reached. Below the cross-over line, $\tilde{Z}_\sigma$ begins to grow rapidly, strongly suppressing longitudinal fluctuations of the order parameter. The structure of the FP in dimension $d = 2.05$ characterized by a steep local potential and suppressed longitudinal fluctuations, effectively trapping the order parameter in the vicinity of the local potential's minimum, is reminiscent of the nonlinear-σ model. Let us note that topological excitations such as vortices and hedgehogs induce strong longitudinal fluctuations of the order parameter. Therefore, our results suggest a decreasing proliferation of such excitations in the critical state with the lowering dimension. Furthermore, the evolution of the FP structure implies that the observed cross-over line might be interpreted as a rapid yet smooth transition between the perturbative regimes of the $2 + \epsilon$ and the $4 - \tilde{\epsilon}$ expansions.

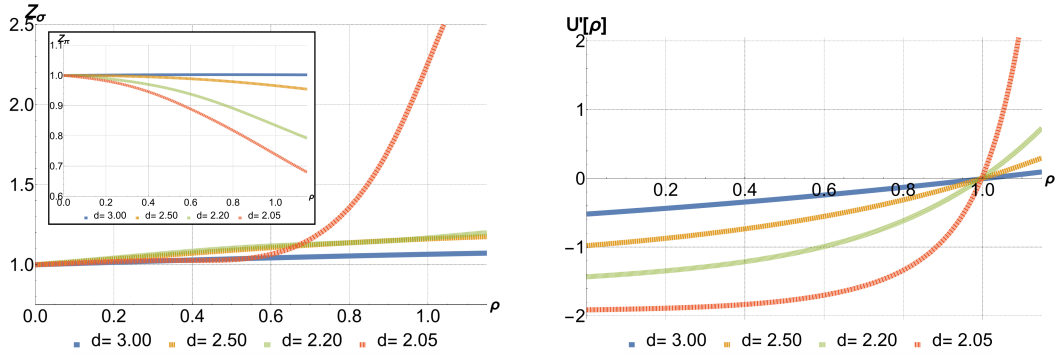

Figure 3.12: Critical fixed points for $N = 2.5$ in a series of dimensions. The left panel shows the fluctuations suppressors: longitudinal $\tilde{Z}_\sigma(\tilde{\rho})$ [main plot] and transverse $\tilde{Z}_\pi(\tilde{\rho})$ [inset]. Particularly visible is the drastic [but smooth] increase of $\tilde{Z}_\sigma(\tilde{\rho})$ upon crossing the CH line located slightly below $d = 2.2$. The right panel shows the derivative of the local potential $\tilde{U}'(\tilde{\rho})$. The axes were rescaled, so that the minimum of the local potential always lies at $\tilde{\rho} = 1$. Figure from Ref. [2].

Let us explore further the FP structure around the minimum of the local potential $\tilde{\rho}_0$. Fig. 3.13 presents the dimension dependence of the fluctuation suppressors $\tilde{Z}_\sigma$ and $\tilde{Z}_\pi$ as well as the second derivative of the local potential $\tilde{U}''$ evaluated at $\tilde{\rho}_0$. Like in Fig 3.7, we observe the curves corresponding to different values of N follow a common trajectory in high dimensions and detach from it one by one upon crossing some characteristic dimension. The cross-over dimensions, defined

by the local maxima of $U''(\tilde{\rho}_0)$, the local minima of $\tilde{Z}_\sigma(\tilde{\rho}_0)$, as well as the inflection points of $\tilde{Z}_\pi(\tilde{\rho}_0)$, lie very close to each other and coincide with the CH line of cross-overs described in Sec. 3.3.2. This shows that the unusual behavior of the critical exponents is also reflected by the changing structure of the FPs. Importantly, the investigated quantities show no indication of nonanalyticity providing further evidence against the FP collision predicted in the CH scenario.

Fig. 3.12 can also serve to illustrate the numerical difficulties encountered in our calculations. The first problem is related to the propagator poles and was discussed in more detail in Sec. 2.4.2. The right panel of Fig. 3.12 shows how the minimal value of $\tilde{U}'(\tilde{\rho})$ steadily converges to $-\alpha$ as the dimension approaches two[3]. As this happens, the propagator poles, located close to $q^2 = -\alpha - \tilde{U}'(\tilde{\rho})$, approach the real axis greatly inflating the numerical effort necessary for accurate resolution of the momentum integrals in the β functions.

The second problem is related to the accuracy of the employed discretization scheme. The error of the discretization is bounded by the magnitude of high-order derivatives of the discretized function. In Fig. 3.12, we observe that $\tilde{U}'$, $\tilde{Z}_\sigma$, and to a lesser extent $\tilde{Z}_\pi$ develop more complex shapes as the dimension approaches two. As a consequence, their derivatives grow in magnitude and increase the discretization errors. Further discussion of the discretization scheme is presented in Appendix B.1.

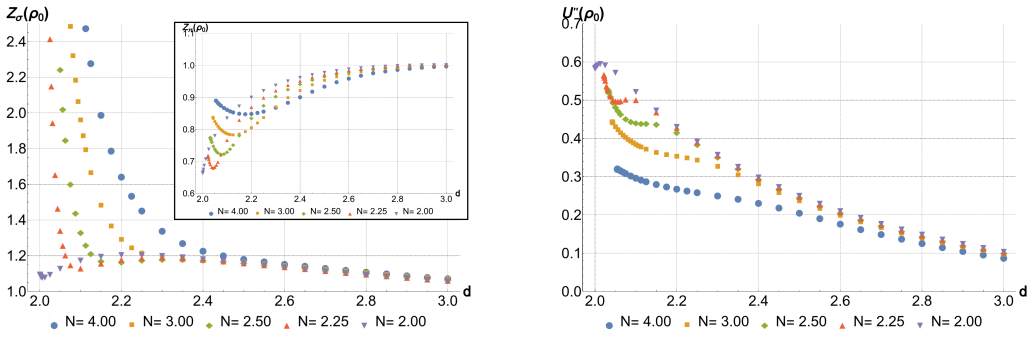

Figure 3.13: Critical fixed-point parameters at the minimum $\tilde{\rho}_0$ of the local potential as a function of the dimension and N. The left panel shows the fluctuations suppressors: longitudinal $\tilde{Z}_\sigma(\tilde{\rho}_0)$ [main plot] and transverse $\tilde{Z}_\pi(\tilde{\rho}_0)$ [inset]. The right panel shows the second derivative of the local potential $\tilde{U}''(\tilde{\rho}_0)$. Figure from Ref. [2].

[3]In the present calculation $\alpha = 2$.

3.3.5 Summary

In this section, we have explored the CH scenario in the top-right $[d > 2,\ N > 2]$ quadrant of the (d, N) plane from the NPRG perspective. Firstly, we have investigated the evolution of the inverse correlation length exponent ν^{-1} and the anomalous dimension η across the quadrant. Our calculations have provided no indication of the nonanalytic behavior of these exponents except at the KT point $(d, N) = (2, 2)$. Instead, we have observed a smooth cross-over between two clearly distinct regimes of exponents' behavior. Curiously, the cross-over closely coincides with the departure of our results from the predictions of the $2 + \epsilon$ expansion and occurs in close proximity to the expected position of the CH line. It might be argued that the cross-over line is related to the changing relevance of the vortices, although a mechanism through which this might occur remains unclear.

Further, we have analyzed the behavior of the subdominant RG eigenvalue e_2 across the top-right quadrant of the (d, N) plane. Knowing that the FP collision predicted by the CH-style analysis cannot take place without vanishing e_2, we have searched for a domain in the quadrant where $e_2 = 0$. Our results present e_2 widely separated from zero in dimensions $d \gtrsim 2.2$ for any value of N. Although our methodology did not allow for an accurate resolution of the subdominant eigenvalue in dimensions very close to two, our calculations unambiguously exclude the possibility of the CH-predicted FP collision. We cannot rule out that the CH scenario does take place in a narrow strip around two dimensions. However, such a phenomenon is supported by neither the CH-style analysis, our results, nor the $2 + \epsilon$ and large-N expansions. On the other hand, it is also possible that the FP collision is an artifact of the perturbative expansion, and that it disappears in the exact treatment or when higher-order terms are included.

Finally, we have examined the evolution of the functional profiles of the FP profiles upon shifting the dimension. The structure of the FP effective action interpolates between the forms resembling the ϕ^4 model in high dimensions and the nonlinear-σ model in dimensions close to two. Importantly, the FP structure presents no indication of nonanalyticity anywhere in the investigated region. However, some FP couplings do exhibit a smooth cross-over behavior coinciding with the cross-overs of the critical exponents.

In summary, our NPRG calculations stand in strong disagreement with the CH scenario. Although we do observe cross-over behaviors in close vicinity of the predicted position of the CH line, our results clearly reject the FP-collision scenario except possibly in dimensions very close to two. Furthermore, our results indicate that the CH line, although possibly physically relevant, is just a line of cross-overs that sharpen to a true nonanalyticity only in the limit $(d, N) \to (2, 2)$.

3.4 QLRO low-temperature phase

In the previous section, we have shown that our NPRG calculations do not support the CH scenario for the nonanalyticity of the critical exponents in the $d > 2$, $N > 2$ quadrant of the (d, N) plane. In this section, we turn our attention to the bottom-left quadrant [$d < 2$, $N < 2$]. There, CH scenario predicts that a low-temperature phase takes the form of the QLRO rather than the long-range order. Moreover, we search for the universal exponents characterizing the critical point and the QLRO phase, and for the line of the lower critical dimensions $N_c(d)$.

In the bottom-left quadrant of the (d, N) plane, the FP collision scenario is strongly supported by the NPRG calculations. This is clearly shown in Fig. 3.14 presenting the evolution of the anomalous dimensions of the critical and the QLRO[4] RG FPs upon decreasing the dimension. For $1 < N < 2$, the two anomalous dimensions rise slowly with the decreasing dimension and converge rapidly upon the FP collision at the lower critical dimension $d_c(N)$. The data presented in Fig. 3.14 has been obtained at the LPA' level with a minimal field truncation [see Sec. 2.2.3]. Throughout this section, this minimal scheme will serve a supplementary role to the functional $O(\partial^2)$-order DE scheme whenever the functional results could not be obtained. The rest of the present section provides a detailed description of this phenomenon from the NPRG perspective with a direct comparison to the predictions of the CH scenario. Results regarding the critical exponents presented throughout this section have been optimized according to the PMS [see Sec. 2.3.1].

3.4.1 Critical exponents

To explore the FP-collision scenario, we first analyze the inverse correlation length exponent ν^{-1} and the anomalous dimension η_c of the critical FP. This analysis is analogous to that of Sec. 3.3.1. Firstly, we identify an approximation of the critical FP in three dimensions by integrating the flows. Subsequently, we gradually decrease the dimension and solve the FP equation using the FP of dimension $d + \delta d$ as a guess in dimension d.

Fig. 3.15 presents the dependence of the leading RG eigenvalue $e_1 = \nu^{-1}$ on the dimension calculated for several values of N close to two. Once again, at high dimensions, we observe a similar trajectory followed by all the curves. However, the cross-over behavior observed for $N > 2$ is absent for $N \leq 2$. All the curves corresponding to $N \leq 2$ behave quite similarly approaching the lower critical dimension $d_c(N)$ [defined by $e_1 = 0$] in a singular fashion. The picture provided

[4]The name "QLRO FP" refers to the stable, finite-temperature FP controlling the QLRO, low-temperature phase in parts of the bottom-left quadrant of the (d, N) plane.

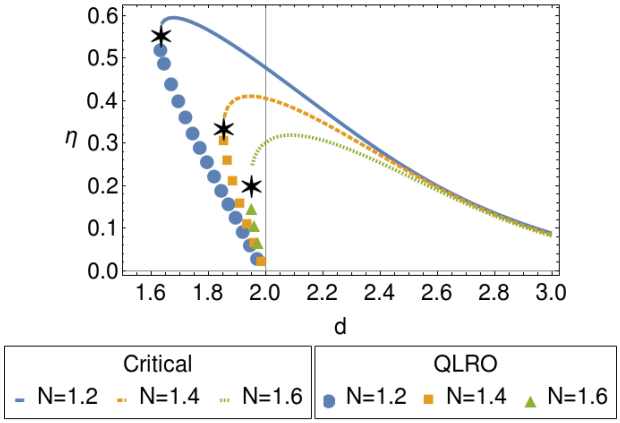

Figure 3.14: The dependence of the anomalous dimension of the critical and the QLRO fixed points on the dimension for a sequence of values of N within the minimal truncation. The points denote the anomalous dimension of the QLRO FP and the lines - the critical FP. The stars mark the collision of the FPs at the lower critical dimension as obtained within the minimal truncation. Figure from Ref. [3].

by our results for N below two is fully consistent with the CH-style analysis.

In Fig. 3.15, our results are juxtaposed with the predictions of the CH-style analysis. Attention should be paid to a remarkable agreement between the two calculations. We particularly emphasize, the agreement in the determination of the lower critical dimension in the direct vicinity of two dimensions. This is somewhat surprising taking into account the relatively low order of expansions employed in both calculations. However, we do note some quantitative differences. In particular, the CH scenario predicts a square-root-like behavior of e_1 in the vicinity of the lower critical dimension. The behavior of our results, although clearly nonanalytical, exhibits a decay with an exponent of around 0.5 only for $N = 2$, which then falls rapidly to around 0.3 for $N = 1.8$ and 0.2 for $N = 1.2$.

Let us now turn our attention to the anomalous dimension of the critical FP η_c. We emphasize, that the CH-style analysis does not offer any predictions for η_c. In Fig. 3.16 we compare the dimension dependence of the critical anomalous dimension as calculated by the functional scheme at the $O(\partial^2)$ order of the DE and the minimal scheme. Interestingly, the results of the functional approach show much weaker N-dependence than the minimal truncation and do not feature a sudden drop in η_c close to the lower critical dimension. The figure also highlights the well-established fact, that the minimal scheme tends to significantly overestimate the anomalous dimension; for our calculation, the minimal scheme inflates η_c by a factor between 1.5 and 2 compared to the functional approach.

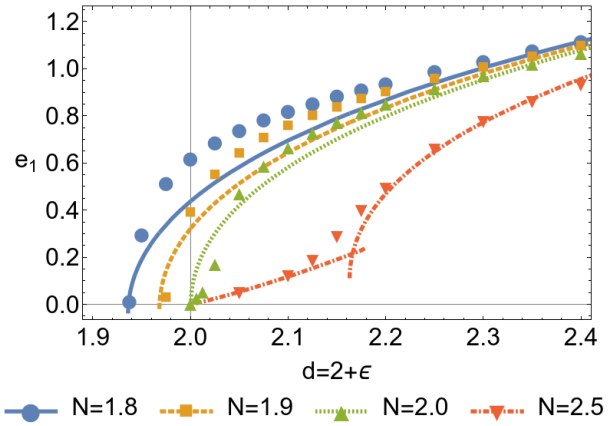

Figure 3.15: The dependence of the leading RG eigenvalue $e_1 = \nu^{-1}$ on the dimension for a series of values of N. The points denote our results from the functional calculation and lines - the predictions from the CH-type analysis. The red line corresponding to $N = 2.5$ features a discontinuity of the first derivative predicted by the CH-type analysis [1], notably absent in the corresponding NPRG calculations [see Sec. 3.3]. Figure from Ref. [3].

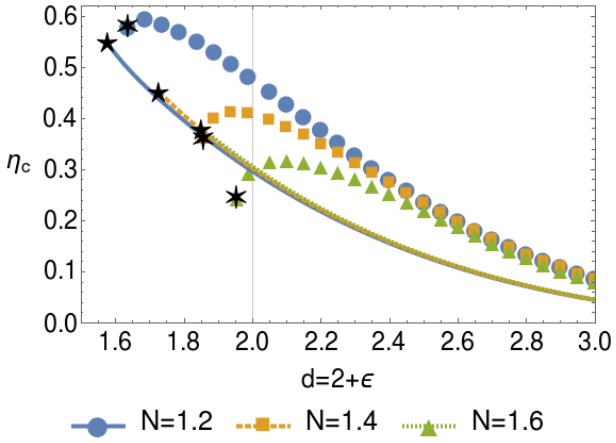

Figure 3.16: The dependence of the anomalous dimension of the critical FP η_c on the dimension for a series of values of N. The points denote the results from the minimal truncation and the lines - the data from the functional calculation. The values at the N-dependent lower critical dimensions $\eta_c(d_c(N))$ are marked by the stars: five-pointed for the functional calculations and six-pointed for the minimal truncation. Figure from Ref. [3].

3.4.2 Low-temperature phase

The QLRO FP is somewhat elusive; it cannot be extracted from the perturbative regime of the $4-\tilde{\epsilon}$ like the critical FP. The QLRO FP is subject to the perturbative description of the $2+\epsilon$ expansion, however, this expansion is performed around the zero-temperature FP which takes a nonanalytical form in the functional approach to the NPRG. Thus, the functional structure of the QLRO FP cannot be inferred perturbatively within the framework of the DE, and capturing it requires an alternative strategy.

The QLRO FP is infrared stable, meaning that the low-temperature RG flows converge to it in the limit $k \to 0$ [$t \to \infty$]. We can use this fact to extract the QLRO FP from the flow. Although, in principle, capturing this FP should be relatively straightforward as it does not require fine-tuning of the initial condition, it turns out to be substantially more difficult. The difficulties with capturing the QLRO FP have numerical origins and are mostly caused by two factors. The first factor is connected to the poles of the propagators and has been discussed in detail in Sec. 2.4.2. It can only be mitigated by adopting a very precise method for performing the momentum integrals.

The second problem arises due to the rapidity of the RG flow in the transient regime in between the critical and the QLRO FPs, which may cause numerical instabilities. A direct solution is to adopt a more precise flow-integration method, but this requires a highly inflated numerical effort. An interesting alternative is to fine-tune the initial condition very close to, but slightly below, the critical temperature. Such an initial condition leads to an RG flow spending long RG time in the proximity of the critical FP and, in our experience, a significantly improved stability in the transient regime of the flow.

An example of an RG flow allowing for the extraction of the QLRO FP is presented in Fig. 3.17. The figure overlays flows of two quantities: the dimensionless potential minimum $\tilde{\rho}_0$ and the anomalous dimension η for $(d, N) = (1.75, 1.3)$ slightly below the critical temperature. The presented flow features two distinct plateaus related to the two RG FPs.

Having identified the critical and the QLRO FPs we can compare their structures. The functions parametrizing the two FPs in the point $(d, N) = (1.75, 1.3)$ are plotted in Fig. 3.18. Both qualitatively resemble the KT FP [$(d, N) = (2, 2)$] presented in Ref. [114] recovered in the same approximation scheme [after a necessary reparametrization] and are broadly similar. This should not come as a surprise since the two FPs evolve smoothly across the (d, N) plane and collide in the lower critical dimension. Nevertheless, we observe several key differences between the two FPs. Compared to the critical FP, the QLRO FP is characterized by a larger value of the local potential's minimum $\tilde{\rho}_0$ and significantly steeper potential barrier beyond the minimum. The QLRO FP also features a very small difference between

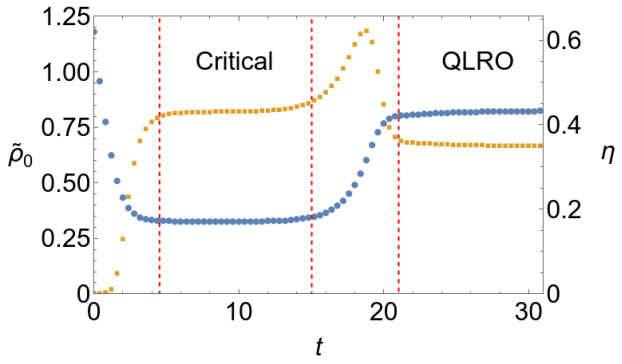

Figure 3.17: Flow of the dimensionless potential minimum $\tilde{\rho}_0$ [left axis, blue circles] and the anomalous dimension η [right axis, orange squares] for $(d, N) = (1.75, 1.3)$ slightly below the critical temperature calculated within the functional scheme. The red vertical lines roughly demarcate the scales at which the flow is controlled by the critical and the QLRO FPs. Figure from Ref. [3].

$\tilde{U}'(0)$ and $-\alpha$ which, as discussed earlier, complicates the numerical computation. We, finally, highlight the relatively complex shape of the $\tilde{Z}_\sigma$ function of the QLRO FP featuring two maxima. The physical consequences of the FP structure remain somewhat unclear and this field requires further investigation.

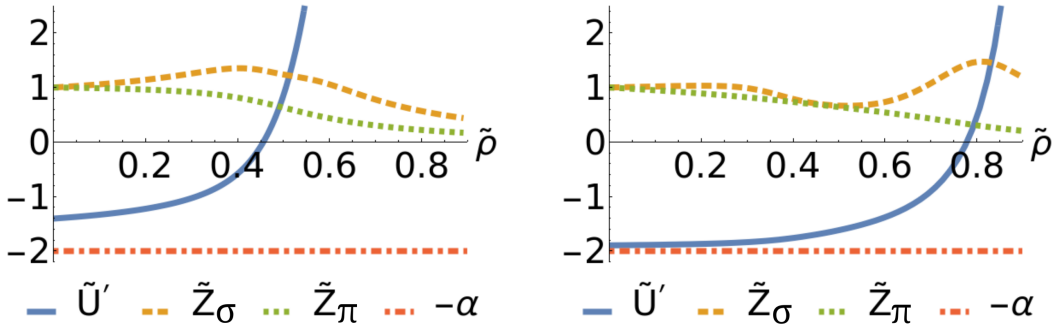

(a) Critical FP (b) QLRO FP

Figure 3.18: The fixed-point functions for $(d, N) = (1.75, 1.3)$. The red horizontal line marks $-\alpha$ corresponding to the propagator pole. Upon decreasing N towards 1, the local potential of the QLRO FP builds up a singularity as the range of values of $\tilde{\rho}$ where $\tilde{U}'(\tilde{\rho})$ is close to $-\alpha$ increases. Figure from Ref. [3].

In the present setting, the QLRO phase is characterized by an algebraic decay of correlation function with a universal exponent $d - 2 + \eta_{\mathrm{QLRO}}$ where η_{QLRO} is the anomalous dimension of the QLRO FP. In the analysis of the QLRO FP, we were faced with a difficulty; close to two dimensions, we were unable to recover the

functional QLRO FP due to its proximity to the nonanalytic, zero-temperature FP. In this regime, however, the results of the minimal scheme coincide with the $2+\epsilon$ expansion at the one-loop level. Thus, in the regime where the functional results are unavailable, the minimal scheme is the most accurate and can serve as a useful supplement. Our results regarding the correlation function exponent $d-2+\eta_{\mathrm{QLRO}}$ are presented in Fig. 3.19. The figure shows a staggering agreement between the predictions of the $2+\epsilon$ expansion and the results of the functional scheme in all dimensions. The results of the minimal scheme, on the other hand, significantly deviate from the perturbative predictions except for the very close proximity of two dimensions.

At this point, a question could be asked about how the NPRG results behave in the relatively well-understood limiting cases of the two-dimensional models [$d=2$] and the Ising universality class [$N=1$]. In two dimensions [for $1<N<2$], the QLRO FP and the zero-temperature FP overlap. As a consequence, the low-temperature phase is characterized by a vanishing anomalous dimension. This fact, along with more exact information about the direct proximity of two dimensions, is captured by the $2+\epsilon$ expansion. We once again emphasize that the $O(\partial^2)$ order of the DE is one-loop exact in $d=2+\epsilon$ and therefore exactly recovers the expected behavior in two dimensions [for $1<N<2$ and $N>2$]. The comparison with the Ising UC, on the other hand, cannot be performed as easily. Due to the lack of the transverse mode [or at least its fraction] the Ising UC is governed by completely different physics than the $O(N)$ models with $N>1$. More technically, for $N>1$ the proper low-temperature behavior can only be recovered if the order-parameter renormalization is defined through Z_π as $Z_k=Z_{\pi,k}(\rho_\eta)$. For $N=1$, however, the transverse mode is absent. As a consequence, Z_π becomes decoupled from physics and to recover the proper low-temperature behavior the order-parameter renormalization has to be defined through Z_σ. We note that this distinction comes about due to eccentricities of the low-temperature phase and that in the investigation of the critical behavior either of the functions can be used to define the the order-parameter renormalization. Due to the significant differences between the $O(N)$ models with $N>1$ and the Ising UC, we refrain from comparison between them throughout this section.

Let us now investigate the FP collision. Fig. 3.20 presents how the correlation function exponents $d-2+\eta$ of the QLRO and the critical FPs vary across the (d,N) plane. Analogously to Fig. 3.19, this figure uses the data from the functional scheme whenever available and supplements it with the results of the minimal truncation close to two dimensions. The figure presents a picture of the FP collision similar to the one obtained within the minimal scheme [see Fig. 3.14]. However, the collision presented here seems sharp, with a clear cusp, aligning well with the picture of the CH scenario [see Fig. 3.4], whereas the minimal scheme

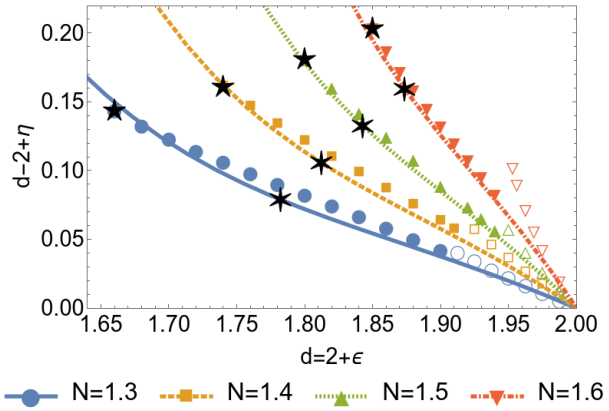

Figure 3.19: The dependence of the correlation function exponent of the QLRO FP on the dimension for a series of values of N. The filled points denote the results from the functional scheme, empty - from the minimal truncation and the lines - the predictions of the $2+\epsilon$ expansion [Ref. [131]]. The stars mark the lower critical dimensions: five-pointed as obtained in the functional scheme and six-pointed from the CH scenario. The lines are extended to dimensions below the point of the FP collision [where the BZJ FP is no longer infrared stable] along the prediction $2+\epsilon$ expansion. Figure from Ref. [3].

predicts an almost smooth merging of the two FPs. We note that, due to limited numerical accuracy, the functional scheme predicts slightly different values of the lower critical dimension as defined through the analysis of either the critical or the QLRO FP.

3.4.3 Lower critical dimension

Finally, we turn our attention to the line of lower critical dimensions $d_c(N)$. Let us recall that below two dimensions, the zero-temperature FP becomes unstable and the low-temperature behavior is controlled by the QLRO FP. The mechanism for the disappearance of the phase transition, as presented by the CH-style analysis and confirmed by our NPRG calculations, is based on a collision and disappearance of the critical and the QLRO FPs taking place at the lower critical dimension.

In the NPRG calculations, the lower critical dimension as defined by the FP collision is subject to a substantial regulator dependence. To minimize this effect we optimized the lower critical dimension in the spirit of the PMS. In practice, this was achieved by defining $d_c(N)$ as the lowest dimension in which the PMS-optimized value of e_1 can be identified[5]. Various estimates for the shape of the line

[5]This definition is in fact equivalent to optimizing the lower critical dimension $d_c(N,\alpha)$ with

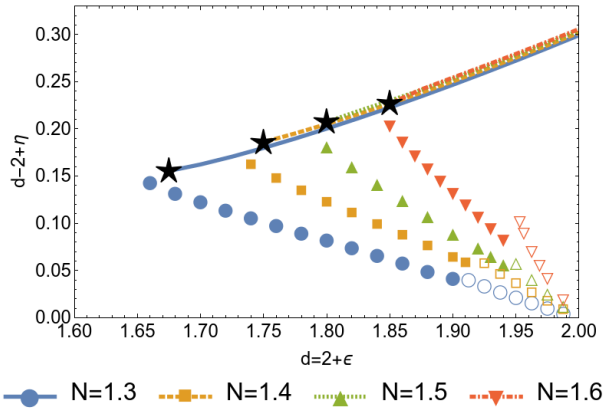

Figure 3.20: The correlation function exponent $d-2+\eta$ of the critical and QLRO FPs as functions of dimension for a series of values of N. The points denote the exponent of the QLRO FP: filled - from the functional scheme, empty - from the minimal truncation, and the lines denote the exponent of the critical FP. The stars mark the lower critical dimensions from the analysis of the critical FPs in the functional scheme. Figure from Ref. [3].

of lower critical dimensions $d_c(N)$ are compared in Fig. 3.21. The figure shows how our results relate to the real-space RG calculations of Ref. [58], and two alternative estimates from the perturbative CH-style analysis. We recall from Sec. 3.1 that the CH line is defined by:

$$0 = \Delta = \epsilon\frac{\pi}{2} - (N-2)f\left(\frac{\pi}{2}, N\right) + O(\epsilon^2). \tag{3.9}$$

The first estimate for the CH line follows the original reasoning of Cardy and Hamber which is based on an additional postulate that $f(g=\pi/2, N=2) = 2/\pi$ [6]. In the alternative estimation, we employ the perturbative expansion of $f(g,N)$ presented in Eq. (3.2).

Our results align well with those of Ref. [58] across a wide range of N as well as with the predictions of the CH-style analysis close to two dimensions. Interestingly, the CH line of lower critical dimensions merges smoothly with the line of cross-overs obtained in the previous section around the KT point $(d,N) = (2,2)$. We find it instructive to analyze the slope of the CH line around the KT point. Various estimates of the slope are shown in Table 3.1. The results of our calculations are situated in between the predictions of other methods. We also observe that the perturbative CH prediction varies strongly with the employed order of the g

respect to α and is somewhat more practical.

[6] This postulate was introduced to satisfy the analytic form for the first RG eigenvalue conjectured by the authors.

expansion of the function f and could be not sufficiently converged at the present order.

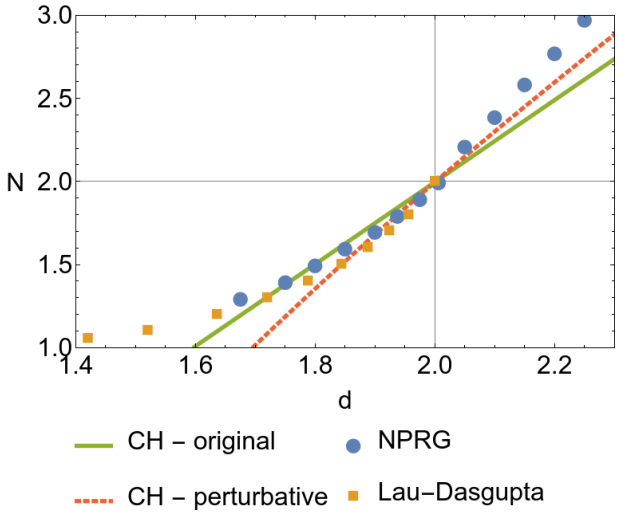

Figure 3.21: Comparison of different estimates of the shape of the line of the lower critical dimension. The lines denote two different ways of charting the CH line based on the perturbative RG calculations. The points denote the results of our calculations and from Ref. [58]. The NPRG points for $d > 2$ mark the position of the CH line estimated within the functional RG scheme in Sec. 3.3, where it was obtained in a form of a cross-over. Figure from Ref. [3].

Calculation	$\frac{\partial N_c(d)}{\partial d}\Big\vert_{d=2}$
CH - original	$\frac{\pi^4}{4} \approx 2.5$
CH - perturbative	3.1
NPRG	4.3
Ref. [58]	5.8

Table 3.1: Different estimates of the slope of the CH line at the KT point $(d, N) = (2, 2)$. Table from Ref. [3].

3.4.4 Summary

In this section, we addressed the CH scenario for the bottom-left $[d < 2,\ N < 2]$ quadrant of the (d, N) plane from the perspective of the NPRG. We traced the behavior of the correlation length exponent ν^{-1}, the anomalous dimension η_c of

the critical FP, and the anomalous dimension η_{QLRO} of the QLRO FP throughout the quadrant. We emphasize that our results present the first time these exponents were calculated in this part of the (d, N) plane. Whenever possible we have compared our results with the perturbative predictions of the CH scenario showing a surprisingly good agreement between the approaches near two dimensions. Particularly noteworthy is the agreement between the results of $2 + \epsilon$ and our calculations at the $O(\partial^2)$ order of the DE regarding the η_{QLRO} exponent in the entire range of dimensions $d_c(N) < d < 2$ [for $1 < N < 2$].

Our NPRG results firmly support the CH scenario in the bottom-left quadrant of the (d, N) plane. In this region, we were able to identify two nontrivial RG FPs: the critical FP, and the stable QLRO FP. We have discussed the differences in the structure of the two FPs and have shown how they collide upon approaching the lower critical dimension $d_c(N)$. Finally, we have charted the line of lower critical dimensions. In the vicinity of two dimensions, our estimates align fairly well with the predictions of the CH scenario and show quite a good agreement with the results of Ref. [58].

3.5 Conclusion

Throughout this chapter, we explored the topic of the critical phase transitions in the $O(N)$ models. We delved deeply into the perturbative analysis of Cardy and Hamber [1] predicting that quite unusual phenomena should occur in certain regions of the (d, N) plane. In the quadrant $d > 2$, $N > 2$, the CH scenario predicts nonanalyticity of the critical exponents, while in the quadrant $d < 2$, $N < 2$, it describes the shape of the line of the lower critical dimensions and predicts the presence of a QLRO phase characterized by a universal anomalous dimension. To verify the CH scenario in a nonperturbative setting, we employed the functional RG and the derivative expansion at the order $O(\partial^2)$.

Strikingly, our NPRG results imply that the CH scenario does take place in the bottom-left quadrant [$d < 2$, $N < 2$] and does not occur in the top-right quadrant [$d > 2$, $N > 2$]. For $N > 2$, we have found no indication of nonanalyticities of the critical exponents consistent with the CH picture of the FP collision. Instead, we identified a smooth cross-over between two distinct regions of the (d, N) plane. On the other hand, we recover a sharp FP collision for $N < 2$ and a QLRO phase as predicted by the CH analysis. We find it somewhat puzzling that our analysis agrees with the CH scenario in one region of the (d, N) plane and disagrees in another. We do, however, emphasize several arguments in favor of the picture provided by our NPRG results.

Firstly, the CH scenario for the nonanalyticity of the critical exponents requires that the subdominant RG eigenvalue e_2 vanishes. This seems highly unlikely ex-

cept for the direct vicinity of two dimensions. In three dimensions, the critical exponents of the $O(N)$ models have been calculated to great precision, not only with the NPRG but also with other methods. We are not aware of any study showing even an indication that e_2 could be close to zero for any $N > 2$ in three dimensions. Therefore, the FP collision envisaged by Cardy and Hamber could only take place in dimensions lower than and largely separated from three, with the CH line becoming very steep and reaching some finite dimension in the limit $N \to \infty$.

Secondly, the presence of the QLRO phase predicted by the CH scenario for $N < 2$ has been confirmed not only by the NPRG calculations but also the real-space RG [58]. Moreover, the shape of the line of the lower critical dimensions $N_c(d)$ as predicted by the CH scenario does agree quite well both with our results and those of Ref. [58]. Finally, the CH scenario seems to be fairly accurate in predicting the leading RG eigenvalue [see Fig. 3.15]. This is true also for $N > 2$ everywhere except for the direct vicinity of the supposed FP collision [see the red curve of Fig. 3.15]. If the CH analysis is fundamentally wrong, the achieved level of accuracy would have to be purely coincidental.

We, finally, observe that the line $N_c(d)$ obtained below two dimensions merges smoothly at the KT point $(d, N) = (2, 2)$ with the line of cross-overs of the critical exponents found above two dimensions. Based on the ample evidence, it seems reasonable to conclude that the FP collision observed for $N < 2$ becomes smoothed when crossing the KT point and survives only as a cross-over for $N > 2$.

A resolution of this apparent contradiction might be possible to reach by considering higher-order terms in the CH analysis. At the present order, the CH equations harbor a subtle symmetry between the bottom-left and top-right quadrants of the (d, N) plane, which leads to a prediction of an almost identical collision for $N < 2$ and $N > 2$. This symmetry, however, becomes broken when the higher-order terms are taken into account. Possibly, with this symmetry broken, the CH analysis would align with the results found with other methods. Obtaining these higher-order terms, however, is an arduous [and maybe impossible] task as it would require performing the KT style analysis in $2 + \epsilon$ dimensions for $2 + \delta$ order-parameter components.

Chapter 4

$O(2)$ model with cubic perturbations

> And what exactly is a dream
> And what exactly is a joke
>
> Pink Floyd, *Jugband Blues*

In the present chapter, we shift our attention away from the isotropic $O(N)$ models and investigate weak cubic perturbations to the $O(2)$ model. Of our primary interest is the leading renormalization group (RG) eigenvalue associated with an anisotropic perturbation to the $O(2)$-symmetric fixed point. We analyze this eigenvalue in three dimensions and subsequently follow its evolution upon continuously decreasing the dimension from three towards two, where it is expected to vanish - marking the onset of nonuniversal critical behavior. This chapter is based on the results originally published in Ref. [4].

In Sec. 4.1, we analyze the three-dimensional model. The previous best nonperturbative renormalization group (NPRG) estimate for the leading anisotropic exponent y_4 of this model underestimates its value by a factor of over two. Using the derivative expansion (DE) at the order $O(\partial^2)$ we aim to improve this estimate. Applying the error estimate methodology developed in Refs. [20, 21] and summarized in Sec. 2.3.2 we obtain the value of y_4 and the error bars fully compatible with the most accurate results obtained with various methods. In Sec. 4.2, we move to dimensions lower than three. We analyze the evolution of several leading RG eigenvalues upon shifting the dimension. Upon approaching two dimensions, we capture the approach of the anisotropic eigenvalue towards zero and the emergence of the Kosterlitz-Thouless (KT) physics.

In addition to providing a better understanding of the physics of the investigated model, this chapter presents important advancements for the NPRG methodology and aims to assess the accuracy of popular simplified approaches to the DE. In our calculations, we employ two alternative schemes described in detail in Sec.

2.4.3. The first of the schemes, hereafter referred to as "full" or the Γ_{F} approach, retains the full functional dependence on the polar coordinates ρ and θ defined via

$$\phi_1 = \sqrt{2\rho}\cos(\theta), \quad \phi_2 = \sqrt{2\rho}\sin(\theta). \tag{4.1}$$

The effective action ansätze imposed in the full approach at the local potential approximation (LPA) and the $O(\partial^2)$ levels of the DE read

$$\Gamma_{\mathrm{F}}^{\mathrm{LPA}} = \int_{\boldsymbol{x}} \Big\{ U(\rho,\theta) + \frac{1}{2}\left(\partial_\mu \phi^i\right)^2 \Big\}, \tag{4.2a}$$

$$\begin{aligned}\Gamma_{\mathrm{F}}^{\partial^2} &= \int_{\boldsymbol{x}} \Big\{ U(\rho,\theta) + \frac{Z(\rho,\theta)}{2}\left(\partial_\mu \phi^i\right)^2 + T(\rho,\theta)\phi_1\phi_2\partial_\mu\phi_1\partial_\mu\phi_2 \\ &\qquad + \frac{W(\rho,\theta)}{4}\left[\left(\phi^1\right)^2 - \left(\phi^2\right)^2\right]\left[\left(\partial_\mu\phi^1\right)^2 - \left(\partial_\mu\phi^2\right)^2\right] \Big\},\end{aligned} \tag{4.2b}$$

and the parametrizing functions are represented on a two-dimensional grid $\rho \in [0, \rho_{\mathrm{Max}}]$, $\theta \in [0, \pi/4]$. The implementation of the discretization in this scheme involves imposing the symmetry constraints in a manner described in Sec. 2.4.3. We emphasize that this work presents the complete $O(\partial^2)$ order of the derivative expansion successfully implemented in a functional setting on a two-dimensional grid for the first time.

The alternative scheme is based on an expansion of the parametrizing functions in the anisotropic invariant $\tau = \left(\phi^1\phi^2\right)^2/2$ up to the linear terms while retaining the full functional dependence on the isotropic invariant $\rho = \phi^i\phi^i/2$. The effective action ansätze for this scheme read:

$$\Gamma_{\mathrm{E}}^{\mathrm{LPA}} = \int_{\boldsymbol{x}} \Big\{ U(\rho) + \tau U^1(\rho) + \frac{1}{2}\left(\partial_\mu \phi^i\right)^2 \Big\}, \tag{4.3a}$$

$$\begin{aligned}\Gamma_{\mathrm{E}}^{\partial^2} &= \int_{\boldsymbol{x}} \Bigg\{ U(\rho) + \tau U^1(\rho) + \frac{Z_\sigma(\rho) + \tau Z_\sigma^1(\rho)}{2}\left(\partial_\mu\phi^i\right)^2 \\ &\qquad - \frac{Z_\sigma(\rho) - Z_\pi(\rho) + \tau\left[Z_\sigma^1(\rho) - Z_\pi^1(\rho)\right]}{4\rho}\left[\left(\phi^1\partial_\mu\phi^2\right)^2 + \left(\phi^2\partial_\mu\phi^1\right)^2\right] \\ &\qquad + T(\rho)\phi^1\phi^2\partial_\mu\phi^1\partial_\mu\phi^2 \Bigg\}.\end{aligned} \tag{4.3b}$$

This scheme, called the "expanded" or the Γ_{E} approach, is expected to perform reasonably well, since we are considering only the infinitesimally weak anisotropic perturbations around the isotropic models and, crucially, offers a huge decrease in numerical complexity. We compare the two truncations described above [the full and expanded schemes] and point out that while in three dimensions their predictions are practically equivalent, important differences appear in lower dimensions.

In Sec. 4.3, we address the ansatz and the truncated variants of the DE discussed in Sec. 2.2.1. We calculate several critical exponents of the $O(2)$ model with cubic anisotropies as functions of dimension in each of the approaches. The comparison of the two variants shows that while in three dimensions the differences between them are completely negligible, they grow in lower dimensions. In particular, the truncated variant does not properly recover the onset of the KT physics in two dimensions.

The NPRG flow equations employed in the present chapter appear very lengthy and rather useless for a human reader. We refrain from quoting them in the text. They are available online in Ref. [137].

4.1 Three dimensions

We first address the cubic anisotropy in the three-dimensional model. The several leading RG eigenvalues as calculated with the $O(\partial^2)$ order DE are plotted in Fig 4.1 as functions of the regulator parameter α. The eigenvalues presented in the figure are divided into two categories. The isotropic eigenvalues, labeled with the superscript "iso", are associated with perturbations conserving the $O(2)$ symmetry and can be found in the isotropic model. The anisotropic eigenvalues, labeled with the superscript "aniso", are associated with perturbations explicitly breaking the $O(2)$ symmetry into $\mathbb{Z}_4$ symmetry and consequently are present only in the anisotropic model. Fig. 4.1 compares the predictions of the Γ_{F} and Γ_{E} schemes. The chart exhibits no visible differences between the two schemes regarding either the isotropic or the anisotropic eigenvalues. We emphasize that the two schemes are equivalent in their treatment of the *isotropic* eigenvalues and any possible discrepancies arise solely due to differences between their numerical implementations.

The eigenvalues presented in Fig. 4.1 are connected to the observable critical exponents. e_1^{iso} is the inverse correlation length exponent ν^{-1}, while the subsequent isotropic eigenvalues are connected to the correction to scaling exponents present in the pure $O(2)$ model. All the anisotropic eigenvalues are connected to the correction to scaling exponents, as well, but these corrections can be observed only in the anisotropic models. Importantly, the e_1^{aniso} eigenvalue can be identified with y_4 - the leading exponent of the cubic field. The value of y_4 predicted by the $O(\partial^2)$ order of the DE lies much closer to the results of other methods [$y_4 \simeq -0.11$] compared to the previous NPRG results [$y_4 = -0.044$]. Let us, finally, note that, although most of the leading eigenvalues are real, some are complex and appear as pairs of complex conjugates. Throughout this section, whenever a pair of complex eigenvalues is encountered, only its real part is plotted and the pair is labeled with a double subscript, e.g. $e_{3,4}^{\mathrm{iso}}$ in Fig. 4.1.

Let us focus on the leading cubic eigenvalue $e_1^{\mathrm{aniso}} = y_4$. Fig. 4.2 presents

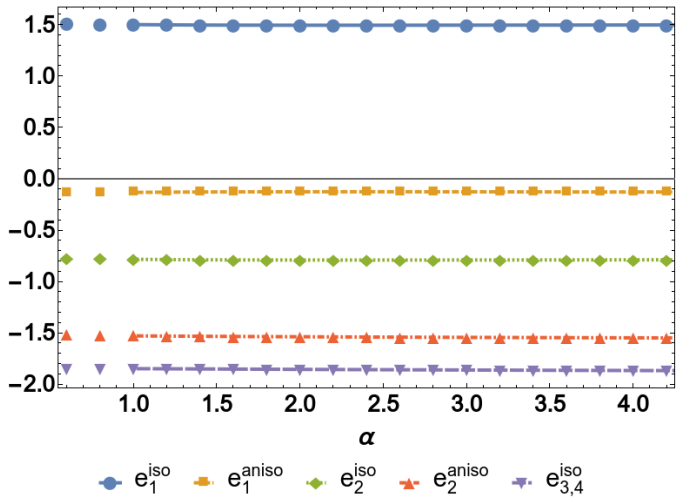

Figure 4.1: The leading stability matrix eigenvalues obtained at the order $O(\partial^2)$ displayed as function of the cutoff parameter α in three dimensions. The results obtained within the $\Gamma_{\rm F}$ and $\Gamma_{\rm E}$ schemes are represented by lines and points respectively. The relevant eigenvalue $e_1^{\rm iso}$ determines the correlation length exponent ν. The leading irrelevant eigenvalue $y_4 = e_1^{\rm aniso}$ emerges due to the anisotropy; the dominant irrelevant isotropic eigenvalue $e_2^{\rm iso}$ is significantly further from zero as compared to $e_1^{\rm aniso}$. The results obtained within the two schemes practically coincide. Figure from Ref. [4].

the dependence of y_4 on the regulator parameter α at the LPA and the $O(\partial^2)$ levels of the DE in the full and τ-expanded schemes. The figure shows substantial differences between the results of the two subsequent orders of the DE. Particularly noteworthy is the fact that at the LPA level y_4 changes sign at low enough α. At the scale of the plot, the differences between the estimates of the full and τ-expanded schemes can hardly be observed and they are completely negligible in comparison with the error bars of the DE.

The final estimate for y_4 and the associated error bars presented in Fig. 4.2 are calculated according to the prescriptions of Sec. 2.3.2. As a consequence of the substantial spread between the LPA values of y_4 at the subsequent orders of the DE the [most likely very conservative] error bars are quite wide. Table 4.1 compares our estimate for y_4 with those obtained by other methods, including perturbation theory, Monte Carlo (MC) simulations, and the large charge expansion. Our results lie in between the other estimates are remain compatible with all of them [except for the outlying estimate of LPA']. Note a significant tension present between the large charge expansion and the remaining methods, in particular with the estimate of the perturbation theory.

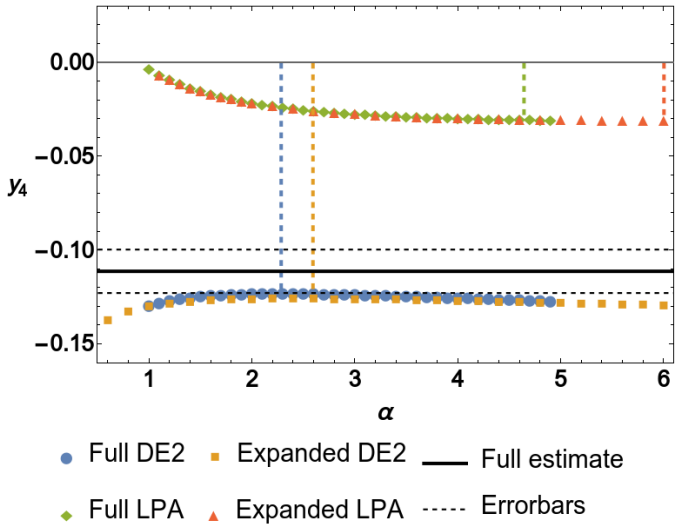

Figure 4.2: The dependence of y_4 on the regulator parameter α, comparing the LPA and the $O(\partial^2)$ DE orders in the full and τ-expanded schemes in three dimensions. The vertical dashed lines indicate the principle of minimal sensitivity (PMS) values corresponding to the four sets of data. The bold line indicates our final estimate of $y_4 = -0.111$ at the order $O(\partial^2)$ and is accompanied by the error bars [horizontal dashed lines]. Figure from Ref. [4].

Methodology	y_4
PT [6 loop] - Ref. [70]	-0.103(8)
MC - Refs. [66, 138]	-0.108(6)
LCE - Ref. [139]	-0.128(6)
MC / RG - Ref. [67]	-0.114(2)
LPA' DE - Ref [65]	-0.042
$O(\partial^2)$ DE - This work	-0.111(12)

Table 4.1: Comparison of the values of y_4 obtained within different theoretical and simulation approaches including perturbation theory (PT), MC simulations, and large charge expansion (LCE). Note a substantial spread of the values, in particular the differences between the LCE and MC / PT predictions. Table from Ref. [4].

We finally point out that an accurate parametrization of the momentum dependencies is crucial for an accurate computation of y_4 within the NPRG methodology. While the accuracy of our results obtained at order $O(\partial^2)$ is comparable to the other approaches listed in Table 4.1, one may expect that a calculation reaching

the order $O(\partial^4)$ would surpass in accuracy all the estimates currently available.

4.2 Below three dimensions

Having established a well-controlled result in the three-dimensional model we turn our attention to lower dimensions. The procedure for the fixed point (FP) search is analogous to that of the previous chapter; we gradually decrease the dimension using the FP in the dimension d as a guess in the dimension $d - \delta d$. In fact, since our analysis is only performed around the $O(2)$ symmetric FPs, the equations used to obtain the FPs are identical to those of the previous chapter [taking $N = 2$]. The anisotropic RG-flow equations are only used later to obtain the stability matrices and extract the RG eigenvalues. Although we were able to recover the FPs in the entire range $d \in [2, 3]$, the eigenvalues in Fig. 4.3 are presented only for the dimensions larger than two. This choice is dictated by a failure of the PMS related to the physical existence of the line of FPs in two dimensions. Although an alternative method for fixing the regulator in two dimensions was proposed in the literature [see Sec. 2.4.1 and Ref. [114]], we refrain from employing it in this chapter so as not to obscure the picture.

Fig. 4.3 compares the evolution of several leading, PMS-optimized RG eigenvalues as calculated within the τ-expanded and full schemes. The two schemes remain in complete agreement regarding the isotropic eigenvalues, demonstrating the fact that they treat the isotropic sector in an equivalent manner. The figure shows the leading isotropic eigenvalue e_1^{iso} approaching zero for $d \to 2^+$ marking the onset of the KT physics characterized by the essential singularity of the correlation length [6]. e_1^{iso} exhibits a square-root-like nonanalyticity upon approaching two dimensions in agreement with the perturbative predictions of Ref. [56]. The figure also reveals a known deficiency of the $O(\partial^2)$ order DE; the subleading isotropic eigenvalue, predicted to vanish in two dimensions by the KT theory [75], reaches a finite value $e_2^{\text{iso}}(d = 2) \simeq -0.5$.

In the anisotropic sector, the Γ_{E} and the Γ_{F} approaches completely agree close to three dimensions. Significant differences arise around dimension $d = 2.5$. In that dimension, the eigenvalues e_2^{aniso} and e_3^{aniso} calculated within the Γ_{E} scheme collide and become complex conjugates[1]. The eigenvalues in the Γ_{E} scheme also exhibit several crossings, which could lead to significant physical consequences. The exponent of the anisotropic field y_4 is defined as the leading anisotropic eigenvalue. Due to crossing this exponent will be associated with various eigenvalues

[1]Due to crossing of the eigenvalues their order changes. The labels $e_i^{\text{iso/aniso}}$ are imposed on the eigenvalues according to their order in three dimensions. Upon crossing the labels are determined in the way that the eigenvalues and the associated eigenvectors remain continuous as functions of the dimension.

depending on dimensions which implies its nonanalytic [yet continuous] behavior. However, not observing any such crossings in the Γ_{F} scheme we presume their presence in the Γ_{E} scheme to appear as an artifact of the field expansion.

In both schemes, the leading anisotropic eigenvalue e_1^{aniso} exhibits nonmonotonous behavior, increasing in absolute value when lowering dimension before approaching zero in the limit $d \to 2^+$. However, below the dimension $d \simeq 2.4$, the predictions of the two schemes differ substantially. In the τ-expanded scheme, e_1^{aniso} reaches the minimal value in dimension $d \simeq 2.2$ and approaches zero in a smooth fashion. In the full scheme, the situation is different. The minimal value is reached just above two dimensions [$d \simeq 2.03$] and in the lowest dimensions in which we were able to apply the PMS [$d = 2.01$], y_4 takes the relatively large value of around -0.25. This, however, represents a sudden and significant rise from $y_4 \simeq -0.4$ in $d = 2.03$. Additionally, in two dimensions, we find that y_4 vanishes for the value of α corresponding to $\eta \simeq 1/4$. Taking into account the significant uncertainties around two dimensions, which we discuss in the following section, we are confident to conclude that the full scheme predicts that y_4 approaches zero on an apparently nonanalytic trajectory as $d \to 2^+$.

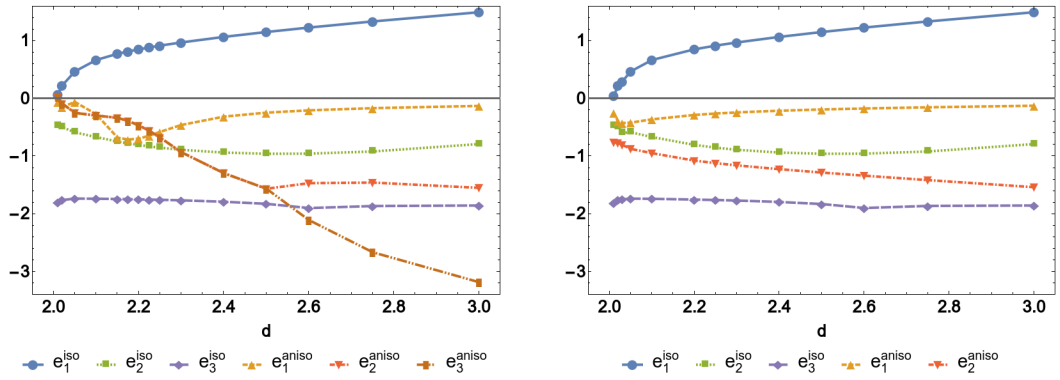

(a) Results of the Γ_{E} scheme.

(b) Results of the Γ_{F} scheme.

Figure 4.3: Comparison between the leading, PMS-optimized RG eigenvalues as obtained within the Γ_{F} and Γ_{E} schemes, varying the dimension between three and two. Figure from Ref. [4].

To comprehend the entire picture, let us explore the behavior of the eigenvalues before the PMS optimization. Fig. 4.4, presents the leading *anisotropic* eigenvalues as functions of the regulator parameter α in several dimensions $d \in]2, 3]$. The figure allows us to better appreciate the differences arising between the two schemes. In three dimensions, the two schemes practically coincide, and down to $d = 2.5$ the differences between them, particularly concerning e_1^{aniso}, remain relatively modest. Below $d = 2.5$, however, the two schemes begin to substantially diverge. In the

τ-expanded scheme for $d = 2.2$ and below, we can observe the crossing of the eigenvalues, notably absent in the full scheme. We reiterate that in two dimensions the PMS cannot be employed in the usual manner and, to avoid obscuring the picture, we present the results in dimension $d = 2.01$.

Fig. 4.4 showcases the degradation of the accuracy control of our approach. The differences between the results of the Γ_{F} and the Γ_{E} truncations indicate that, at the employed order, the τ-expansion is not yet converged. We should note, however, that a similar problem arises with the order-parameter expansion in the isotropic models; in three dimensions the expansion converges quickly, while below it becomes divergent [see Sec. 2.2.3]. It is, therefore, not obvious if including the higher-order anisotropic terms would actually improve the quality of the τ-expanded scheme. Nevertheless, we emphasize that both schemes capture the subtle effects of marginal operators arising in two dimensions, standing as a hallmark of the KT transition. This, together with the accurate resolution of y_4 in three dimensions constitutes a significant improvement as compared to the previous NPRG studies of this system.

4.3 Ansatz and truncated variants of the derivative expansion

In Sec. 2.2.1 we introduced two different ways of implementing the DE: the "ansatz" variant, and the "strict" or "truncated" variant. The flow equations of these two approaches are not identical and it remains unclear to what extent the results they yield are equivalent. As is well known, both variants yield very accurate, and consequently similar, critical exponents of the three-dimensional $O(N)$ models. However, we are not aware of any analysis of the differences between the variants and their comparative precision below three dimensions. In this section, we address this point at the order $O(\partial^2)$ in the $O(2)$ model for dimensions between three and two for both isotropic exponents and for $\mathbb{Z}_4$-symmetric perturbations.

Before discussing the results, we offer a brief reminder of the two variants. Let us recall that the DE flow equations take the form of one-loop 1PI diagrams [see e.g. Fig. 4.5]. These diagrams consist of vertices representing the n-point functions and lines representing the "dressed" propagators obtained from the 2-point functions:

$$G_{ij}(\boldsymbol{q}^2) = \left(\Gamma^{(2)}_{ij}(\boldsymbol{q}^2) + R_k(\boldsymbol{q}^2)\delta_{ij}\right)^{-1}. \tag{4.4}$$

Thus, to deduce the flow equations we first construct the appropriate diagrams and subsequently translate them into expressions by plugging in the appropriate n-point functions. This is the prescription of the ansatz approach - the vertex

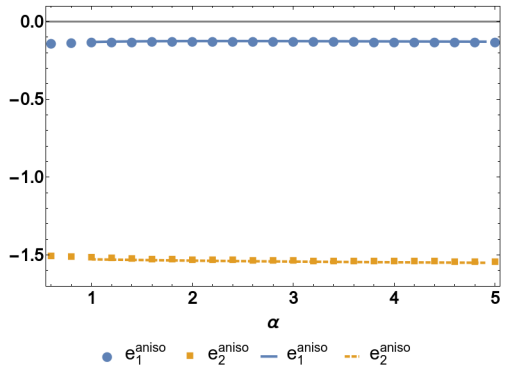

(a) $d = 3.00$.

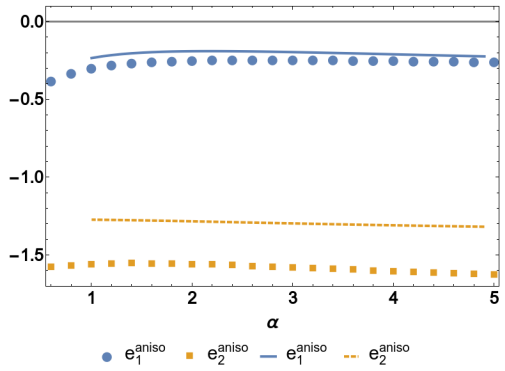

(b) $d = 2.50$.

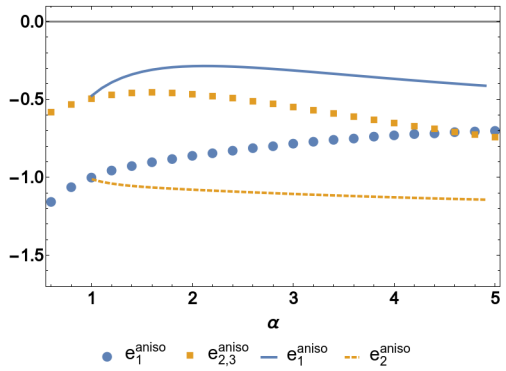

(c) $d = 2.20$.

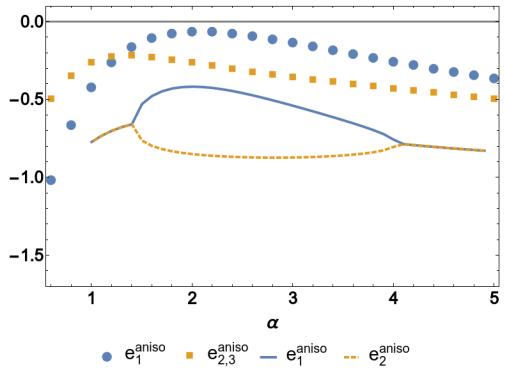

(d) $d = 2.05$.

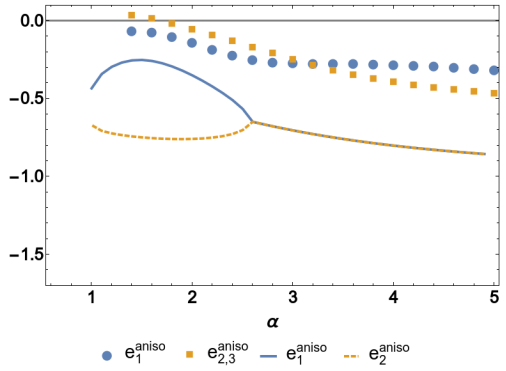

(e) $d = 2.01$.

Figure 4.4: The leading stability matrix eigenvalues related to the anisotropy obtained at the order $O(\partial^2)$ displayed as a function of the cutoff parameter α in a sequence of dimensions. The results obtained within the Γ_{F} and Γ_{E} schemes are exhibited with the lines, and the points respectively. For $d = 2.2$ the leading, anisotropic eigenvalue y_4 corresponds to e_1^{aniso} within the Γ_{F} scheme, and to $e_{2,3}^{\mathrm{aniso}}$ within the Γ_{E} scheme. In dimensions approaching two, the PMS value of $y_4 = e_1^{\mathrm{aniso}}$ becomes very close to zero. In Figs. 4.4(d) and 4.4(e) two of the eigenvalues are real and take distinct values near the PMS but cross and become complex conjugates far from the PMS. This results in some bifurcations in the curves in these figures. Figure from Ref. [4].

functions are directly extracted from the ansatz and no further truncations are imposed.

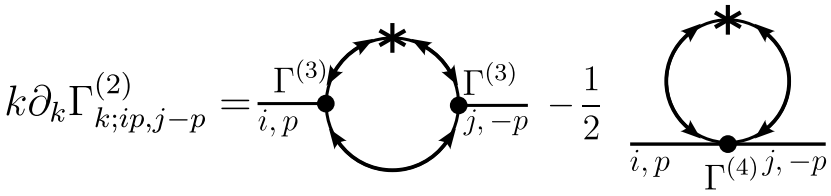

Figure 4.5: Diagrammatic representation of the flow equation for the $\Gamma^{(2)}_{k;i\boldsymbol{p},j-\boldsymbol{p}}$ function. The continuous lines with arrows denote the "dressed propagator" $\left(\Gamma^{(2)}_k + R_k\right)^{-1}$, the asterisks denote the scale derivative of the regulator $\dot{R}_k$ and the dots with n lines denote the n-point vertex functions. The external legs of the diagram are labeled with corresponding field indices and momenta.

Recently Balog et al. [23] proposed an alternative procedure relying on the interpretation of the DE as a truncation of the n-point functions in the external momenta. From this perspective, the ansatz prescription is not consistent, since the flow equations contain contributions of the same order in momenta as the terms already truncated due to imposition of the ansatz. For example, at the order $O(\partial^2)$, the "bubble" diagram [see Fig. 4.5] contains contributions of order $O(q^4)$ coming from the product of the two $\Gamma^{(3)}$ vertices. However, the terms of order $O(q^4)$ were already truncated in the ansatz. Thus, a prescription of the truncated scheme is to remove such higher-order contributions from the flow equations.

Each of the approaches comes with its advantages. The ansatz approach is arguably more aesthetic and easier to implement since tracking all the higher-order terms can be quite an arduous task, especially at the order $O(\partial^4)$ and above. Moreover, treating the effective action ansatz in the same way for all vertices automatically ensures the satisfaction of all relations coming from symmetries or relations between response functions and correlation functions. On the other hand, the truncated approach leads to flow equations of reduced complexity. At low orders of the expansion the gain is modest, the two variants even yield the identical flow equations at the LPA level. However, at the order $O(\partial^4)$, there is a huge amount of higher-order terms and their truncation leads to flow equations many times shorter than in the ansatz variant.

The existence of the two versions of the DE raises the question of their compatibility. Implementing one of the variants, we should make sure that the other yields the equivalent results [within the corresponding error bars]. The comparison between the two versions of the DE was previously performed in three dimensions at the order $O(\partial^2)$ for the $O(N)$ models and at the order $O(\partial^4)$ for the $N = 1$ case [21]. In Ref. [112], the $O(\partial^4)$ DE equations in the ansatz variant are truncated in

powers of the order parameter and yield results fully compatible with those previously obtained in the truncated variant without the field expansion. All these comparisons indicate that, in three dimensions, the difference between the two variants of the DE is considerably smaller than the error bars estimated to a given order and allow us to conclude that the two procedures are essentially equivalent for the purpose of studying universal properties of the three-dimensional $O(N)$ models.

In our calculations regarding the three-dimensional model, we confirm the previously reported [21] compatibility between the ansatz and the truncated variants for the isotropic exponents ν and η. Furthermore, we reach a similar conclusion for the anisotropic exponent y_4. In Table 4.2, we present the comparison of the PMS optimized values of y_4 as calculated within ansatz or truncated variants. In addition, the table shows how the y_4 estimate depends on the regulator family and the scheme for the treatment of the anisotropy. Clearly, in three dimensions the difference between the truncated and the ansatz variant of the DE is well below the margin of error. Moreover, in that dimension, the truncation in the anisotropic invariant [at the order indicated in the equation Eq. (4.3)] or the choice of the regulator family[2] also have effects below the margin of error.

Version	Field truncation	Regulator	y_4
Ansatz	Full	Wetterich	-0.111 ± 0.012
Ansatz	Full	Exponential	-0.112 ± 0.012
Truncated	Full	Wetterich	-0.113 ± 0.012
Truncated	Full	Exponential	-0.114 ± 0.012
Ansatz	Expanded	Wetterich	-0.114 ± 0.012
Truncated	Expanded	Wetterich	-0.114 ± 0.012

Table 4.2: Comparison of the values of y_4 obtained within different versions of the DE at the order $O(\partial^2)$ in three dimensions. The field truncation refers to either the fully functional approach treating both variables ρ and θ on a functional level or the expanded scheme retaining the functional dependence on the ρ variable but involving an expansion in the cubic invariant τ. Table from Ref. [4].

Below three dimensions we observe a general trend of deteriorating accuracy of various approximate schemes in the NPRG. Let us recall that, in the isotropic case, the expansion in powers of the order parameter becomes unstable around dimension $d \lesssim 2.5$ [see Sec. 2.2.3], the results of the τ-expanded approach significantly deviate from the results of the fully functional scheme below dimension $d \approx 2.5$

[2]One must, however, stress that the dependence on the regulator is higher if the results are not optimized via the PMS.

[see Sec. 4.2], and the DE itself becomes less accurate as the dimension decreases. The last point is visualized in Fig. 4.6 showing the dimension dependence of the $O(\partial^2)$-order DE estimates for several critical exponents along with the estimated error bars. In the dimensions approaching two, the error bars become very large due to an increasing spread between the results of the consecutive orders of the DE. Below the dimension $d = 2.1$ [$d = 2.2$ in Fig. 4.6(c)], the error bars are not displayed because we were unable to identify the fixed-point solution at the LPA level required in our error bar estimation procedure.

It is, therefore, expected that the spread between the results of the ansatz and the truncated variants should increase with the decreasing dimension. This is confirmed in Fig. 4.6 comparing the estimates and the error bars for the critical exponents: η, ν and y_4 as calculated with the two variants. Let us note that, except for the direct vicinity of two dimensions, the differences between the results of the two variants remain relatively small and the estimates of the two variants remain compatible within the error bars.

The increasing differences in low dimensions can be attributed to the increasing importance of the terms of the higher order in derivatives. In fact, the difference between the ansatz and the truncated variants should be of order $O(\partial^4)$ in derivatives. Thus, one might argue, that the increasing discrepancy is a manifestation of the fact that the effects induced by the higher orders of the DE become much more significant in the dimensions $d \lesssim 2.5$.

Nevertheless, it should be noted that the ansatz variant captures the KT physics in two dimensions [including the effects of the cubic anisotropy] not only qualitatively but largely also quantitatively. In the truncated approach, on the other hand, the leading isotropic and anisotropic RG eigenvalues do not vanish in two dimensions. As a consequence, the lines of FPs - the hallmark of the KT physics cannot be reproduced even qualitatively in the truncated variant of the DE. The difference in the quality of the results obtained in two dimensions indicates an apparent superiority of the ansatz approach. This topic requires further clarifying studies.

Although, at the moment, we do not have a conclusive explanation, we permit ourselves to conjecture a possible reason for this substantial difference in quality between the two variants of the DE close to two dimensions. As mentioned before, the ansatz variant has the property of exactly preserving the generalized response-fluctuation relations, as well as the Ward identities for the $O(2)$ symmetry[3]. The truncated variant, by treating each vertex independently, satisfies these relations only up to corrections of the higher order in the momentum expansion. Such

[3]Ward identities and response-fluctuation relations depend only on the existence of an ansatz with symmetry from which all vertices are extracted; it does not require that the ansatz provides an accurate description of the physics.

relationships are key in the study of the broken phase in the presence of continuous symmetry. Although, strictly speaking, the isotropic $O(2)$ model does not exhibit the symmetry-broken phase in two dimensions, the line of KT FPs springs from the zero-temperature FP [controlling the symmetry-broken phase]. We do believe that the proximity to the zero-temperature FP might be causing the underperformance of the truncated variant due to the violation of the generalized response-fluctuation relations. The resolution of this point calls for an extension of the present study to the order $O(\partial^4)$.

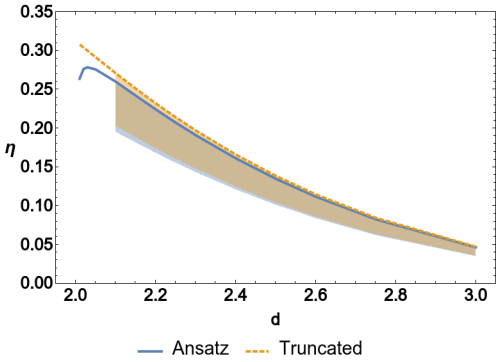

(a) Anomalous dimension η.

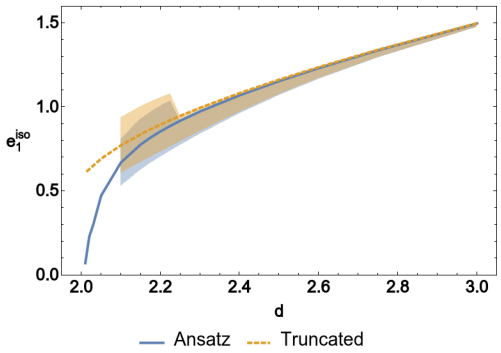

(b) Inverse correlation length exponent $\nu^{-1} = e_1^{\mathrm{iso}}$.

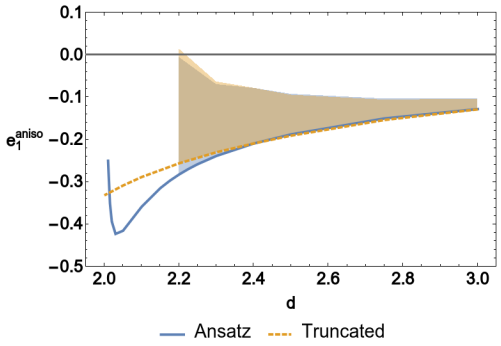

(c) Anisotropic field exponent $y_4 = e_1^{\mathrm{aniso}}$ as calculated within the full scheme.

Figure 4.6: The dependence of several critical exponents on the implementation of the DE as functions of the dimension. The lines represent the raw values from the ansatz and truncated variants of the DE at the order $O(\partial^2)$. The marked regions represent $O(\partial^2)$ confidence intervals for each implementation. Figure from Ref. [4].

4.4 Conclusion

In very recent years, the derivative expansion of the NPRG has been shown to provide a computational tool capable of delivering accurate and highly precise results with controllable error estimates for the universal properties of the $O(N)$ models in three dimensions. In the present chapter, we have presented an extension of this approach to a model involving discrete $\mathbb{Z}_4$-symmetric perturbations, dangerously irrelevant at the isotropic $O(2)$-symmetric fixed point. An accurate treatment of such a model within nonperturbative RG requires substantial methodological advancements as compared to the isotropic case since the effective action depends in an essential way on two field variables.

We have provided an accurate estimate of the leading RG eigenvalue related to the discrete anisotropy y_4 in three dimensions. Our result represents the first NPRG estimation of y_4 compatible [within the error bars] with the values calculated with other methods. We emphasize that such a feat required a systematical implementation of the DE up to order $O(\partial^2)$. In the anisotropic models, it seems, it is not sufficient to consider the dependence of the parametrizing functions on two parameters [as has been previously done], the effective action ansatz itself has to be promoted to the most general anisotropic form. In our case, the promotion of the ansatz relied on splitting the $O(2)$-symmetric $(\partial_\mu\rho)^2$ term into two independent $\mathbb{Z}_4$-symmetric terms:

$$\phi^1\phi^2\partial_\mu\phi^1\partial_\mu\phi^2 \quad \text{and} \quad \left[\left(\phi^1\right)^2-\left(\phi^2\right)^2\right]\left[\left(\partial_\mu\phi^1\right)^2-\left(\partial_\mu\phi^2\right)^2\right], \tag{4.5}$$

each associated with a separate parametrizing function in the ansatz. Our results indicate, that accurately capturing the anisotropic eigenvalues requires introducing the anisotropic structure not just in the local potential, but also in the momentum-dependent parts of the two-point function. Interestingly, this is not the case for the leading *isotropic* eigenvalues, which can be quite accurately calculated already at the LPA order of the DE where the momentum dependence of the two-point function is greatly simplified. The nature of the relation between the momentum structure of the correlation functions and the anisotropic couplings presents an interesting area for future research.

Furthermore, we have demonstrated that a truncation in the $\mathbb{Z}_4$ invariant $\tau=\frac{1}{2}\left(\phi^1\phi^2\right)^2$ including just the terms up to the order $O(\tau)$ yields results practically equivalent to those obtained within the complete $O(\partial^2)$ DE approach in three dimensions. This is, however, no longer the case in lower dimensions. The results obtained from the τ expansion deviate significantly from the fully functional calculation below dimension $d\lesssim 2.5$, suggesting a failure of the order-parameter truncation similar to that observed in the isotropic $O(N)$ models.

We have analyzed the dependence of y_4 and subsequent irrelevant eigenvalues

on the dimension. The exponent y_4 has a nonmonotonous character as a function of the dimension, reaching a minimal value in a dimension slightly above two. After reaching its minimal value, y_4 rapidly approaches zero when the dimension reaches two, marking the onset of nonuniversal critical behavior. Previous NPRG studies, while providing the correct resolution of the interplay between the different fixed points and the rich and interesting cross-over behavior of the system, did not deliver the accurate eigenvalues describing the cubic perturbation [neither in three nor in two dimensions]. Our present study demonstrates how this is achieved via a systematic implementation of the derivative expansion.

Finally, we have discussed and compared the different implementations of the DE [the ansatz and the truncated variants]. While in the vicinity of three dimensions these yield practically identical results, substantial differences occur in lower dimensions. We do note, however, that the two variants remain compatible, in every dimension for which the error bars could be provided. The crucial difference occurs very close to two dimensions, where only the ansatz variant correctly accounts for the divergence of the correlation length exponent accompanying the onset of the KT physics. This discrepancy calls for further clarifying studies, going beyond the $O(\partial^2)$ truncation level.

The results discussed in this chapter also point to the fertility of the methodology developed recently in Refs. [20, 21, 23, 48] in situations reaching beyond the paradigm of the isotropic $O(N)$ models. It would be very interesting to extend the present study to the order $O(\partial^4)$ of the DE. We expect that in three dimensions this would allow for obtaining the estimate of y_4 with an accuracy better than in all the studies performed so far. On the other hand, in two dimensions we anticipate that the $O(\partial^4)$ calculation might be capable of capturing the KT physics fully accurately and, in any case, would provide a stringent test of the NPRG error estimate methodology developed recently. Such calculation would additionally shed more light on the differences between the ansatz and truncated variants of the DE approximation scheme.

Contribution statement

The results presented in this chapter are a product of a collaboration between Andrzej Chlebicki, Carlos A. Sánchez-Villalobos, Paweł Jakubczyk, and Nicolás Wschebor. The numerical calculations in the τ-expanded scheme were performed solely by Andrzej Chlebicki. The numerical full scheme calculations, treating the two field variables ρ and θ on a functional basis, were performed by Carlos Sánchez with support from Andrzej Chlebicki regarding the efficiency and the accuracy of the numerical implementation.

Appendix A

Functional RG flow equations

I've got a bike, you can ride it if you like
It's got a basket, a bell that rings
And things to make it look good
I'd give it to you if I could, but I borrowed it

Pink Floyd, *Bike*

In this section, we present the renormalization-group equations that were used in the calculations of Chapter 3. To simplify the expressions we denote the "dressed propagators" as follows:

$$G_\sigma(\rho) = \left[U'(\rho) + 2\rho U''(\rho) + Z_\sigma(\rho)q^2 + R(\boldsymbol{q}^2)\right]^{-1}, \tag{A.1}$$

$$G_\pi(\rho) = \left[U'(\rho) + Z_\pi(\rho)q^2 + R(\boldsymbol{q}^2)\right]^{-1}. \tag{A.2}$$

Additionally, we introduce the following notation:

$$\dot{R}\left(q^2\right) = k\partial_k R\left(q^2\right), \quad R'\left(q^2\right) = \partial_{q^2} R\left(q^2\right), \quad R''\left(q^2\right) = \partial_{q^2}^2 R\left(q^2\right), \tag{A.3}$$

and we suppress the k dependence to simplify the notation. The β functions employed in the functional calculation read:

$$\begin{aligned}\beta_{U'}(\rho) &= k\partial_k U'(\rho) \\ &= -\frac{1}{2}\int_q \dot{R}\left(q^2\right)\Big\{G_\sigma(\rho)^2\left[q^2 Z'_\sigma(\rho) + 2\rho U^{(3)}(\rho) + 3U''(\rho)\right] \\ &\qquad + G_\pi(\rho)^2(N-1)\left[q^2 Z'_\pi(\rho) + U''(\rho)\right]\Big\},\end{aligned} \tag{A.4}$$

$$
\begin{aligned}
&\beta_{Z_\sigma}(\rho) = k\partial_k Z_\sigma(\rho) = -\frac{1}{2d}\int_q \dot{R}\left(q^2\right)\Big[4(N-1)\rho G_\pi(\rho)^4\left[q^2 Z'_\pi(\rho) + U''(\rho)\right] \\
&\big\{-\left[R'\left(q^2\right) + Z_\pi(\rho)\right]\left[(d+4)q^2 Z'_\pi(\rho) + dU''(\rho)\right] - 2q^2 R''\left(q^2\right)\left[q^2 Z'_\pi(\rho) + U''(\rho)\right]\big\} \\
&+ 4(N-1)G_\pi(\rho)^3\left\{d\left[Z_\sigma(\rho) - Z_\pi(\rho)\right]\left[q^2 Z'_\pi(\rho) + U''(\rho)\right] + q^2\rho Z'_\pi(\rho)^2\right\} \\
&+ 4\rho G_\sigma(\rho)^4\Big[q^2 Z'_\sigma(\rho) + 2\rho U^{(3)}(\rho) + 3U''(\rho)\Big] - dG_\sigma(\rho)^2\left[Z'_\sigma(\rho) + 2\rho Z''_\sigma(\rho)\right] \\
&\Big(-\left[R'\left(q^2\right) + Z_\sigma(\rho)\right]\Big\{(d+4)q^2 Z'_\sigma(\rho) + d\Big[2\rho U^{(3)}(\rho) + 3U''(\rho)\Big]\Big\} \\
&- 2q^2 R''\left(q^2\right)\Big[q^2 Z'_\sigma(\rho) + 2\rho U^{(3)}(\rho) + 3U''(\rho)\Big]\Big) \\
&+ 4\rho G_\sigma(\rho)^3 Z'_\sigma(\rho)\Big[(2d+1)q^2 Z'_\sigma(\rho) + 4d\rho U^{(3)}(\rho) + 6dU''(\rho)\Big] \\
&+ 16(N-1)q^2\rho G_\pi(\rho)^5\left[R'\left(q^2\right) + Z_\pi(\rho)\right]^2\left[q^2 Z'_\pi(\rho) + U''(\rho)\right]^2 \\
&+ 16q^2\rho G_\sigma(\rho)^5\left[R'\left(q^2\right) + Z_\sigma(\rho)\right]^2\Big[q^2 Z'_\sigma(\rho) + 2\rho U^{(3)}(\rho) + 3U''(\rho)\Big]^2 \\
&- d(N-1)\rho^{-1}G_\pi(\rho)^2\left[\rho Z'_\sigma(\rho) - Z_\sigma(\rho) + Z_\pi(\rho)\right]\Big],
\end{aligned}
\tag{A.5}
$$

$$
\begin{aligned}
&\beta_{Z_\pi}(\rho) = k\partial_k Z_\pi(\rho) = -\frac{1}{2d\rho}\int_q \dot{R}\left(q^2\right)\Big[4q^2 G_\sigma(\rho)^3\left[R'\left(q^2\right) + Z_\sigma(\rho)\right]^2 \\
&+ G_\pi(\rho)^2\big\{-d\left[(N-1)\rho Z'_\pi(\rho) + 2R'\left(q^2\right) + 2Z_\pi(\rho)\right] - 4q^2 R''\left(q^2\right) \\
&- 4q^2 G_\sigma(\rho)\left[R'\left(q^2\right) - \rho Z'_\pi(\rho) + Z_\pi(\rho)\right]\left[R'\left(q^2\right) + \rho Z'_\pi(\rho) + Z_\pi(\rho)\right]\big\} \\
&+ G_\sigma(\rho)^2\left\{-d\left[2R'\left(q^2\right) + 2\rho^2 Z''_\pi(\rho) + 5\rho Z'_\pi(\rho) + Z_\sigma(\rho) + Z_\pi(\rho)\right] - 4q^2 R''\left(q^2\right)\right\} \\
&+ G_\pi(\rho)\Big(G_\sigma(\rho)\left\{4d\left[R'\left(q^2\right) + \rho Z'_\pi(\rho) + Z_\pi(\rho)\right] + 8q^2 R''\left(q^2\right)\right\} \\
&+ 4q^2 G_\sigma(\rho)^2\left[R'\left(q^2\right) + \rho Z'_\pi(\rho) + Z_\pi(\rho)\right]\left[-R'\left(q^2\right) + \rho Z'_\pi(\rho) - 2Z_\sigma(\rho) + Z_\pi(\rho)\right]\Big) \\
&+ 4q^2 G_\pi(\rho)^3\left[R'\left(q^2\right) + Z_\pi(\rho)\right]^2\Big].
\end{aligned}
\tag{A.6}
$$

Appendix B

Overview of numerical techniques

Hello
Is there anybody in there?
Just nod if you can hear me

Pink Floyd, *Comfortably Numb*

B.1 Finite grid representation for functions

The functional approach to the nonperturbative renormalization group (NPRG) described in Chapter 2 relies on the numerical treatment of partial and ordinary differential equations. The numerical analysis cannot be, however, performed in a continuous space. Thus, developing a well-controlled discretization procedure becomes a crucial step in implementing the NPRG.

In the DE treatment of the $O(N)$ models, every parametrizing function f is a real function of a nonnegative real parameter $\tilde{\rho}$

$$f : \mathbb{R}_0^+ \ni \tilde{\rho} \mapsto f(\tilde{\rho}) \in \mathbb{R}. \tag{B.1}$$

Therefore, there are two steps to discretization: restricting the $\tilde{\rho}$ domain to a compact set and discretizing the domain. The first step relies on selecting some value $\tilde{\rho}_{\mathrm{Max}}$ and restricting the domain of f to a set $\tilde{\rho} \in [0, \tilde{\rho}_{\mathrm{Max}}]$. Our analysis shows that the performance of the NPRG treatment is very weakly dependent on $\tilde{\rho}_{\mathrm{Max}}$ provided that $\frac{4}{3}\tilde{\rho}_0 \lesssim \tilde{\rho}_{\mathrm{Max}} \lesssim 10\tilde{\rho}_0$, where $\tilde{\rho}_0$ is the minimum of the fixed-point local potential.

The second step is substantially more involved. The domain of the function f is further reduced to an N_ρ-element discrete grid $\tilde{\rho} \in \{\tilde{\rho}_0, \tilde{\rho}_1, \ldots, \tilde{\rho}_{N_\rho - 1}\}$. It is typical and convenient, although not necessary, to work with an equispaced grid

$\tilde{\rho}_i = i\epsilon$ with $\epsilon(N_\rho - 1) = \tilde{\rho}_{\mathrm{Max}}$. Such representation reduces differential equations to algebraic equations making them suitable for numerical analysis. However, on a finite grid, we do not have access to the analytically calculated $\tilde{\rho}$ derivatives and they have to be approximated by finite differences.

The idea of a finite difference approximation for derivatives follows from the Taylor series expansion. The lowest-order finite difference formula can be derived as:

$$f(x+\epsilon) = f(x) + f'(x)\epsilon + O(\epsilon^2) \implies f'(x) = \frac{f(x+\epsilon) - f(x)}{\epsilon} + O(\epsilon). \quad \text{(B.2)}$$

The error associated with that expression, however, is of order $O(\epsilon)$ which is often unsatisfactory. To find a formula with a lower truncation error we need to use more evaluation points.

We define a stencil s - a set of n integer numbers $\{s_i\}_{i\in\{0,\ldots,n-1\}}$ that indicates the grid points that will be involved in the derivative calculation. We write:

$$f(x + s_i\epsilon) = \sum_{m=0}^{n-1} \frac{s_i^m \epsilon^m f^{(m)}(x)}{m!} + O\left(\epsilon^n\right). \quad \text{(B.3)}$$

To calculate the d-th order derivative $f^{(d)}(x)$ we want to find a linear combination $\sum c_i^{(d)} f(x + s_i\epsilon)$ such that the largest possible number of corrections is cancelled out. We find that:

$$\begin{aligned}\sum_{i=0}^{n-1} c_i^{(d)} f(x+s_i\epsilon) &= f(x)\sum_{i=0}^{n-1} c_i^{(d)} + \epsilon f'(x)\sum_{i=0}^{n-1} c_i^{(d)} s_i + \frac{\epsilon^2 f''(x)}{2}\sum_{i=0}^{n-1} c_i^{(d)} s_i^2 + \ldots \\ &= \sum_{m=0}^{n-1} \frac{\epsilon^m f^{(m)}(x)}{m!}\sum_{i=0}^{n-1} c_i^{(d)} s_i^m + O(\epsilon^n). \quad \text{(B.4)}\end{aligned}$$

Using the matrix notation Eq. (B.4) can be rewritten as

$$\begin{aligned}\sum_{i=0}^{n-1} c_i^{(d)} f(x+s_i\epsilon) = &\left(\begin{array}{cccc} f^{(0)}(x)\frac{\epsilon^0}{0!} & f^{(1)}(x)\frac{\epsilon^1}{1!} & \ldots & f^{(n-1)}(x)\frac{\epsilon^{n-1}}{(n-1)!}\end{array}\right)\cdot \\ &\left(\begin{array}{cccc} s_0^0 & s_1^0 & \ldots & s_{n-1}^0 \\ s_0^1 & s_1^1 & & s_{n-1}^1 \\ \vdots & & \ddots & \vdots \\ s_0^{n-1} & s_1^{n-1} & \ldots & s_{n-1}^{n-1}\end{array}\right)\left(\begin{array}{c} c_0^{(d)} \\ c_1^{(d)} \\ \vdots \\ c_{n-1}^{(d)}\end{array}\right) + O(\epsilon^n). \quad \text{(B.5)}\end{aligned}$$

To find the expression for $f^{(d)}(x)$ we need to cancel contributions from all of the derivatives $f^{(i)}(x)$ but $f^{(d)}(x)$ in Eq. (B.5). We achieve that by solving a set

of linear equations

$$\begin{pmatrix} s_0^0 & s_1^0 & \dots & s_{n-1}^0 \\ s_0^1 & s_1^1 & & s_{n-1}^1 \\ \vdots & & \ddots & \vdots \\ s_0^{n-1} & s_1^{n-1} & \dots & s_{n-1}^{n-1} \end{pmatrix} \begin{pmatrix} c_0^{(d)} \\ c_1^{(d)} \\ \vdots \\ c_{n-1}^{(d)} \end{pmatrix} = d! \begin{pmatrix} \delta_{0,d} \\ \delta_{1,d} \\ \vdots \\ \delta_{n-1,d} \end{pmatrix}. \tag{B.6}$$

for the coefficients $c_i^{(d)}$.

Having found the coefficients $c_i^{(d)}$ from Eq. (B.6) we can express the derivative as:

$$f^{(d)}(x) = \frac{\sum_{i=0}^{n-1} c_i^{(d)} f(x + \epsilon s_i)}{\epsilon^d} + O(\epsilon^{n-d}). \tag{B.7}$$

If the stencil s is symmetric [taking the form $\{-k, -(k-1), \dots, 0, \dots, k-1, k\}$] the corrections to the finite difference approximation (B.7) can be of an order higher than $O(\epsilon^{n-d})$. The algorithm outlined above along with the finite difference coefficients for calculating derivatives with various stencils can be found in Ref. [140].

To check the accuracy of our discretization scheme we calculate the two leading renormalization group (RG) eigenvalues of the three-dimensional $O(2)$ model at the $O(\partial^2)$ order of the DE with different numbers of stencil points and varying grid spacing ϵ. In Fig. B.1 we present the absolute value of the deviation $\Delta e_i = \left| e_i - e_i^{\text{ref}} \right|$ as a function of the number of grid points [for constant $\tilde{\rho}_{\text{Max}}$] calculated with 3−, 5−, 7−, and 9−point $\tilde{\rho}$ derivatives. As the reference value e_i^{ref} we chose the intersection of the two asymptotic lines for the 9−point derivative calculation at $N_\rho = 76$.

We find that for very low grid sizes, the discretization error follows the power laws and slowly flattens as N_ρ increases. The error profile is very similar for both the leading and the subleading eigenvalue, but the associated best-fit power-laws somewhat differ; the low-N_ρ asymptotic power-law fits are presented in Table B.1. As expected, the power-law exponents increase in absolute value with the increasing number of points used to calculate the derivatives, but interestingly they do not take integer values. This primarily shows that the discretization error propagates in a nonlinear fashion to the error in the eigenvalue calculation. We also note, that even on very sparse grids $N_\rho \approx 20$ the 9−point calculations yield a precision of 6 digits, which is often sufficient for most purposes.

When the grid becomes too tight the error starts to increase at a staggering rate of N_ρ^{16}. This is probably due to the rounding errors occurring in the calculation of the characteristic polynomial of very large matrices. We note that the number of nonzero entries in the stability matrix is almost exactly proportional to the number of points used in the calculation of $\tilde{\rho}$ derivatives. It is therefore expected that the

rounding errors will be more severe in the calculations involving more points in the derivative approximation. We further note that the eigenvalue calculation was performed with the "Eigenvalues" function of Wolfram Mathematica [141]. We emphasize that point because Mathematica allows for arbitrary machine precision in the calculation. When a finite-precision C++ library "Eigen" [142] was employed the rounding errors were much more severe, even when the 80-bit "long double" precision was employed.

The results of the present section can serve to both reassure and caution. On one hand, our results indicate a rapid convergence of our discretization scheme on very sparse grids. Moreover, we see that even when the derivatives are approximated on the crude 3−point stencil the leading eigenvalue can be obtained with a reasonable precision. Simultaneously, we show that the finite floating-point precision can have severe consequences and has to be treated with care. Finite machine precision leads to rapid degradation of the eigenvalue precision on very dense grids. For this reason, N_ρ cannot be increased indefinitely, and a comprehensive convergence analysis of the discretization scheme should be performed for each calculation. We finally note that the error seems to grow quite rapidly with each subsequent eigenvalue, which can become a significant issue when studying a large number of eigenvalues, e.g. in investigations of multicritical points.

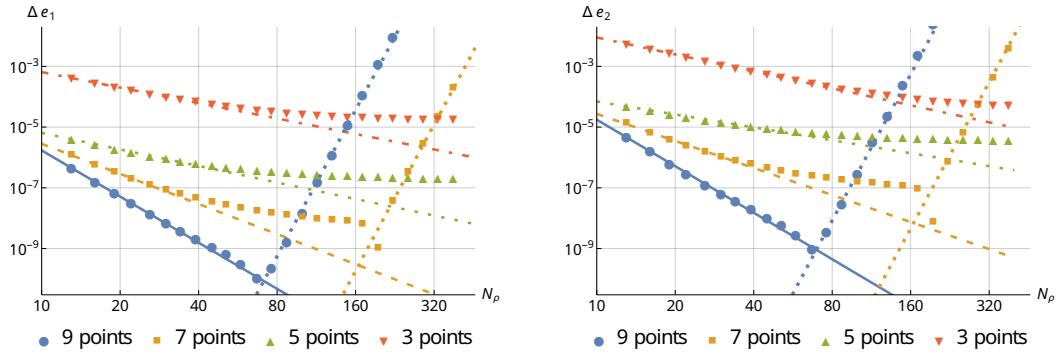

(a) Error of the dominant eigenvalue. (b) Error of the subdominant eigenvalue.

Figure B.1: Absolute deviation of the leading RG eigenvalues from the reference values $\Delta e_i = \left|e_i - e_i^{\text{ref}}\right|$ as a function of the number of grid points N_ρ. Series of data correspond to calculations using varying numbers of points in approximations of $\tilde{\rho}$ derivatives. Lines denote the best power-law fits for low- and large-N_ρ asymptotic behaviors. The charts feature a logarithmic scale on both axes.

n_ρ	9	7	5	3
Δe_1	$0.2N_\rho^{-5.1}$	$0.6 \cdot 10^{-2} N_\rho^{-3.3}$	$0.4 \cdot 10^{-3} N_\rho^{-1.8}$	$0.03N_\rho^{-1.7}$
Δe_2	$2N_\rho^{-5.1}$	$0.03N_\rho^{-3.0}$	$0.2 \cdot 10^{-2} N_\rho^{-1.4}$	$0.6N_\rho^{-1.9}$

Table B.1: Low-N_ρ asymptotic power-law fits to the absolute deviation of the leading RG eigenvalues from the reference values $\left|e_i - e_i^{\text{ref}}\right|$ for different numbers of points used in approximations of $\tilde{\rho}-$derivatives n_ρ.

B.2 Finite difference approximation for the Jacobian

In section 2.2.2 we defined the Jacobian - the matrix of the first derivatives of the flow equations:

$$M(\mathcal{F})_{a\tilde{\rho}_i, b\tilde{\rho}_j} := \frac{\partial \left(\partial_t \mathcal{F}_{a\tilde{\rho}_i}\right)}{\partial \mathcal{F}_{b\tilde{\rho}_j}}. \tag{B.8}$$

We recall that $\mathcal{F}$ stands for a vector of dimensionless functions parametrizing the effective action Γ_k. The indices a, b enumerate the functions and $\tilde{\rho}_i$, $\tilde{\rho}_j$ enumerate the discrete grid points. We stress that when some constraints are imposed on the function $\mathcal{F}_c$ at some point $\tilde{\rho}_k$ the corresponding row $M(\mathcal{F})_{c\tilde{\rho}_k,..}$ and column $M(\mathcal{F})_{..,c\tilde{\rho}_k}$ are removed from the matrix. Examples of such constraints include $\tilde{Z}(\tilde{\rho}_\eta) = 1$ and $\tilde{Z}_\sigma(0) = \tilde{Z}_\pi(0)$.

The expression for the Jacobian defined in Eq. (B.8) can be given analytically. Let us recall Eq. (2.23) for the dimensionless form of the flow equations:

$$\partial_t \mathcal{F}_a(\tilde{\rho}) = d_a \mathcal{F}_a(\tilde{\rho}) - (d - 2 + \eta_k)\tilde{\rho}\mathcal{F}'_a(\tilde{\rho}) - \tilde{\beta}_a(\tilde{\rho}), \tag{B.9}$$

with d_a denoting the canonical dimension of the function $\mathcal{F}_a$ and $\tilde{\beta}_a$ denoting the dimensionless loop contribution to the flow of $\mathcal{F}_a$. With that in mind, the Jacobian can then be expressed as:

$$M(\mathcal{F})_{a\tilde{\rho}_i, b\tilde{\rho}_j} = \delta_{a,b}\left(d_a \delta_{\tilde{\rho}_i,\tilde{\rho}_j} - (d - 2 + \eta_k)\tilde{\rho}_i \delta'_{\tilde{\rho}_i,\tilde{\rho}_j}\right) - \frac{\partial \beta_a(\tilde{\rho}_i)}{\partial \mathcal{F}_{b\tilde{\rho}_j}}, \tag{B.10}$$

where δ denotes the discrete counterpart of the Dirac delta - the Kronecker delta and δ' denotes the discrete counterpart of the derivative of the Dirac delta. The form of δ' depends on the employed discretization scheme [see Appendix B.1] and can be written as:

$$\delta'_{i,j} = \sum_{k=0}^{n-1} c_k^{(1)} \delta_{i+s_k,j} \tag{B.11}$$

where $c_k^{(1)}$ are the finite difference coefficients and s_k are the stencil points used to calculate the discretized approximation of the first derivative [see Eq. (B.7)].

The expressions for the derivatives $\frac{\partial \beta_a(\tilde{\rho}_i)}{\partial \mathcal{F}_{b\tilde{\rho}_j}}$ can be found analytically and later evaluated numerically. The exact expressions, however, heavily depend on the employed discretization scheme due to the presence of derivatives of the Dirac delta function. Additionally, the expressions for the functional derivatives of the β functions become very lengthy. This approach can be efficiently implemented with software for symbolic calculations, e.g. in Mathematica [141], where the derivatives can be calculated analytically after the discretization is performed. In purely numerical calculations, on the other hand, it is much more convenient to approximate the derivatives involved in calculating the Jacobian by finite differences.

The finite difference approximation in the functional space is applied similarly to that in the $\tilde{\rho}$ grid. We just need to define the stencil points s_i and the perturbation parameter ϵ. To find the entry of the matrix $M(\mathcal{F})_{a\tilde{\rho}_i, b\tilde{\rho}_j}$, we first need to perturb the entry $\mathcal{F}_{b\tilde{\rho}_j}$ of the parametrization by the value ϵs_k for each of the stencil points s_k. We define a family of perturbed actions:

$$\mathcal{F}^{k,b\tilde{\rho}_j}_{a\tilde{\rho}_i} = \mathcal{F}_{a\tilde{\rho}_i} + \epsilon s_k \delta_{a,b} \delta_{\tilde{\rho}_i, \tilde{\rho}_j}. \tag{B.12}$$

Then, we calculate the $(a\tilde{\rho}_i)$ component of the time derivative for each member of the family $\mathcal{F}^{k,b\tilde{\rho}_j}$. Finally, the derivative is found from Eq. (B.7):

$$M(\mathcal{F})_{a\tilde{\rho}_i, b\tilde{\rho}_j} = \frac{1}{\epsilon} \sum_{k=0}^{n-1} c_k^{(1)} \partial_t \left(\mathcal{F}^{k,b\tilde{\rho}_j}_{a\tilde{\rho}_i} \right) + O\left(\epsilon^{n-1}\right). \tag{B.13}$$

The expression (B.13) can seem somewhat convoluted at first but its implementation is easier than an analogous discretization in the $\tilde{\rho}$ space. This is due to the fact, that in the functional space, there are no boundaries so we can always choose the same symmetric stencil which allows for a straightforward implementation and oftentimes yields an improved precision.

The finite difference approximation of the Jacobian relies on a small parameter ϵ. It is therefore necessary to assess the quality of the approximation and find the optimal value for ϵ. In Fig. B.2 we compare the performance of 9− 7−, 5−, and 3−point derivative approximations in the calculation of the Jacobian. Like in sec. B.1, we look at the absolute differences of the leading RG eigenvalues from the reference values $\Delta e_i = \left| e_i - e_i^{\text{ref}} \right|$, where e_i^{ref} is found at the intersection of the two asymptotic behaviors; in this analysis we find e_i^{ref} at $\epsilon \approx 5 \cdot 10^{-6}$. The calculations are performed at the $O(\partial^2)$ level of the DE in the three-dimensional $O(2)$ model.

We find that for large ϵ, the accuracy of the eigenvalue calculation follows the same asymptotic behavior as the theoretically expected accuracy of the finite difference derivatives; the power-laws read ϵ^8, ϵ^6, ϵ^4, and ϵ^2 for 9− 7−, 5−, and

3−point derivatives respectively. As for the small ϵ asymptotics, there seems to be a universal line $\sim \epsilon^{-1}$ that serves as a lower bound for the possible eigenvalue accuracy. This behavior is related most likely to the rounding errors and the finite numerical precision. We also note a significant, approximately 10 times, drop in precision between the first and the second eigenvalue.

In Eq. (B.13) we used the same value of ϵ at every point $\mathcal{F}_{a\tilde{\rho}_i}$. There is, however, no fundamental reason to do that. Moreover, a drawback of that approach lies in the fact, that when the functions $\mathcal{F}$ span many orders of magnitude a perturbation suitable for at one point might be too large or too small at another. One of the alternative approaches is to introduce a proportional parameter $\epsilon_{a\tilde{\rho}_i} = \tilde{\epsilon}|\mathcal{F}_{a\tilde{\rho}_i}|$. Such a method has to be implemented with a threshold value ϵ_{Min}, such that $\epsilon_{a\tilde{\rho}_i}$ does not become too small when $\mathcal{F}_{a\tilde{\rho}_i}$ becomes too close to zero. We have tested the approach with $\epsilon_{a\tilde{\rho}_i}$ proportional to the value of the parametrizing function and observed no significant change in the precision of the calculated RG eigenvalues as compared to the fixed value of ϵ.

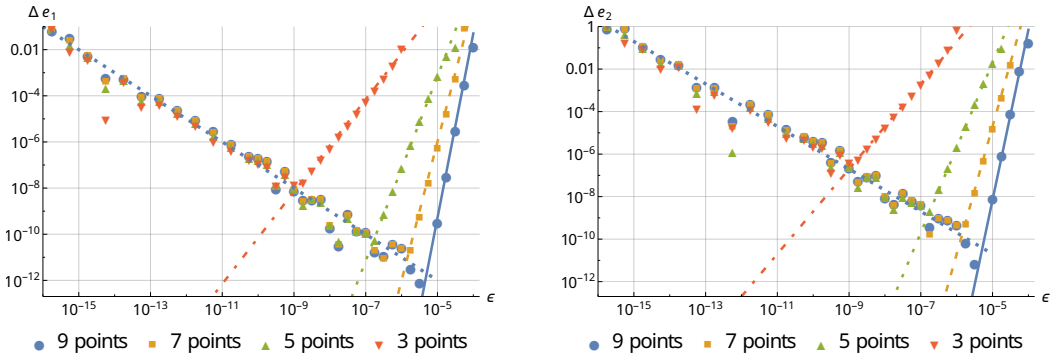

(a) Error of the dominant eigenvalue.

(b) Error of the subdominant eigenvalue.

Figure B.2: Absolute deviation of the leading RG eigenvalues from the reference values $\Delta e_i = \left|e_i - e_i^{\mathrm{ref}}\right|$ as a function of the perturbation ϵ used in the finite difference approximation of the Jacobian [see Eq. (B.13)]. Series of data correspond to calculations using varying numbers of points in the finite difference method. Lines denote the best power-law fit with integer exponents. The charts feature a logarithmic scale on both axes.

As in the previous section, our analysis indicates that our methodology can reach appropriate precision in a wide range of numerical parameters. However, whenever an arbitrary parameter appears in the methodology, a comprehensive analysis of its effects should be performed and caution is advised. Our results clearly show that too small a value of ϵ leads to a degradation of precision just as a value too large does. Interestingly, in the analysis of the finite-difference approximation of the Jacobian, there is no obvious disadvantage of using a larger

stencil [9−point vs 3−point] besides a slight increase in the required numerical effort. We once again emphasize that the subleading eigenvalue is determined with precision substantially worse than the leading one and that this trend continues with subsequent eigenvalues.

B.3 Newton-Raphson method

The Newton-Raphson (NR) method is a root-finding algorithm characterized by quick convergence and a straightforward formulation. It is very widely known and implemented in all areas of numerical analysis. In the NPRG context, the NR method is used in a search for RG fixed points.

Suppose we have a function $\boldsymbol{f} : \mathbb{R}^n \to \mathbb{R}^n$ and we are searching for a good approximation of its root $\boldsymbol{f}(\boldsymbol{x}^*) = 0$. We begin the search with a guess vector $\boldsymbol{x}_0$. From the Taylor series expansion, we have

$$\boldsymbol{f}(\boldsymbol{x}_0) = \underbrace{\boldsymbol{f}(\boldsymbol{x}^*)}_{0} + M(\boldsymbol{x}^*)\Delta\boldsymbol{x}_0 + O\left(\Delta\boldsymbol{x}_0^2\right), \tag{B.14}$$

where

$$M(\boldsymbol{x}')_{ij} = \left.\frac{\partial f_i(\boldsymbol{x})}{\partial x_j}\right|_{\boldsymbol{x}=\boldsymbol{x}'} \tag{B.15}$$

is the Jacobian matrix and $\Delta\boldsymbol{x}_0 = \boldsymbol{x}_0 - \boldsymbol{x}^*$ is the distance between the guess and the root. Inverting this relation to find $\Delta\boldsymbol{x}_0$ we find

$$\Delta\boldsymbol{x}_0 = M(\boldsymbol{x}^*)^{-1}\boldsymbol{f}(\boldsymbol{x}_0) + O(\Delta\boldsymbol{x}^2). \tag{B.16}$$

Not knowing the root $\boldsymbol{x}^*$ we are unable to calculate the Jacobian $M(\boldsymbol{x}^*)$. We note, however, that

$$\left(M(\boldsymbol{x}_0)^{-1} - M(\boldsymbol{x}^*)^{-1}\right)\boldsymbol{f}(\boldsymbol{x}_0) = O(\Delta\boldsymbol{x}^2) \tag{B.17}$$

so we can replace $M(\boldsymbol{x}^*)^{-1}$ with $M(\boldsymbol{x}_0)^{-1}$ in Eq. (B.16) without altering the order of the correction.

We thus formulate an iterative scheme

$$\boldsymbol{x}_{n+1} = \boldsymbol{x}_n - M(\boldsymbol{x}_n)^{-1}\boldsymbol{f}(\boldsymbol{x}_n). \tag{B.18}$$

Tracking the quadratic correction from the Taylor series one easily finds that

$$|\Delta\boldsymbol{x}_{n+1}| = \frac{1}{2}\left|M(\boldsymbol{x}_n)^{-1}\left(\Delta\boldsymbol{x}_n^T H(\boldsymbol{x}_n)\Delta\boldsymbol{x}_n\right)\right| + O(\Delta x_n^3) \tag{B.19}$$

where $H(\boldsymbol{x}_n)$ denotes the tensor of second derivatives of $\boldsymbol{f}$. Eq. (B.19) implies a rapid, quadratic convergence of the NR algorithm when the three conditions are met:

1. $\Delta \boldsymbol{x}_n$ is sufficiently small - $\boldsymbol{x}_n$ is not too far from the root;
2. $M(\boldsymbol{x}_n)^{-1}$ is finite - the Jacobian is not singular or near-singular
3. $H(\boldsymbol{x}_n)$ is small enough - the system is not too stiff.

The NR method, though very effective, can sometimes suffer from poor convergence. This can happen due to several reasons, the most severe of which include: poor initial guess, overshooting, and singularity of the Jacobian.

A good initial guess is not difficult to find in the NPRG context. A very simple approach is to start the fixed point (FP) search sufficiently close to the upper critical dimension. In the perturbative regime, the critical action can be well approximated by the perturbative action. Thus, the initial guess can also be inferred from perturbative calculations. From the upper critical dimension one can slowly lower the dimension, taking the FP of the dimension d as the initial condition in dimension $d - \delta d$.

The problem of overshooting is not difficult to overcome either. Most often, it occurs when the initial guess is too far from the root, and the higher-order corrections in Eq. (B.16) cannot be neglected. In those cases, it is convenient to introduce a "damping coefficient" $\alpha < 1$ and modify the NR method as follows:

$$\boldsymbol{x}_{n+1} = \boldsymbol{x}_n - \alpha M(\boldsymbol{x}_n)^{-1} \boldsymbol{f}(\boldsymbol{x}_n). \tag{B.20}$$

The value of α cannot be found from first principles and has to be determined phenomenologically. Typically, this is done by performing a series of calculations with varying α in a search for the value yielding the best improvement in $\boldsymbol{f}$.

On the other hand, the singularity of the Jacobian is a very severe issue. Typically, such situations call for the adoption of different numerical methods. In the NPRG context, the Jacobian can become singular when some coupling is close to marginality. This happens primarily close to a critical dimension [lower or upper] and when the relevance of some operator changes. One can expect, that numerical treatment of the FP search will be particularly difficult in studying such problems and additional effort will be necessary. It might prove fruitful to identify root-finding methods that might offer better convergence in the NPRG applications in situations in which the NR method fails.

For more details on NR method and other numerical techniques, we refer to Ref. [104].

B.4 Runge-Kutta methods

Methods of the Runge-Kutta (RK) family are techniques for finding numerical solutions to ordinary differential equations. Similarly to the discretization scheme

i	τ_i	ξ_{ij}			I_i
		$j=1$	$j=2$	$j=3$	
1	0				1/6
2	1/2	1/2			1/3
3	1/2	0	1/2		1/3
4	1	0	0	1	1/6

Table B.2: Coefficients of the RK4 method.

discussed in sec. B.1 they rely on the Taylor expansion to find solutions that are correct up to some power of the small discretization parameter h.

Let us consider an initial value problem with an ODE of form

$$\partial_t \boldsymbol{x}(t) = \boldsymbol{f}(t, \boldsymbol{x}), \quad \boldsymbol{x}(t_0) = \boldsymbol{x}_0, \tag{B.21}$$

where $\boldsymbol{f} : \mathbb{R} \otimes \mathbb{R}^n \to \mathbb{R}^n$ is real-vector valued smooth function. In the RK type methods, a discrete step $\boldsymbol{x}(t) \to \boldsymbol{x}(t+h)$ is calculated through consecutive evaluations of the function $\boldsymbol{f}$ at several intermediate points and linearly combining them in a way that cancels the corrections of low-order in h. Let n denote the number of intermediate points.

The RK methods involve three families of coefficients: the intermediate time-increment coefficients τ_i, the intermediate position-increment coefficients ξ_{ij}, and the final position-increment coefficients I_i. The general formula for the position after the time increment reads

$$\boldsymbol{x}(t+h) = \boldsymbol{x}(t) + h \sum_{i=1}^{n} I_i \boldsymbol{k}_i, \tag{B.22}$$

where $\boldsymbol{k}_i$ denotes the time derivative $\boldsymbol{f}$ calculated at the intermediate position $\boldsymbol{x}_i$

$$\boldsymbol{k}_i = \boldsymbol{f}(t + h\tau_i, \boldsymbol{x}_i), \quad \boldsymbol{x}_i = \boldsymbol{x}(t) + h \sum_{j<i} \xi_{ij} \boldsymbol{k}_j. \tag{B.23}$$

One of the most popular and widely employed methods of the RK family is the 4−step method often called the RK4 method. The coefficients of the RK4 method are presented in Table B.2. The RK4 method is subject to a local truncation error of order $O(h^5)$ and a total accumulated truncation error of order $O(h^4)$.

Besides precision, efficiency is one of the most important considerations for a numerical algorithm. In a fixed-step RK method discussed above, the truncation error can vary significantly during the simulation; in more steady periods the truncation error will be comparatively low, and in volatile periods - comparatively high. This leads to inefficiencies since the gain in precision achieved in the steady

periods is overshadowed by the loss in precision incurred in the volatile periods, typically by orders of magnitude.

A relatively simple solution is to adjust the time step h at each step in a way that keeps the truncation error approximately constant throughout the simulation. This idea lies at the center of the adaptive RK methods. In the adaptive methods, the position after a time increment is calculated identically to the fixed-step methods based on Eqs. (B.22) and (B.23). The adaptive methods, however, feature a truncation error estimator E_{T} based on an additional family of coefficients E_i:

$$E_{\mathrm{T}} = h \sum_{i=1}^{n} \|E_i \boldsymbol{k}_i\|, \tag{B.24}$$

where $\|\cdot\|$ refers to a norm on $\mathbb{R}^n$.

After each step, a new value of the time increment is calculated according to the formula:

$$h_{\mathrm{New}} = h \left(\frac{E_{\mathrm{T}}}{E_{\mathrm{T}}^{\mathrm{Max}}} \right)^{1/q} f_{\mathrm{Safety}}, \tag{B.25}$$

where $E_{\mathrm{T}}^{\mathrm{Max}}$ is the predefined maximal accepted truncation error and q is the order of the error estimator. The safety factor f_{Safety} is introduced so that the error will be acceptable in the next step with high probability. Typically, f_{Safety} is set equal to 0.8, 0.9, $0.25^{1/q}$ or $0.38^{1/q}$ [143]. If $E_{\mathrm{T}} > E_{\mathrm{T}}^{\mathrm{Max}}$ the step is repeated with a new, lower value of the time increment; if $E_{\mathrm{T}} \leq E_{\mathrm{T}}^{\mathrm{Max}}$ the step is completed and h_{New} is accepted as the time increment for the next step.

Typically, the adaptive RK methods are embedded - the points $(t + h\tau_i, \boldsymbol{x}_i)$ used to calculate the new position feature in methods of two consecutive orders. Thus, the difference between the two methods can be used as an error estimator with a minimal number of evaluations of the time derivative $\boldsymbol{f}$. The Runge-Kutta-Fehlberg method employed in this thesis is a fourth-order method with an embedded fifth-order error estimator [143]. Its coefficients are presented in Table B.3.

For further discussion of the Runge-Kutta methods, we refer to Refs. [143, 144]. We also note that implementations of the RK methods are easily accessible via open-source numeric libraries such as Boost [145] for C++ and SciPy for Python [146].

i	τ_i	ξ_{ij}					I_i	E_i
		$j=1$	$j=2$	$j=3$	$j=4$	$j=5$		
1	0						$\frac{16}{135}$	$\frac{1}{360}$
2	$\frac{1}{4}$	$\frac{1}{4}$					0	0
3	$\frac{3}{8}$	$\frac{3}{32}$	$\frac{9}{32}$				$\frac{6656}{12825}$	$-\frac{128}{4275}$
4	$\frac{12}{13}$	$\frac{1932}{2197}$	$-\frac{7200}{2197}$	$\frac{7296}{2197}$			$\frac{28561}{56430}$	$-\frac{2197}{75240}$
5	1	$\frac{439}{216}$	-8	$\frac{3680}{513}$	$-\frac{845}{4104}$		$-\frac{9}{50}$	$\frac{1}{50}$
6	$\frac{1}{2}$	$-\frac{8}{27}$	2	$-\frac{3544}{2565}$	$\frac{1859}{4104}$	$-\frac{11}{40}$	$\frac{2}{55}$	$\frac{2}{55}$

Table B.3: Coefficients of the adaptive step Runge-Kutta-Fehlberg method.

Bibliography

[1] J. L. Cardy and H. W. Hamber, "O(n) Heisenberg model close to n=d=2", Phys. Rev. Lett. **45**, 499–501 (1980).

[2] A. Chlebicki and P. Jakubczyk, "Analyticity of critical exponents of the O(N) models from nonperturbative renormalization", SciPost Phys. **10**, 10.21468/SciPostPhys.10.6.134 (2021).

[3] A. Chlebicki and P. Jakubczyk, "Low-temperature behavior of the O(N) models below two dimensions", Physical Review E **107**, 10.1103/PhysRevE.107.014121 (2023).

[4] A. Chlebicki, C. A. Sánchez-Villalobos, P. Jakubczyk, and N. Wschebor, "$\mathbb{Z}_4$-symmetric perturbations to the XY model from functional renormalization", Phys. Rev. E **106**, 10.1103/PhysRevE.106.064135 (2022).

[5] N. Goldenfeld, *Lectures on phase transitions and the renormalization group*, 1st Edition (CRC Press, Boca Raton, 1992).

[6] P. M. Chaikin and T. C. Lubensky, *Principles of Condensed Matter Physics* (Cambridge University Press, Cambridge, 1995).

[7] J. Berges, N. Tetradis, and C. Wetterich, "Non-perturbative renormalization flow in quantum field theory and statistical physics", Phys. Rep. **363**, 223–386 (2002).

[8] D. J. Amit and V. Martin-Mayor, *Field Theory, the Renormalization Group, and Critical Phenomena* (World Scientific, 2005).

[9] J. Cardy, *Scaling and Renormalization in Statistical Physics* (Cambridge University Press, Apr. 1996).

[10] J. Zinn-Justin, *Phase Transitions and Renormalization Group* (Oxford University Press, July 2007).

[11] F. Parisen Toldin, "Boundary Critical Behavior of the Three-Dimensional Heisenberg Universality Class", Phys. Rev. Lett. **126**, 135701 (2021).

[12] M. Hu, Y. Deng, and J.-P. Lv, "Extraordinary-Log Surface Phase Transition in the Three-Dimensional XY Model", Phys. Rev. Lett. **127**, 120603 (2021).

[13]F. Parisen Toldin and M. A. Metlitski, "Boundary Criticality of the 3D O(N) Model: From Normal to Extraordinary", Phys. Rev. Lett. **128**, 215701 (2022).

[14]J. Padayasi, A. Krishnan, M. A. Metlitski, I. A. Gruzberg, and M. Meineri, "The extraordinary boundary transition in the 3d O(N) model via conformal bootstrap", SciPost Phys. **12**, 10.21468/SciPostPhys.12.6.190 (2022).

[15]S. Yabunaka and B. Delamotte, "Surprises in $O(N)$ Models: Nonperturbative Fixed Points, Large N Limits, and Multicriticality", Phys. Rev. Lett. **119**, 191602 (2017).

[16]S. Yabunaka and B. Delamotte, "Why Might the Standard Large N Analysis Fail in the O(N) Model: The Role of Cusps in Fixed Point Potentials", Phys. Rev. Lett. **121**, 231601 (2018).

[17]V. Abhignan and R. Sankaranarayanan, "Continued Functions and Perturbation Series: Simple Tools for Convergence of Diverging Series in $O(n)$-Symmetric ϕ^4 Field Theory at Weak Coupling Limit", J. Stat. Phys. **183**, 1–29 (2021).

[18]S. El-Showk, M. F. Paulos, D. Poland, S. Rychkov, D. Simmons-Duffin, and A. Vichi, "Solving the 3d Ising Model with the Conformal Bootstrap II. c-Minimization and Precise Critical Exponents", J. Stat. Phys. **157**, 869–914 (2014).

[19]F. Kos, D. Poland, and D. Simmons-Duffin, "Bootstrapping mixed correlators in the 3D Ising model", J. High Energy Phys. **2014**, 10.1007/JHEP11(2014)109 (2014).

[20]G. De Polsi, G. Hernández-Chifflet, and N. Wschebor, "Precision calculation of universal amplitude ratios in $O(N)$ universality classes: Derivative expansion results at order $\mathcal{O}(\partial^4)$", Phys. Rev. E **104**, 064101 (2021).

[21]G. De Polsi, I. Balog, M. Tissier, and N. Wschebor, "Precision calculation of critical exponents in the O(N) universality classes with the nonperturbative renormalization group", Phys. Rev. E **101**, 1–24 (2020).

[22]M. Hasenbusch, "Monte Carlo study of an improved clock model in three dimensions", Phys. Rev. B **100**, 1–19 (2019).

[23]I. Balog, H. Chaté, B. Delamotte, M. Marohnić, and N. Wschebor, "Convergence of Nonperturbative Approximations to the Renormalization Group", Phys. Rev. Lett. **123**, 240604 (2019).

[24]M. V. Kompaniets and E. Panzer, "Minimally subtracted six-loop renormalization of $O(N)$-symmetric ϕ^4 theory and critical exponents", Phys. Rev. D **96**, 1–26 (2017).

[25]D. Simmons-Duffin, "The lightcone bootstrap and the spectrum of the 3d Ising CFT", J. High Energy Phys. **2017**, 10.1007/JHEP03(2017)086 (2017).

[26]A. C. Echeverri, B. von Harling, and M. Serone, "The effective bootstrap", J. High Energy Phys. **2016**, 10.1007/JHEP09(2016)097 (2016).

[27]F. Kos, D. Poland, D. Simmons-Duffin, and A. Vichi, "Precision islands in the Ising and O(N) models", J. High Energy Phys. **2016**, 10.1007/JHEP08(2016)036 (2016).

[28]J. A. Lipa, J. A. Nissen, D. A. Stricker, D. R. Swanson, and T. C. P. Chui, "Specific heat of liquid helium in zero gravity very near the lambda point", Phys. Rev. B **68**, 174518 (2003).

[29]M. Campostrini, M. Hasenbusch, A. Pelissetto, and E. Vicari, "Theoretical estimates of the critical exponents of the superfluid transition in ^{4}He by lattice methods", Phys. Rev. B **74**, 144506 (2006).

[30]R. Guida and J. Zinn-Justin, "Critical exponents of the N-vector model", J. Phys. A. Math. Gen. **31**, 8103–8121 (1998).

[31]S. M. Chester, W. Landry, J. Liu, D. Poland, D. Simmons-Duffin, N. Su, and A. Vichi, "Carving out OPE space and precise O(2) model critical exponents", Journal of High Energy Physics **2020**, 10.1007/JHEP06(2020)142 (2020).

[32]D. J. Binder and S. Rychkov, "Deligne categories in lattice models and quantum field theory, or making sense of O(N) symmetry with non-integer N", J. High Energy Phys. **2020**, 117 (2020).

[33]O. Boada, A. Celi, J. I. Latorre, and M. Lewenstein, "Quantum simulation of an extra dimension", Phys. Rev. Lett. **108**, 133001 (2012).

[34]O. Boada, A. Celi, J. Rodríguez-Laguna, J. I. Latorre, and M. Lewenstein, "Quantum simulation of non-trivial topology", New J. Phys. **17**, 045007 (2015).

[35]H. Yi, "Quantum critical behavior of the quantum Ising model on fractal lattices", Phys. Rev. E **91**, 012118 (2015).

[36]Z. Zhou, X.-F. Zhang, F. Pollmann, and Y. You, "Fractal Quantum Phase Transitions: Critical Phenomena Beyond Renormalization", pre-print, 1–15 (2021).

[37]Q. Liu, Y. Deng, T. M. Garoni, and H. W. Blöte, "The O(n) loop model on a three-dimensional lattice", Nucl. Phys. B **859**, 107–128 (2012).

[38]S. El-Showk, M. Paulos, D. Poland, S. Rychkov, D. Simmons-Duffin, and A. Vichi, "Conformal Field Theories in Fractional Dimensions", Phys. Rev. Lett. **112**, 141601 (2014).

[39]J. Henriksson, "The critical O(N) CFT: Methods and conformal data", Phys. Rep. **1002**, 1–72 (2023).

[40]M. Moshe and J. Zinn-Justin, "Quantum field theory in the large N limit: A review", Phys. Rep. **385**, 69–228 (2003).

[41]A. Polyakov, "Interaction of goldstone particles in two dimensions. Applications to ferromagnets and massive Yang-Mills fields", Phys. Lett. B **59**, 79–81 (1975).

[42]E. Brézin and J. Zinn-Justin, "Renormalization of the nonlinear σ model in $2+\epsilon$ dimensions-application to the Heisenberg ferromagnets", Phys. Rev. Lett. **36**, 691–694 (1976).

[43]T. H. Berlin and M. Kac, "The Spherical Model of a Ferromagnet", Phys. Rev. **86**, 821–835 (1952).

[44]H. E. Stanley, "Spherical model as the limit of infinite spin dimensionality", Phys. Rev. **176**, 718–722 (1968).

[45]J. F. Nicoll, T. S. Chang, and H. E. Stanley, "Approximate renormalization group based on the Wegner-Houghton differential generator", Phys. Rev. Lett. **33**, 540–543 (1974).

[46]C. Wetterich, "Exact evolution equation for the effective potential", Phys. Lett. B **301**, 90–94 (1993).

[47]T. R. Morris, "The exact renormalization group and approximate solutions", Int. J. Mod. Phys. A **09**, 2411–2449 (1994).

[48]I. Balog, G. De Polsi, M. Tissier, and N. Wschebor, "Conformal invariance in the nonperturbative renormalization group: A rationale for choosing the regulator", Phys. Rev. E **101**, 062146 (2020).

[49]N. D. Mermin and H. Wagner, "Absence of ferromagnetism or antiferromagnetism in one- or two-dimensional isotropic Heisenberg models", Phys. Rev. Lett. **17**, 1133–1136 (1966).

[50]J. M. Kosterlitz and D. J. Thouless, "Ordering, metastability and phase transitions in two-dimensional systems", J. Phys. C Solid State Phys. **6**, 1181–1203 (1973).

[51]G. Kohring, R. E. Shrock, and P. Wills, "Role of vortex strings in the three-dimensional O(2) model", Phys. Rev. Lett. **57**, 1358–1361 (1986).

[52]S. R. Shenoy, "Vortex-loop scaling in the three-dimensional XY ferromagnet", Phys. Rev. B **40**, 5056–5068 (1989).

[53]M.-h. Lau and C. Dasgupta, "Numerical investigation of the role of topological defects in the three-dimensional Heisenberg transition", Phys. Rev. B **39**, 7212–7222 (1989).

[54]M. Kamal and G. Murthy, "New O(3) transition in three dimensions", Phys. Rev. Lett. **71**, 1911–1914 (1993).

[55]O. I. Motrunich and A. Vishwanath, "Emergent photons and transitions in the O(3) sigma model with hedgehog suppression", Phys. Rev. B - Condens. Matter Mater. Phys. **70**, 10.1103/PhysRevB.70.075104 (2004).

[56]D. R. Nelson and D. S. Fisher, "Dynamics of classical XY spins in one and two dimensions", Phys. Rev. B **16**, 4945–4955 (1977).

[57]M. Tissier and G. Tarjus, "Unified picture of ferromagnetism, quasi-long-range order, and criticality in random-field models", Phys. Rev. Lett. **96**, 12–15 (2006).

[58]M.-h. Lau and C. Dasgupta, "Critical behavior of the n-vector model for $1 < n < 2$", Phys. Rev. B **35**, 329–332 (1987).

[59]R. Skomski, P. Manchanda, and A. Kashyap, "Anisotropy and Crystal Field", in *Handbook of magnetism and magnetic materials*, edited by J. M. D. Coey and S. S. Parkin (Springer International Publishing, Cham, 2021), pp. 103–185.

[60]D. R. Nelson, "Coexistence-curve singularities in isotropic ferromagnets", Phys. Rev. B **13**, 2222–2230 (1976).

[61]A. V. Chubukov, S. Sachdev, and J. Ye, "Theory of two-dimensional quantum Heisenberg antiferromagnets with a nearly critical ground state", Phys. Rev. B **49**, 11919–11961 (1994).

[62]S. Miyashita, "Nature of the Ordered Phase and the Critical Properties of the Three Dimensional Six-State Clock Model", J. Phys. Soc. Japan **66**, 3411–3420 (1997).

[63]M. Oshikawa, "Ordered phase and scaling in models and the three-state antiferromagnetic Potts model in three dimensions", Phys. Rev. B - Condens. Matter Mater. Phys. **61**, 3430–3434 (2000).

[64]J. Lou, A. W. Sandvik, and L. Balents, "Emergence of U(1) symmetry in the 3D XY model with Z_q anisotropy", Phys. Rev. Lett. **99**, 207203 (2007).

[65]F. Léonard and B. Delamotte, "Critical Exponents Can Be Different on the Two Sides of a Transition: A Generic Mechanism", Phys. Rev. Lett. **115**, 200601 (2015).

[66]T. Okubo, K. Oshikawa, H. Watanabe, and N. Kawashima, "Scaling relation for dangerously irrelevant symmetry-breaking fields", Phys. Rev. B - Condens. Matter Mater. Phys. **91**, 174417 (2015).

[67]H. Shao, W. Guo, and A. W. Sandvik, "Monte Carlo Renormalization Flows in the Space of Relevant and Irrelevant Operators: Application to Three-Dimensional Clock Models", Phys. Rev. Lett. **124**, 080602 (2020).

[68]P. Patil, H. Shao, and A. W. Sandvik, "Unconventional U(1) to Z_q crossover in quantum and classical q-state clock models", Phys. Rev. B **103**, 1–24 (2021).

[69]A. Aharony, "Critical behavior of anisotropic cubic systems", Phys. Rev. B **8**, 4270–4273 (1973).

[70]J. Manuel Carmona and A. Pelissetto, "Component Ginzburg-Landau Hamiltonian with cubic anisotropy: A six-loop study", Phys. Rev. B - Condens. Matter Mater. Phys. **61**, 15136–15151 (2000).

[71]S. M. Chester, W. Landry, J. Liu, D. Poland, D. Simmons-Duffin, N. Su, and A. Vichi, "Bootstrapping Heisenberg magnets and their cubic instability", Phys. Rev. D **104**, 105013 (2021).

[72]H. Kleinert and V. Schulte-Frohlinde, "Exact five-loop renormalization group functions of θ^4-theory with O(N)-symmetric and cubic interactions. Critical exponents up to ϵ^5", Phys. Lett. B **342**, 284–296 (1995).

[73]M. Hasenbusch, "Cubic fixed point in three dimensions: Monte Carlo simulations of the ϕ^4 model on the simple cubic lattice", Phys. Rev. B **107**, 24409 (2023).

[74]P. Calabrese and A. Celi, "Critical behavior of the two-dimensional N-component Landau-Ginzburg Hamiltonian with cubic anisotropy", Phys. Rev. B **66**, 184410 (2002).

[75]J. V. José, L. P. Kadanoff, S. Kirkpatrick, and D. R. Nelson, "Renormalization, vortices, and symmetry-breaking perturbations in the two-dimensional planar model", Phys. Rev. B **16**, 1217–1241 (1977).

[76]G. Delfino and N. Lamsen, "Critical points of coupled vector-Ising systems. Exact results", J. Phys. A Math. Theor. **52**, 10.1088/1751-8121/ab3055 (2019).

[77]A. Chlebicki and P. Jakubczyk, "Criticality of the $O(2)$ model with cubic anisotropies from nonperturbative renormalization", Phys. Rev. E **100**, 052106 (2019).

[78]E. Rastelli, S. Regina, and A. Tassi, "Monte Carlo simulation of a planar rotator model with symmetry-breaking fields", Phys. Rev. B **69**, 174407 (2004).

[79]E. Rastelli, S. Regina, and A. Tassi, "Monte Carlo simulation for square planar model with a small fourfold symmetry-breaking field", Phys. Rev. B **70**, 174447 (2004).

[80]A. Taroni, S. T. Bramwell, and P. C. Holdsworth, "Universal window for two-dimensional critical exponents", J. Phys. Condens. Matter **20**, 275233 (2008).

[81]J. Tobochnik and G. V. Chester, "Monte Carlo study of the planar spin model", Physical Review B **20**, 3761–3769 (1979).

[82]S. T. Bramwell and P. C. W. Holdsworth, "Magnetization and universal sub-critical behaviour in two-dimensional XY magnets", J. Phys. Condens. Matter **5**, L53–L59 (1993).

[83]S. T. Bramwell and P. C. W. Holdsworth, "Magnetization: A characteristic of the Kosterlitz-Thouless-Berezinskii transition", Phys. Rev. B **49**, 8811–8814 (1994).

[84]S. T. Bramwell, P. C. Holdsworth, and J. Rothman, "Magnetization in ultrathin films: Critical exponent β for the 2D XY model with 4-fold crystal fields", Mod. Phys. Lett. B **11**, 139–148 (1997).

[85]K. G. Wilson and J. Kogut, "The renormalization group and the ϵ expansion", Phys. Rep. **12**, 75–199 (1974).

[86]F. J. Wegner and A. Houghton, "Renormalization group equation for critical phenomena", Phys. Rev. A **8**, 401–412 (1973).

[87]J. Polchinski, "Renormalization and effective lagrangians", Nucl. Physics, Sect. B **231**, 269–295 (1984).

[88]D. S. Fisher and D. A. Huse, "Wetting transitions: A functional renormalization-group approach", Physical Review B **32**, 247–256 (1985).

[89]R. Lipowsky and M. E. Fisher, "Scaling regimes and functional renormalization for wetting transitions", Physical Review B **36**, 2126–2141 (1987).

[90]R. Lipowsky and S. Leibler, "Unbinding Transitions of Interacting Membranes", Physical Review Letters **56**, 2541–2544 (1986).

[91]G. R. Golner and E. K. Riedel, "Renormalization-group calculation of critical exponents in three dimensions", Physical Review Letters **34**, 856–859 (1975).

[92]K. E. Newman and E. K. Riedel, "Cubic N-vector model and randomly dilute Ising model in general dimensions", Phys. Rev. B **25**, 264–280 (1982).

[93]K. E. Newman and E. K. Riedel, "Critical exponents by the scaling-field method: The isotropic N-vector model in three dimensions", Physical Review B **30**, 6615–6638 (1984).

[94]A. Hasenfratz and P. Hasenfratz, "Renormalization group study of scalar field theories", Nuclear Physics B **270**, 687–701 (1986).

[95]K. E. Newman, E. K. Riedel, and S. Muto, "Q-state Potts model by Wilson's exact renormalization-group equation", Physical Review B **29**, 302–313 (1984).

[96]M. Bonini, M. D'Attanasio, and G. Marchesini, "Perturbative renormalization and infrared finiteness in the Wilson renormalization group: the massless scalar case", Nuclear Physics B **409**, 441–464 (1993).

[97]P. Kopietz, L. Bartosch, and F. Schütz, *Introduction to the Functional Renormalization Group*, 1st ed. (Springer Berlin, Heidelberg, 2010).

[98]H. Gies, "Introduction to the functional RG and applications to gauge theories", in *Lect. notes phys.* Vol. 852, edited by A. Schwenk and J. Polonyi (Springer Berlin Heidelberg, Berlin, Heidelberg, 2012), pp. 287–348.

[99]N. Dupuis, L. Canet, A. Eichhorn, W. Metzner, J. M. Pawlowski, M. Tissier, and N. Wschebor, "The nonperturbative functional renormalization group and its applications", Phys. Rep. **910**, 1–114 (2021).

[100]B. Delamotte, "An introduction to the nonperturbative renormalization group", in *Renormalization group and effective field theory approaches to many-body systems*, edited by A. Schwenk and J. Polonyi (Springer Berlin Heidelberg, Berlin, Heidelberg, 2012), pp. 49–132.

[101]T. R. Morris, "Derivative expansion of the exact renormalization group", Phys. Lett. B **329**, 241–248 (1994).

[102]J. Berges and D. Mesterházy, "Introduction to the nonequilibrium functional renormalization group", Nucl. Phys. B - Proc. Suppl., Lecture Notes in Physics **228**, 37–60 (2012).

[103]B. Delamotte, D. Mouhanna, and M. Tissier, "Nonperturbative renormalization-group approach to frustrated magnets", Physical Review B - Condensed Matter and Materials Physics **69**, 10.1103/PhysRevB.69.134413 (2004).

[104]E. Süli and D. F. Mayers, *An Introduction to Numerical Analysis* (Cambridge University Press, Aug. 2003), p. 433.

[105]A. Pelissetto and E. Vicari, "Critical phenomena and renormalization-group theory", Physics Reports **368**, 549–727 (2002).

[106]M. Gräter and C. Wetterich, "Kosterlitz-Thouless Phase Transition in the Two Dimensional Linear σ Model", Physical Review Letters **75**, 378–381 (1995).

[107]K.-I. Aoki, K. Morikawa, W. Souma, J.-I. Sumi, and H. Terao, "Rapidly Converging Truncation Scheme of the Exact Renormalization Group", Progress of Theoretical Physics **99**, 451–466 (1998).

[108]S.-B. Liao, J. Polonyi, and M. Strickland, "Optimization of renormalization group flow", Nuclear Physics B **567**, 493–514 (2000).

[109]D. F. Litim, "Critical exponents from optimised renormalisation group flows", Nuclear Physics B **631**, 128–158 (2002).

[110]L. Canet, B. Delamotte, D. Mouhanna, and J. Vidal, "Optimization of the derivative expansion in the nonperturbative renormalization group", Physical Review D **67**, 065004 (2003).

[111]L. Canet, B. Delamotte, D. Mouhanna, and J. Vidal, "Nonperturbative renormalization group approach to the Ising model: A derivative expansion at order ∂^4", Physical Review B **68**, 064421 (2003).

[112]Z. Péli, "Derivative expansion for computing critical exponents of O(N) symmetric models at next-to-next-to-leading order", Physical Review E **103**, 032135 (2021).

[113]G. D. Polsi and N. Wschebor, "Regulator dependence in the functional renormalization group: A quantitative explanation", Physical Review E **106**, 10.1103/PhysRevE.106.024111 (2022).

[114]P. Jakubczyk, N. Dupuis, and B. Delamotte, "Reexamination of the nonperturbative renormalization-group approach to the Kosterlitz-Thouless transition", Phys. Rev. E **90**, 062105 (2014).

[115]G. v. Gersdorff and C. Wetterich, "Nonperturbative renormalization flow and essential scaling for the Kosterlitz-Thouless transition", Physical Review B - Condensed Matter and Materials Physics **64**, 0545131–0545135 (2001).

[116]P. Jakubczyk and W. Metzner, "Longitudinal fluctuations in the Berezinskii-Kosterlitz-Thouless phase", Phys. Rev. B **95**, 085113 (2017).

[117]P. Jakubczyk and A. Eberlein, "Thermodynamics of the two-dimensional XY model from functional renormalization", Physical Review E **93**, 062145 (2016).

[118]S. Nagy, I. Nándori, J. Polonyi, and K. Sailer, "Functional Renormalization Group Approach to the Sine-Gordon Model", Phys. Rev. Lett. **102**, 241603 (2009).

[119]A. Rançon and N. Dupuis, "Higgs amplitude mode in the vicinity of a $(2+1)$-dimensional quantum critical point", Phys. Rev. B **89**, 180501 (2014).

[120]A. Rançon and N. Dupuis, "Kosterlitz-thouless signatures in the low-temperature phase of layered three-dimensional systems", Phys. Rev. B **96**, 214512 (2017).

[121]J. Krieg and P. Kopietz, "Dual lattice functional renormalization group for the Berezinskii-Kosterlitz-Thouless transition: Irrelevance of amplitude and out-of-plane fluctuations", Phys. Rev. E **96**, 042107 (2017).

[122]N. Defenu, A. Trombettoni, I. Nándori, and T. Enss, "Nonperturbative renormalization group treatment of amplitude fluctuations for $|\phi|^4$ topological phase transitions", Physical Review B **96**, 10.1103/PhysRevB.96.174505 (2017).

[123]I. Maccari, N. Defenu, L. Benfatto, C. Castellani, and T. Enss, "Interplay of spin waves and vortices in the two-dimensional XY model at small vortex-core energy", Phys. Rev. B **102**, 104505 (2020).

[124]M. Peláez and N. Wschebor, "Ordered phase of the O(N) model within the nonperturbative renormalization group", Phys. Rev. E **94**, 10.1103/PhysRevE.94.042136 (2016).

[125]F. Rose and N. Dupuis, "Nonperturbative functional renormalization-group approach to transport in the vicinity of a $2+1$-dimensional O(N)-symmetric quantum critical point", Phys. Rev. B **95**, 014513 (2017).

[126]G. von Gersdorff, *Zweidimensionale O(N)-symmetrische systeme im formalismus der exakten renormierungs-gruppe (MSc thesis)* (Heidelberg University (unpublished), 2000).

[127]M. Tissier and G. Tarjus, "Nonperturbative functional renormalization group for random field models and related disordered systems. IV. Supersymmetry and its spontaneous breaking", Physical Review B **85**, 104203 (2012).

[128]B. Delamotte, M. Dudka, D. Mouhanna, and S. Yabunaka, "Functional renormalization group approach to noncollinear magnets", Physical Review B **93**, 064405 (2016).

[129]N. Tetradis, "Renormalization-group study of weakly first-order phase transitions", Phys. Lett. Sect. B Nucl. Elem. Part. High-Energy Phys. **431**, 380–386 (1998).

[130]M. Tissier, D. Mouhanna, J. Vidal, and B. Delamotte, "Randomly dilute Ising model: A nonperturbative approach", Physical Review B **65**, 140402 (2002).

[131]W. Bernreuther and F. J. Wegner, "Four-Loop-Order Function for Two-Dimensional Nonlinear Sigma Models", Phys. Rev. Lett. **57**, 1383–1385 (1986).

[132]H. Kleinert, "Variational resummation for ϵ-expansions of critical exponents of nonlinear O(n)-symmetric σ-model in $2 + \epsilon$ dimensions", Phys. Lett. Sect. A Gen. At. Solid State Phys. **264**, 357–365 (2000).

[133]I. F. Herbut, "Critical behavior at superconductor-insulator phase transitions near one dimension", Phys. Rev. B **58**, 971–981 (1998).

[134]I. F. Herbut, "Critical exponents at the superconductor-insulator transition in dirty-boson systems", Phys. Rev. B **61**, 14723–14726 (2000).

[135]B. Nienhuis, "Exact critical point and critical exponents of O(N) models in two dimensions", Phys. Rev. Lett. **49**, 1062–1065 (1982).

[136]A. Nahum, J. T. Chalker, P. Serna, M. Ortuño, and A. M. Somoza, "Deconfined Quantum Criticality, Scaling Violations, and Classical Loop Models", Phys. Rev. X **5**, 041048 (2015).

[137]A. Chlebicki, C. A. Sánchez-Villalobos, P. Jakubczyk, and N. Wschebor, *Z4-symmetric perturbations to the XY model from functional renormalization*, (2022) `https://doi.org/10.18150/MNMJAO`.

[138]M. Hasenbusch and E. Vicari, "Anisotropic perturbations in three-dimensional O(N)-symmetric vector models", Phys. Rev. B - Condens. Matter Mater. Phys. **84**, 125136 (2011).

[139]D. Banerjee, S. Chandrasekharan, and D. Orlando, "Conformal Dimensions via Large Charge Expansion", Phys. Rev. Lett. **120**, 61603 (2018).

[140]B. Fornberg, "Generation of finite difference formulas on arbitrarily spaced grids", Mathematics of Computation **51**, 699–706 (1988).

[141]W. R. Inc., *Mathematica, Version 13.3*, Champaign, IL, 2023.

[142]J. Benoît and G. Guennebaud, *Eigen C++ Library*, `https://eigen.tuxfamily.org/dox/`, Last accessed 2023-08-07, 2021.

[143]E. Hairer, G. Wanner, and S. P. Nørsett, *Solving ordinary differential equations I*, Vol. 8 (Springer Berlin Heidelberg, 1993).

[144]J. C. Butcher, *Numerical Methods for Ordinary Differential Equations* (Wiley, July 2016).

[145]*Boost C++ Library*, `https://www.boost.org/`, Last accessed 2023-08-14.

[146]P. Virtanen, R. Gommers, T. E. Oliphant, M. Haberland, T. Reddy, D. Cournapeau, E. Burovski, P. Peterson, W. Weckesser, J. Bright, S. J. van der Walt, M. Brett, J. Wilson, K. J. Millman, N. Mayorov, A. R. J. Nelson, E. Jones, R. Kern, E. Larson, C. J. Carey, İ. Polat, Y. Feng, E. W. Moore, J. VanderPlas, D. Laxalde, J. Perktold, R. Cimrman, I. Henriksen, E. A. Quintero, C. R. Harris, A. M. Archibald, A. H. Ribeiro, F. Pedregosa, P. van Mulbregt, and SciPy 1.0 Contributors, "SciPy 1.0: Fundamental Algorithms for Scientific Computing in Python", Nature Methods **17**, 261–272 (2020).